A Driver-Vehicle Model for Impaired Motorists and Strategies for Planning Autonomous Vehicles

Thanh Phuc Le

A Thesis

In the Department

of

Mechanical and Industrial Engineering

Presented in Partial Fulfillment of the Requirements

For the Degree of

Doctor of Philosophy (Mechanical Engineering) at

Concordia University

Montreal, Quebec, Canada

February 2013

CONCORDIA UNIVERSITY

School of Graduate Studies

This is to certify that the thesis prepared

By: **Thanh Phuc Le**

Entitled: **A Driver-Vehicle Model for Impaired Motorists and Strategies for Planning Autonomous Vehicles**

and submitted in partial fulfillment of the requirements for the degree of

Doctor of Philosophy (Mechanical Engineering)

complies with the regulations of the University and meets the accepted standards with respect to originality and quality.

Signed by the final Examining Committee:

_____Chair
Dr. D. Dysart-Gale

_____External Examiner
Dr. D. Necsulescu

_____Examiner to Program
Dr. S. Williamson

_____Examiner
Dr. S. Rakheja

_____Examiner
Dr. R. Sedaghati

_____Thesis Supervisor
Dr. I. Stiharu

Approved by _____
Chair of Department or Graduate Program Director

_____ 2013 _____
Dean of Faculty

ABSTRACT

A Driver-Vehicle Model for Impaired Motorists

and Strategies for Planning Autonomous Vehicles

Thanh Phuc Le

Concordia University, 2013

Vehicle drivers play a vital role in transportation safety and they impose meaningful constraints during the design of the vehicle. Understanding the drivers' behavior, especially the impaired drivers' behavior, is crucial to improve the vehicle safety. The distinctive features of the impaired driver are quantified by using the control theories. The proposed impaired driver model is based on the optimal preview control and the linear quadratic regulator (LQR). Two important parameters that could be counted for in a mathematical model of the driver are the reaction time and the preview time. For the impaired driver model the reaction time is increased while the preview time is decreased. This modifications are consistent with an impaired driver who needs the longer time to react to an incident while observes a shorter preview on the road. The simulation results for the model of the impaired driver and the vehicle yield a larger lateral deviation than the one of a normal driver, as revealed in the experiments conducted by the previous studies. The weaving vehicle is also recognized as a characteristic for the vehicle driven by the impaired drivers. The other parameters such as

the control priority and lateral perception are formulated to introduce the random errors that bring the model closer to the human driver. The investigation on vehicle parameters reveals that the changes of parameters may improve the overall performance of the impaired driver-vehicle system. The results suggest a method to improve the vehicle safety by adapting vehicle parameters to the impaired driver.

The controller for autonomous vehicles is developed from the studies of the driver model representing the human driver. The preview capability of driver is introduced to the design of the controller by using the preview control theory. The preview information of the path in terms of the lateral position and the velocity profile enhances the performance of the autonomous vehicle. The controller uses the coupled linear longitudinal and lateral models to compute the steering angle and the wheel torque that are provided to the model of a nonlinear vehicle. The actual response of the vehicle is approximated by using the Kalman filter. The neural network is presented as a feasible alternative approach to implement the future path in design of autonomous vehicle controller. The neural network weights the path data and provides the adjustment as the preparation to the vehicle.

Acknowledgement

I would like to take this opportunity to thank my supervisor Professor I. Stiharu for his patience and kindness throughout this study. Without his inspiring discussion and invaluable guidance, this thesis would have never been fulfilled.

I wish to express my great appreciation to the Vietnamese Government who granted the scholarship. The financial support gave me the opportunity to pursuit the graduate study in Concordia University.

I want to send the special thanks to my friends and colleagues in the Department of Mechanical and Industrial Engineering for their constant moral support. The enthusiastic encouragement helps me overcome the difficult situations.

Finally, I am very grateful to my parents who are always looking at my steps. Many thanks go to my beloved wife for her priceless love and understanding.

TABLE OF CONTENTS

LIST OF FIGURES ix

NOMENCLATURE xiii

Chapter 1 INTRODUCTION AND LITERATURE REVIEW 1

1.1 GENERAL 1

1.2 LITERATURE REVIEW 3

1.2.1 Vehicle models used in modeling and simulation 3

1.2.2 Driver models for lateral control of a vehicle 12

1.2.3 Effects of alcohol on driving 23

1.2.4 Autonomous vehicles 25

1.3 SCOPE OF THE RESEARCH AND ORGANIZATION OF THE THESIS 28

Chapter 2 AN OPTIMAL PREVIEW CONTROL REPRESENTING THE SYSTEM OF AN IMPAIRED DRIVER AND A NON-LINEAR VEHICLE 31

2.1 INTRODUCTION 31

2.2 LINEAR VEHICLE MODEL 33

2.3 OPTIMAL PREVIEW MODEL OF DRIVER 38

2.4 DRIVER-VEHICLE RESPONSE 43

2.5 THE COUPLING OF DRIVER MODEL AND NON-LINEAR VEHICLE AND THE PRESENTATION OF DETERIORATED DRIVING SKILLS 51

2.6 CONCLUSION 60

Chaper 3 AN IMPAIRED DRIVER MODELAND THE CONTROL OF VEHICLE PARAMETERS 62
3.1 INTRODUCTION 62
3.2 LINEAR QUADRATIC REGULATOR (LQR) CONTROL MODEL OF DRIVER AND VEHICLE 63
3.3 THE IMPAIRED DRIVER MODEL AND THE CONTROL OF VEHICLE PARAMETERS 81
3.4 CONCLUSION 88
Chapter 4 LATERAL AND LONGITUDINAL PLANNING FOR AUTONOMOUS VEHICLES 90
4.1 INTRODUCTION 90
4.2 DESIGN OF LONGITUDINAL AND LATERAL CONTROLLERS 92
4.2.1 Velocity profile of the path 92
4.2.2 Linear model of the vehicle and the preview control for longitudinal direction 94
4.2.3 Lateral controller design 97
4.3 NONLINEAR VEHICLE MODEL 98
4.4 THE OVERALL MODEL AND SIMULATION 110
4.5 CONCLUSION 118
Chapter 5 NEURAL NETWORK USED TO CONTROL AUTONOMOUS VEHICLES 119
5.1 INTRODUCTION 119
5.2 NETWORK ARCHITECTURE 120

5.3 TRAINING ARTIFICIAL NEURAL NETWORK 124
5.4 SIMULATION RESULTS 133
5.5 CONCOLUSION 138
Chapter 6 CONCLUSION AND FUTURE WORK 139
6.1 CONCLUSION 139
6.2 FUTURE WORK 142
REFERENCES 144

LIST OF FIGURES

Figure 1.1 Fatalities in vehicle crashes due to alcohol in Canada 2

Figure 1.2 Vehicle coordinate systems 4

Figure 1.3 The bicycle model 5

Figure 1.4 The roll-able vehicle model 6

Figure 1.5 The 14-DOF vehicle model 8

Figure 1.6 Lateral force as the function of slip angle in the nonlinear tire 9

Figure 1.7 Compensatory tracking driver model 12

Figure 1.8 The typical preview tracking driver model 14

Figure 1.9 The prediction strategy 15

Figure 1.10 The multi loop driver-vehicle model 16

Figure 1.11 Vehicle and previewed road path 18

Figure 1.12 Structure of driver-vehicle model with neuromuscular property 19

Figure 2.1 The 3 DOF linear vehicle model 35

Figure 2.2 The preview path 39

Figure 2.3 The block diagram of the driver-vehicle system 42

Figure 2.4 The relation of the preview time, delay time and cost function 44

Figure 2.5 The root locus of the closed-loop system with a) varying T_p and b) varying τ 45

Figure 2.6 The dynamic response of the modified driver-vehicle model comparing to that of MacAdam model 47

Figure 2.7 The effect of under-steer coefficient (K_{us}) on the performance of the driver model 48
Figure 2.8 Three levels of lane-change and their cost 50
Figure 2.9 The system of driver and non-linear vehicle 52
Figure 2.10 Preview gains of linear vehicle and non-linear vehicle 53
Figure 2.11 Sensitivity of lateral performance to variations in M_y, M_ψ, h and k_p 55
Figure 2.12 Lateral position of the non-linear vehicle with three values of preview time 56
Figure 2.13 Roll angle of the non-linear vehicle with three values of preview time 57
Figure 2.14 The performance of the non-linear vehicle model with levels of deterioration 59
Figure 3.1 (a) The absolute path and (b) the path planned by the driver 65
Figure 3.2 (a) Lateral displacement and (b) driver steering angle of the driver-vehicle system with a lane-change 72
Figure 3.3 Path following with (a) varying preview time and (b) varying delay time 74
Figure 3.4 The road path seen by the driver 75
Figure 3.5 Time history of (a) lateral displacement and (b) driver steering angle for the simulation of driver-vehicle model with the update mechanism 77
Figure 3.6 The performance of the delay system comparing to the system without delay 78
Figure 3.7 The performance of the driver-vehicle system with the decreased preview time and increased delay time 79

Figure 3.8 The relation of standard lateral deviation and preview time 80
Figure 3.9 The standard lateral deviation with changing reaction time 81
Figure 3.10 (a) Lateral position and (b) lateral deviation of the vehicle model with the driver model impairment of 21% 85
Figure 3.11 Mean (SE) standard deviation of lateral position for three levels of impairment. 86
Figure 3.12 The SDLPs when (a) $C_{\alpha f}$ changes and (b) $C_{\alpha r}$ changes 87
Figure 4.1 The observed path and the curvature 92
Figure 4.2 The velocity profile of the path 93
Figure 4.3 The longitudinal vehicle model 95
Figure 4.4 Vehicle coordinate systems 99
Figure 4.5 The simplified vehicle coordinate system 100
Figure 4.6 Forces acting on the planar vehicle. 102
Figure 4.7 Vehicle roll in plane model 105
Figure 4.8 Forces acting on the wheel 106
Figure 4.9 The impact of changing coefficients D and C on the outputs of Magic Formula 108
Figure 4.10 The impact of changing coefficients B and E on the outputs of Magic Formula 109
Figure 4.11 The overall model of vehicle control 110
Figure 4.12 Longitudinal performance 113
Figure 4.13 Lateral performance 115
Figure 4.14 Lateral performance with disturbances 116

Figure 4.15 Longitudinal performance with disturbances 117
Figure 5.1 The contribution of vehicle states and path preview in generating the steering angle 121
Figure 5.2 The NN presenting the path preview 122
Figure 5.3 The structure of autonomous vehicle controller 123
Figure 5.4 Vehicle trajectory with a proportional controller 126
Figure 5.5 NN training with arbitrary pre-defined gains 127
Figure 5.6 Control gains of LQR driver model 128
Figure 5.7 NN weights for nonlinear vehicle 129
Figure 5.8 NN weights for velocity control 130
Figure 5.9 The road path used in the frequency response analysis 131
Figure 5.10 Frequency response of the lateral position 132
Figure 5.11 Frequency response of the vehicle speed 133
Figure 5.12 F1 Montreal Grand Prix circuit 134
Figure 5.13 NN gains after training 135
Figure 5.14 Vehicle speed 136
Figure 5.15 Vehicle position for the section AB 137
Figure 5.16 Vehicle position for the section DE 137

NOMENCLATURE

$\boldsymbol{A}$	State matrix of the vehicle
$\boldsymbol{A_d}$	Discrete **s**tate matrix of the vehicle
$\boldsymbol{B}$	Control matrix of the vehicle
BAC	Blood alcohol concentration
$\boldsymbol{B_d}$	Discrete control matrix of the vehicle
B_r	Reflex damping
$\boldsymbol{C}$	Observer vector
CG	Center of gravity
$C_{\alpha f}$, $C_{\alpha r}$	Cornering stiffness of front tires and rear tires
$c_{\phi f}$, $c_{\phi r}$	Roll damping
DOF	Degree of freedom
d_f	Front track width
d_r	Rear track width
$\boldsymbol{F}$	State matrix
F_x	Longitudinal force
F_y	Lateral force
$f(\eta)$	Preview path input
$\boldsymbol{G}$	Control matrix
h	Height of vehicle Center of Gravity (C.G)
h_s	Distance from roll axis to sprung mass
I_x	Vehicle moment of inertia about x axis
I_{xz}	Vehicle moment of inertia about x and z axis

I_w	Wheel moment of inertia
I_z	Inertial about z axis
$\boldsymbol{i}$, $\boldsymbol{j}$	Unit vectors
J_{dr}, B_{dr}, K_{dr}	Inertia, damping, and stiffness of the steering system
$\boldsymbol{K(k)}$	Matrix of control gains
K_a	Active stiffness
K_d	Driver's gain
$\boldsymbol{K_k}$	Control law matrix
$\boldsymbol{K}_p$	Control gain
K_r	Reflex stiffness
K_{us}	The under-steer coefficient
$k_{\phi f}$, $k_{\phi r}$	Roll stiffness
LQR	Linear quadratic regulator
l	Wheel base
l_f, l_r	Distance of front and rear axle to C.G
M_T	Torque feedback
M_z	Yaw moment
m	Vehicle mass
m_s	Sprung mass
n_{sw}	Steering ratio
n_τ	Delay steps
$\boldsymbol{P_k}$	Riccati matrix
$\boldsymbol{Q}$	Matrix of weighting factors
q_y, q_T, q_ψ	Weight factors of lateral position, muscle torque and head angle
$\boldsymbol{R}$	Position vector of the CG

R	Weighting factors of the steering input
R_i	Effective rolling radius of wheels
R_1, R_2	Weighting factors of the lateral deviation and the steering input
$r(t)$, $\dot{\psi}(t)$	Yaw velocity
SDLP	Standard deviation of lateral position
SE	Standard error
T_p, T^*	Preview time, optimal preview time
T_I	Lag time
T_L	Lead time
T_m	Applied muscle torque
u	Forward speed of the vehicle
v	Lateral velocity
$\boldsymbol{x}(k)$	Vehicle state
$\boldsymbol{y}_p(k)$	Road state
$\boldsymbol{z}(k)$	System state
α_f	Slip angle of front tires
α_r	Slip angle of rear tires
δ_f	Steering angle of front tires
δ_{sw}	Steering wheel angle
$\delta(t)$	Steer angle
ψ	Vehicle head angle
τ	Delay time

Chapter 1

INTRODUCTION AND LITERATURE REVIEW

1.1 GENERAL

Traffic accidents represent one of the largest public safety problems that lead to significant costs to society and individuals [1]. Even though vehicles and road condition have been dramatically improving, deaths and serious injuries from traffic collisions continue to be the key problem of transportation safety partly due to the increase of the traffic and the driver inability. The vehicle driver, an active component of a moving vehicle plays the vital role in road safety. Statistics of road accidents show that major fatal cases come from drivers' lack of ability in controlling a vehicle [2].

Road accidents due to alcohol intoxicated drivers are the increasing problem [1]. During 2005 in Canada, there were 3,226 persons who died in vehicle crashes. Of these cases, 1,100 persons died in alcohol related crashes. Comparing to the data in 2008, 2694 persons died in vehicle crashes and 1,056 of these fatalities are related to driving under the influence of alcohol. Although, total numbers of fatalities are decreased, the percentage of alcohol related fatalities are increased. Figure 1.1 shows the trend of fatal vehicle crashes and alcohol related factor in four years.

An impaired driver is a person who is unable to optimally drive a motor vehicle due to the consumption of alcohol, drugs, excessive fatigue or old age related inabilities (limited visual and listening capability, limited capability to perform the necessary driving maneuvers). This work focuses on the alcohol-affected drivers as impaired

drivers. Usually, the reflection of impaired driving is foreseen when the driver is driving a vehicle too fast or too slow, the vehicle does not follow the direction of the road or the driver is unable to perform a simple task. For drivers under the influence, blood alcohol concentration (BAC) is commonly used to measure impairment. Although, the BAC considered to be illegally driving varies by countries but the BAC of 0.08% is a typical limit to operate a vehicle. The driving regulations have contributed to gradual decrease in road accidents during past years; however they are not either effective or practical as they are not always respected. For examples, a driver who is not over BAC of 0.08 may be seriously impaired because the effect of alcohol varies from person to person depending on age, weight, gender or metabolism.

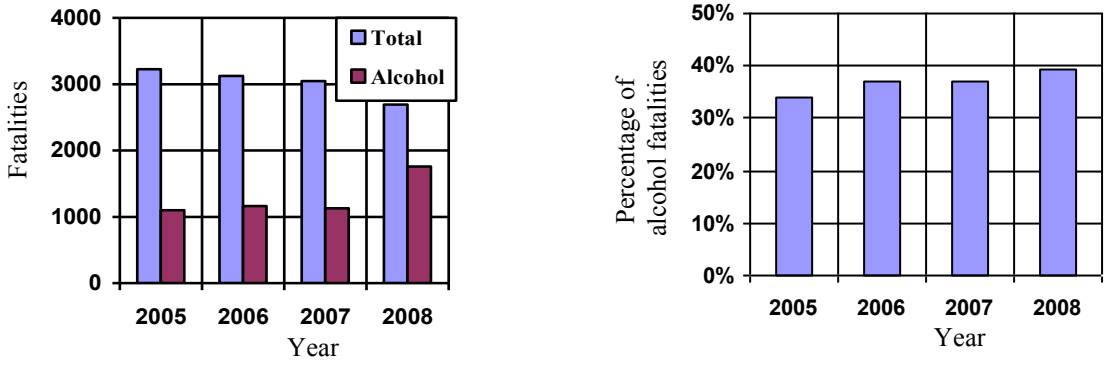

Figure 1.1: Fatalities in vehicle crashes due to alcohol in Canada [1]

Recently, autonomous vehicle became an attractive topic that has intensively been investigated. The autonomous vehicle on road may reduce accidents that occur due to human mistakes and improves the traffic flow on highway [3]. An active control system can react faster than a human driver when a sudden incident happens [4]. The automatic driving also reduces workload of the driver therefore eliminating the effect of impaired

drivers and inexperienced drivers [5]. Under the assumption that all vehicles would be autonomously driven, all "drivers" would experience identical skills that would make the traffic more fluid and safer. Environment benefits are obtained when autonomous vehicles consume less fuel and emit less pollutant [6].

The impact of drivers on transportation safety is significant. This research aims to investigate a driver model that can perform as of the impaired driver. The goal is to establish the threshold for safe driving and adapt vehicle to impaired drivers with various levels of impairment. The research also attempts to develop a controller that may regulate the vehicle speed and steer actively for autonomous vehicles. The design of the controller is based on the studies of driver behavior. The autonomous vehicle with the proposed controller may properly perform various maneuvers.

1.2 LITERATURE REVIEW

1.2.1 Vehicle models used in modeling and simulation

An accurate and realistic vehicle mathematical model is essential to simulate the driver-vehicle system. Many different models ranging from simple to complex have been developed for use in various control applications. More complex models might provide more details on the vehicle response but this comes with the cost of large computational time. Thus, the assumptions to reduce the complexity of vehicle dynamics system and represent the vehicle in form of simplified equations are usually performed.

A vehicle with its coordinate systems is shown in the Figure 1.2 [7]. The global coordinate system *XYZ* is fixed to the ground. The vehicle coordinate system *xyz* is fixed to the moving vehicle with the origin at the center of gravity (*CG*). The vehicle can freely

move in the *xy* plane and perform roll, yaw and pitch motions while maintaining the road path. From various performance evaluations, different models may be investigated. For vehicle directional analysis, an in-plane model could be used.

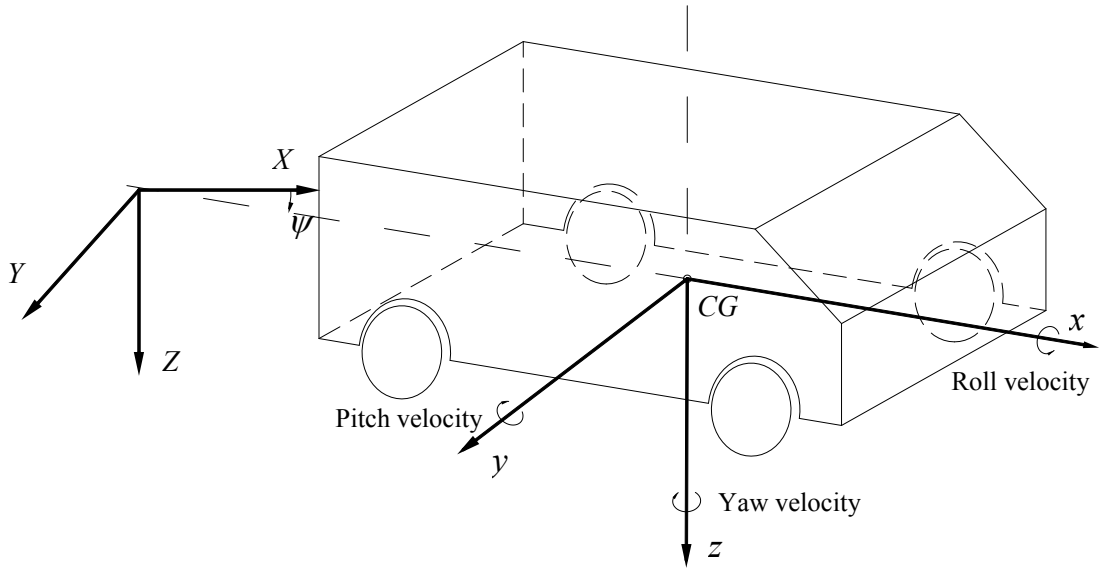

Figure 1.2: Vehicle coordinate systems [7]

The simplest vehicle model is built by assuming that the vehicle is rigid. The vehicle operates under negligible roll and small differences in longitudinal forces. Then the left and right tires are lumped into an equivalent axle. The pair of tires on the axle is represented by a single tire with double cornering stiffness. The vehicle has longitudinal and lateral translation and yaw as shown in the Figure 1.3 [8]. The advantage of the bicycle model is the linearity that is easily combined with the linear control. The traditional methods such as root locus and frequency response analysis may be used to evaluate the performance of the system.

When the vehicle is negotiating a turn at a constant forward speed *(u)*, the centrifugal force acting at the center of gravity will develop appropriate slip angles on tires. The handling characteristics of the vehicle depend on the relationship between the slip angles of the front and rear tires, α_f and α_r respectively. The steady-state handling performance of the vehicle is investigated to determine the yaw velocity, lateral acceleration and curvature responses to a steering input. For the steer angle as a function of time $\delta(t)$, the handling quality of a vehicle depends on its transient behaviors which are the transient values of yaw velocity and lateral acceleration. The bicycle model is able to perform a quick assessment of the vehicle dynamics with fewer parameters. The disadvantage of the bicycle model is on neglecting roll effect. The linear model may not accurately represent the vehicle if the maneuver involves high lateral acceleration.

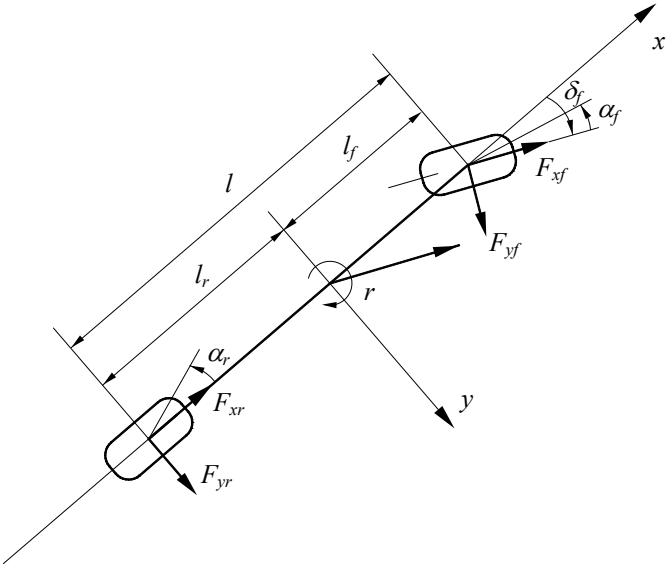

Figure 1.3: The bicycle model [8]

A vehicle is not a unique rigid body but a configuration of coupled masses. It is reasonable to consider for simplification purpose that a vehicle is made of two lumped masses: sprung and un-sprung which are connected by a suspension system. During a cornering maneuver, the sprung mass tends to tilt that significantly affects the directional stability of the vehicle. Besides longitudinal, lateral and yaw motion of bicycle model, roll motion is added as shown in the Figure 1.4 [9]. The magnitude of roll angle depends on roll stiffness and damping coefficient of the suspension system as well as the type of maneuver. The roll effect is perceived as the load transfer from one side to another side of the vehicle. In turn, lateral and longitudinal forces vary due to vertical load transfer.

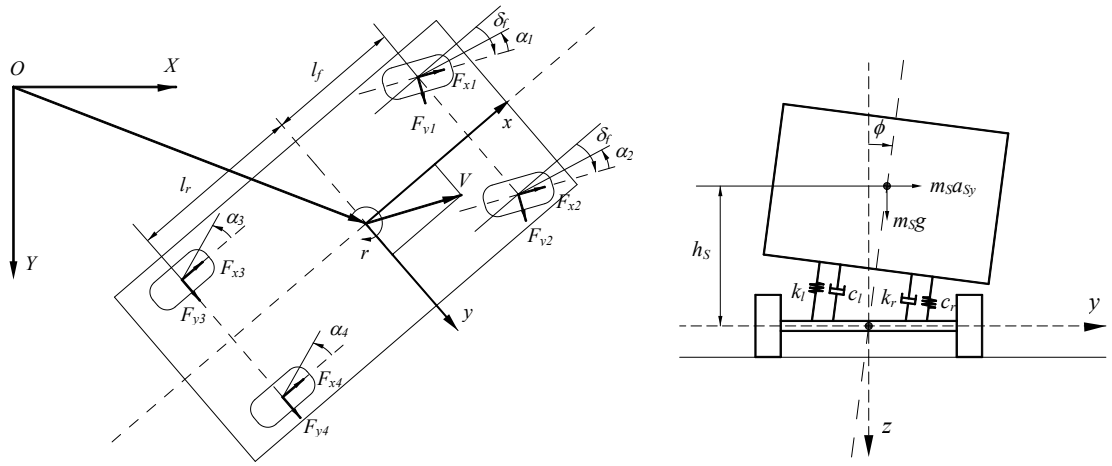

Figure 1.4: The roll-able vehicle model [9]

The comprehensive 14-DOF vehicle model, as shown in Figure 1.5, was introduced to study the vehicle behavior in longitudinal, lateral and vertical directions. The model consists of a sprung mass of the body and four un-sprung masses of the wheels [10]. The sprung mass has six DOF including longitudinal, lateral, vertical, yaw, roll and pitch

motion. Each of the wheels has two DOF which are vertical displacement and wheel spin. Lumped mass model is used to represent the sprung and un-sprung masses. The vehicle body is being modeled as rigid. The model is appropriate to study the ride quality relating vertical oscillation of vehicle body and occupants.

A vehicle is a multi-body system consisting of subsystems like front and rear suspension, steering system, tires and body. Several multi-body simulation programs are capable of creating and analyzing full vehicle models. The most well-known one is being MSC.ADAMS [11]. The program requires full description of the geometric model assembling the model's components to a system; therefore equations are no longer formulated by hand. The program can numerically analyze two or three dimensional mechanical systems including nonlinear geometry, forces and motion. Few template subsystems and full vehicles are available in MSC.ADAMS library. The full vehicle model may be simulated by applying various types of input events. The graphic aid of ADAMS is a very effective interface between the output simulation and the perception and comprehension of a human analyst.

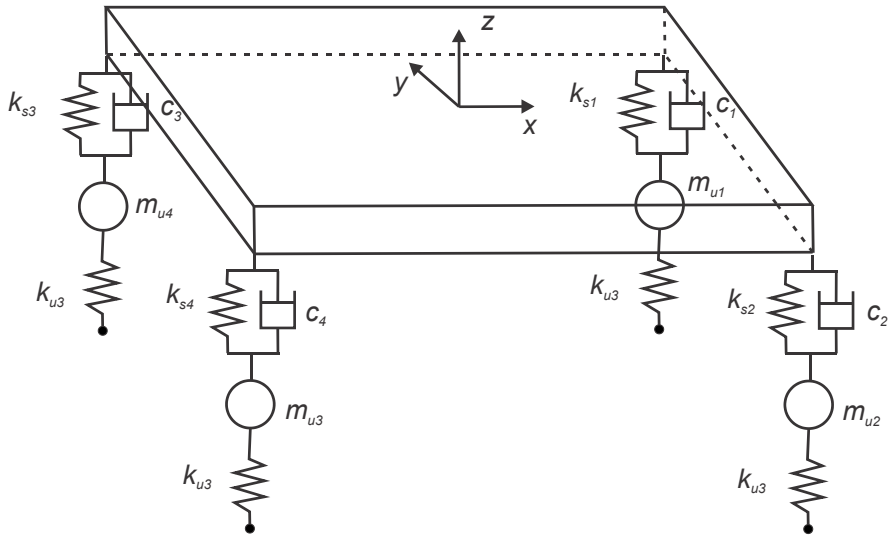

Figure 1.5: The 14-DOF vehicle model [10]

One of the most important components of the vehicle model is the tire model that represents the interface between the vehicle and the road. The dynamic perturbations are introduced at the tire level. The important forces and moments affecting the motion of the vehicle are applied through the tire-ground contact. Therefore, the property of tire-ground contact is essential to characterize the vehicle performance such as ride quality and handling behavior of the vehicle. When a vehicle is negotiating a turn, the treads on tires deform and a side force is generated in the tires. This is the cornering force that will be developed on the contact path and the tire will move along a path drifted by the slip angle α. The relationship between cornering force and slip angle is complex and depends on the normal load, tire properties and road condition. For a small angle and constant normal load, this relationship is considered linear as the following expression:

$$F_{y\alpha} = C_\alpha \alpha \tag{1.1}$$

where C_α represents the cornering stiffness of the tire.

In general, the cornering properties of tires are known to be nonlinearly related to the normal load and slip angle as illustrated in Figure 1.6 [12]. For the region the slip angle larger than 5 degrees, the rate of force change decreases when the slip angle increases. The lateral force is saturated when the slip angle is larger than 10 degrees for all four levels of normal forces. For the normal operating conditions, the slip angle is in the low region. The lateral force is assumed linear relationship with the slip angle. The cornering stiffness is approximated as the slope of the side force curve at zero slip.

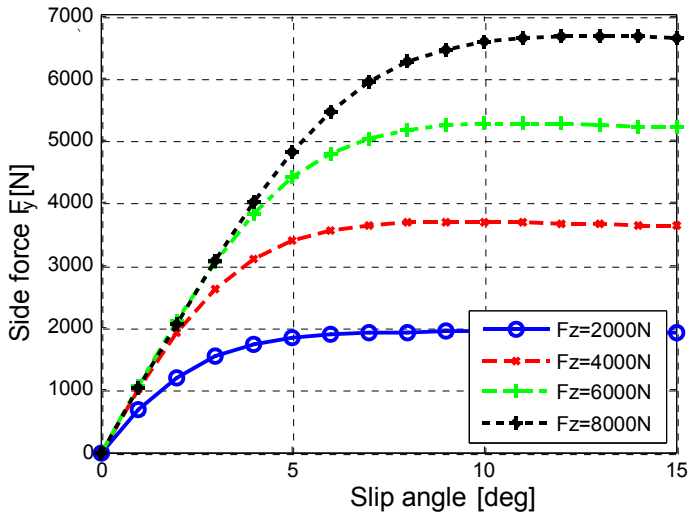

Figure 1.6: Lateral force as the function of slip angle in the nonlinear tire [12]

Table 1.1 summarizes few vehicle models with the order of increasing complexity. The advantages and disadvantages of these models in the aspect of modeling are also indicated. The advantage of the linear model is the simple approximation of the real vehicle. The model works properly with the regular operating conditions such as small

steering angles and low lateral acceleration. The main disadvantage of nonlinear model is the difficulty to couple it with a linear driver models represented as transfer functions. Depending on the problem, the right model may save the cost associated with computation and design of the efficient controllers.

Table 1.1: List of vehicle models

No.	Vehicle model	Descriptions	Advantages	Disadvantages
1	Linear bicycle [8]	- Linear tire and bicycle vehicle model - Output: lateral acceleration and yaw velocity	Simplicity	Does not account for nonlinear characteristic of tires and vehicle roll.
2	Nonlinear 2-DOF [12]	- Nonlinear tire and bicycle model - Output: lateral acceleration and yaw velocity	Tire behavior	- Nonlinear equations - Does not account for vehicle roll and load transfer.
3	8-DOF [9]	- Nonlinear tires with Magic Formula - Output: longitudinal and lateral acceleration, yaw and roll velocity	Introducing roll effect	Nonlinear equations of motion
4	14-DOF (Full vehicle) [10]	- Magic Formula tires and 14 DOF vehicle model -Output: longitudinal, lateral, vertical, yaw, roll and pitch motion	To introduce the vertical and pitch DOF	- Nonlinear equations of motion - Longer computational time
5	Adams/Car [11]	- Multi-body vehicle model - Output: full state of the vehicle and its components	To validate driver-vehicle model.	Difficulty of model modification

Two important states of the vehicle affecting the path following control are the lateral position and head angle of the vehicle. A linear bicycle model provides sufficient feedback for the driver to maintain the vehicle following a path. An 8-DOF model that introduces roll effect is also a suitable model. The increased complexity arising from the nonlinearity of the vehicle model raises difficulties in the modeling and enlarges the computational time. Moreover, most of passenger cars have the rollover thresholds significantly greater than 1.0g, while light trucks, vans and SUVs threshold range from 0.8 to 1.2g and for that of a heavy load truck lies well below 0.5g [13]. The objective of the research leads to the impaired driver-vehicle model where the alcohol affected drivers are mainly considered. Passenger cars involving most of alcohol related road accident represent a reasonable choice as a vehicle model. The model assumes that there is a minor roll effect on driving a passenger car so that it can be neglected at the benefit of a much simplified directional model.

The bicycle model is a linear system that couples easily to the driver model which is also linear. The linear control theory is used to evaluate the driver-vehicle system. For the nonlinear 14-DOF model and the multi-body models, the complexity is significantly increased. As foreseen, the benefits of a more complex dynamic model for the vehicle would bring limited advantages that represent a less of interest issue in the passenger vehicles. These models can be used to validate the driver model with parameters obtained by the linear driver-vehicle model.

1.2.2 Driver models for lateral control of a vehicle

Many driver models of varying complexities have been proposed to study the dynamics of driver-vehicle systems. Most of these models were developed to control the lateral vehicle dynamics. The driver models can be classified into two broad groups based on their tracking objectives: the compensatory tracking models and the preview tracking models.

The structure of a compensatory tracking driver model is illustrated in Figure 1.7, where *H(s)* is the describing function of the driver, which operates on the perceived instantaneous path error of the vehicle and *G(s)* is the vehicle transfer function.

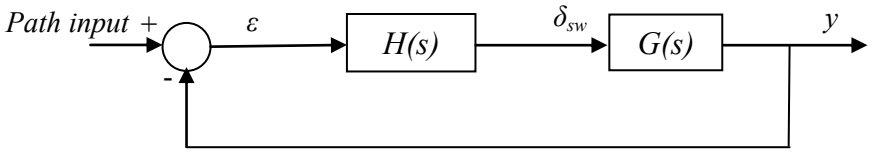

Figure 1.7: Compensatory tracking driver model [14, 15]

In order to achieve the driver transfer function *H(s)*, the driver is modeled as a controller. Firstly, the driver needs time to perform the judgment and take the action. This represents the time delay represented by $e^{-\tau s}$, where τ is the effective time delay. The easy control action is defined as the proportional action that gives the output proportional to the stimulus. The driver is able to predict a change in the input, in other words to perform the derivative control. The driver is also capable of performing integral action where the output signal is proportional to the integrated input signal. The vehicle driver, therefore,

is well defined as a PID controller. However, the system gains of the PID driver function were not related to the driver's physical behavior.

McRuer et al [16-20] proposed the quasi-linear compensatory model adequate for a variety of drivers, inputs, vehicle dynamics, and steering system characteristics. The experiments were carried out to learn the properties of human operator and controlled machine. To cause the system meet desired values, the operator must continuously exert control activities. The operator changes the control strategy with different controlled element dynamics. Although the human's transfer function is different for each controlled element, the product of human's transfer function and controlled element transfer function is essentially the same form. A generic transfer function of the human operator may be applied to most of control tasks. The proposed transfer function is of the form:

$$H(s) = K_d \frac{T_L s + 1}{T_I s + 1} e^{-\tau + T_N s} \tag{1.2}$$

where K_d is the control gain, $\frac{T_L s + 1}{T_I s + 1}$ is a simplified equalization characteristic, τ is time delay, and T_N is the neuromuscular system time constant. The equalizing characteristic and the gain, K_d are adaptive elements of the human driver which enable the model to be implemented on various vehicles. The parameters of the function are evaluated by using an approximate "crossover model". The crossover model of a human operator implies that operators adopt a sufficient lead or lag equalization, such that the slope of the magnitude of the open loop transfer function of the driver-vehicle system is close to 20dB/decade in the region of crossover frequency.

The crossover model is not accurate at frequencies much less or greater than the crossover frequency. Hess and Modjtahedzadeh [21] developed the driver steering

behavior consisting of low and high frequency compensation elements called “structure model”. It gives the more realistic representation of signal processing structure in the driver. The central nervous system consists of a gain and time delay and is a low frequency system. The high frequency representing the neuromuscular system of the driver is a second order system describing the motion of human limbs and the muscular tissue. The structure model is valid for a wider frequency range than the crossover model. Its disadvantage resides in the limitations to tracking task.

The preview tracking model that introduces the future path input performs better than the compensatory tracking model [22]. A typical preview tracking model is illustrated in Figure 1.8. The preview effect of the closed loop system is represented by the function $P(s) = e^{T_P s}$, where T_p is the preview time of the driver which might be in a wide range of values depending on test methods, road conditions, vehicle speeds and the adopted maneuvers.

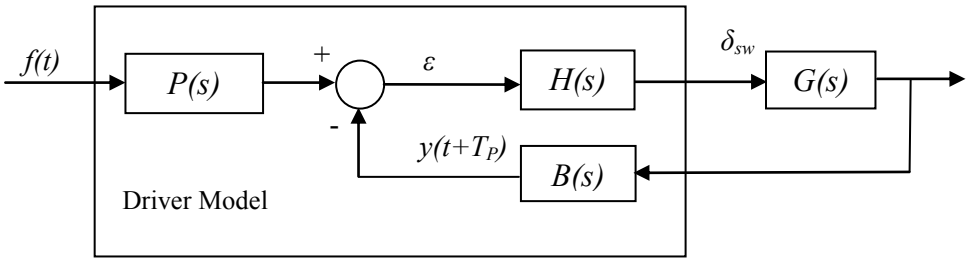

Figure 1.8: The typical preview tracking driver model [23, 24]

The prediction function is *B(s)*. When the vehicle is traveling away from the desired path, the steering strategy of the driver is to diminish the lateral deviation that is the distance between the predicted and the desired position as shown in Figure 1.9. If the

vehicle keeps moving with the unchanged heading angle ψ, the lateral position of the vehicle after a time T_p becomes $y(t+T_P)$ which can be seen as:

$$y(t+T_P)=y(t)+L\psi(t)\cong y(t)+T_P\dot{y}(t) \tag{1.3}$$

Hence, the first order prediction function is $B(s)=1+T_P s$.

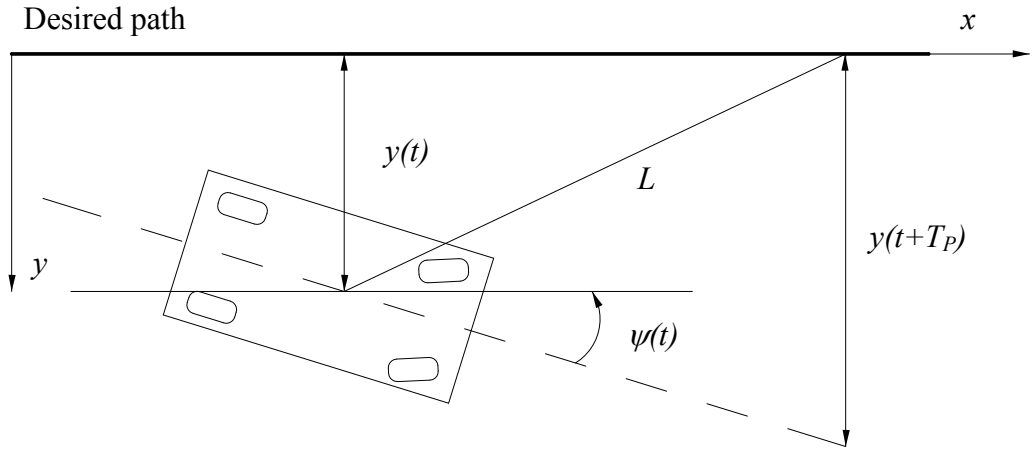

Figure 1.9: The prediction strategy [25]

The optimal preview control model introduces the driver-vehicle tracking problem using a local optimal preview. The driver is always looking at a finite segment of the future path and drives the vehicle to minimize the tracking error. McAdam [26-29] described the vehicle system as a linear state space. In the case of single point preview, the linear vehicle system can described as:

$$\begin{cases}\dot{\boldsymbol{x}}=\boldsymbol{F}\boldsymbol{x}+\boldsymbol{g}\delta_{SW}\\ y=\boldsymbol{m}^{\boldsymbol{T}}\boldsymbol{x}\end{cases} \tag{1.4}$$

where $\boldsymbol{x}$ denotes the state vector of the vehicle system, $\boldsymbol{F}$ the system matrix, $\boldsymbol{g}$ the control matrix, δ_{SW} is the steering input, and y is the lateral position. Then, the optimal steering input becomes:

$$\delta_{SW}^{*}(t) = \delta_{SW}(t) + \frac{\varepsilon(t + T_P)}{A(T_P)} \tag{1.5}$$

where $\varepsilon(t + T_P)$ is the error between the path preview input and the lateral position preview output, $A(T_P)$ the unit step input response of the vehicle system. The result of the experiments shows that the driver steering control strategy during path following can be accurately represented as a time lagged optimal preview control [27].

All the above mentioned models are based on the single loop preview strategy. However, the vehicle performance is influenced by not only the lateral position but also the yaw orientation. Gou and Guan [30] established the position and orientation preview acceleration model based on the optimal preview theory. The model utilizes the information of orientation and predicted trajectory. Simulation studies show that an improvement of tracking performance of the closed loop system is achieved. Yang et al [31] proposed the multi loop structure of driver-vehicle system formulated on the basis of tracking information from the lateral displacement and orientation error. In addition, the roll angle, yaw rate and lateral acceleration are observed. The model requires driver equalization as each loop is characterized by its own gain and time delay. The structure of the multi loop model may be described in Figure 1.10.

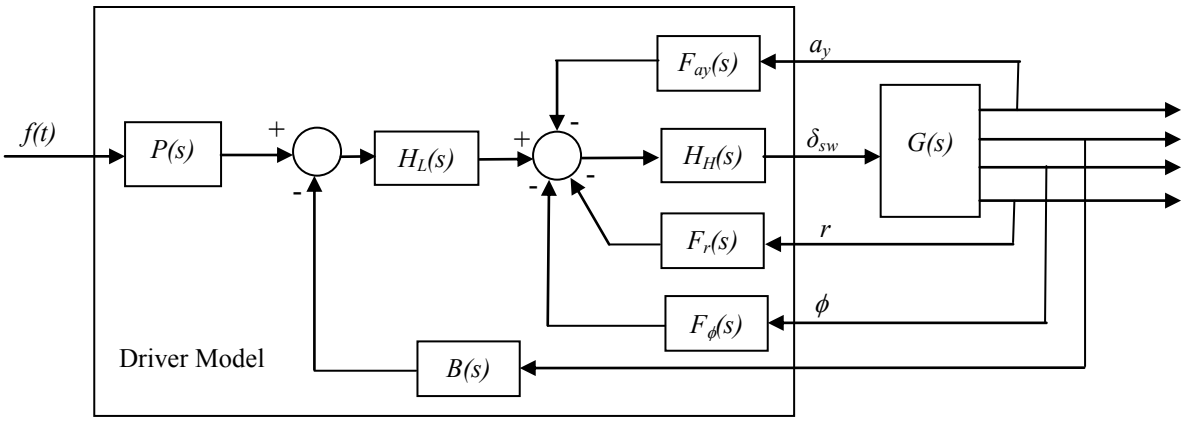

Figure 1.10: The multi loop driver-vehicle model [31]

The functions $H_L(s)$ and $H_H(s)$ represent the low and high frequency of the driver's compensatory characteristics. The functions $F_{ay}(s)$, $F_r(s)$, and $F_\phi(s)$ represent the driver's prediction function for lateral acceleration, yaw rate, and roll angle respectively.

Sharp et al (2001) [32-36] developed the optimal preview control model as a discrete state. The roadway described by its lateral profile $y(k)$ is the discrete function of longitudinal displacement x as shown in Figure 1.11. The driver observes the road path in the finite lateral values ahead of the vehicle equally spaced in x.

The discrete system representation, then, is the road path preview incorporated with the vehicle state space equation. For the linear-quadratic regulator method, the optimal steering wheel angle is given by:

$$\delta_{sw}^{*}(k) = -\boldsymbol{K}_p \begin{bmatrix} \boldsymbol{x}(k) & \boldsymbol{y}_p(k) \end{bmatrix}^T \tag{1.6}$$

where $\boldsymbol{K}_p$ is the full state control gain, $\boldsymbol{x}(k)$ the vehicle state, and $\boldsymbol{y}_p(k)$ the road state. The road model and the controlled vehicle model were assembled in the path following simulation. The vehicle with its steering input derived from the linear-quadratic regulator (LQR) method exhibited a good path following.

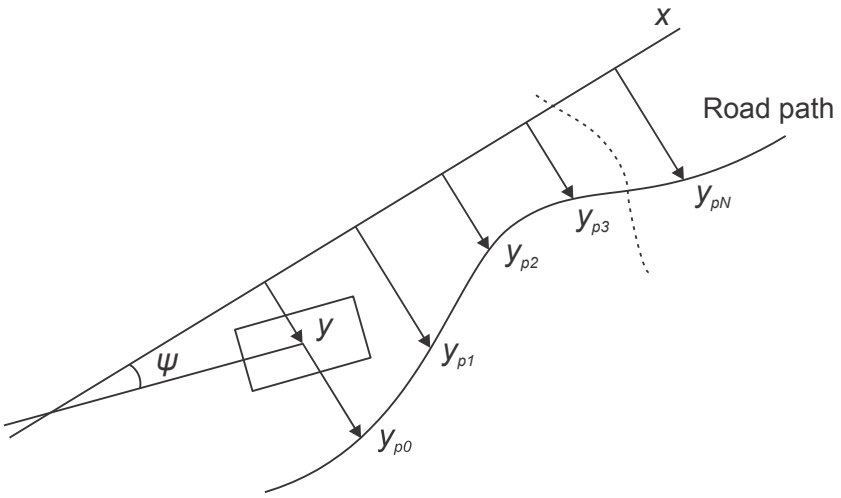

Figure 1.11: Vehicle and previewed road path [35].

The studies of Pick and Cole [36-40] extended the LQR model by adding the neuromuscular module. The path LQR controller acts as the driver's brain and generates a steering wheel angle. Then, through the neuromuscular system, this optimal angle applies to the steering wheel of the vehicle. The neuromuscular system provides control by activating appropriate muscles. A model of driver-vehicle system including neuromuscular dynamics, the LQR control and the vehicle dynamics is illustrated in Figure 1.12.

The driver's arms could be represented by a simple inertia connected to ground via a parallel spring and damper which are passive stiffness and damping of the arms. The arm and steering dynamics are coupled while the driver holding the steering wheel. The equation of motion for the coupling is:

$$\left(J_{dr}+J_{st}\right)\ddot{\delta}_{sw}+\left(B_{dr}+B_{st}\right)\dot{\delta}_{sw}+\left(K_{dr}+K_{st}\right)\delta_{sw}=T_m-\frac{M_T}{n_{sw}} \tag{1.7}$$

where J_{dr}, B_{dr}, and K_{dr} are the inertia, damping and stiffness of the arm. The steering system includes inertia J_{st}, damping B_{st}, and stiffness K_{st}. The applied muscle torque, T_m, is generated by the contractile element. The torque feedback, M_T, arises from the lateral forces and self-aligning moment.

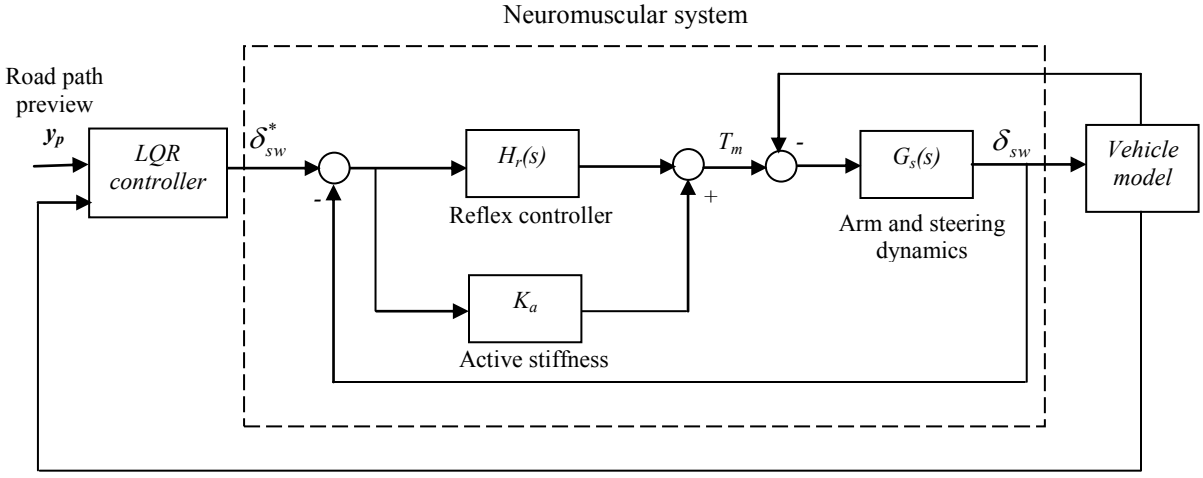

Figure 1.12: Structure of driver-vehicle model with neuromuscular property [40]

The flex control loop maintains the optimal steering angle through muscle control stretch of the arm as an internal feedback. An additional control is possible by varying the parameters of the reflex controller. The transfer function of reflex control can be described as:

$$H_r(s) = \frac{\omega_c (sB_r + K_r) e^{-s\tau}}{s + \omega_c} \tag{1.8}$$

where ω_c is the cut off frequency. Parameters B_r and K_r represent the reflex stiffness and damping. The time delay τ is the transport lag. The active stiffness increases the intrinsic stiffness of the muscle because of the increased muscle activation or co-contraction by applying offset torques to the steering wheel. The simplified active stiffening block

produces a force proportional to the difference between steer angle and required steer angle.

Peng et al [41-45] developed an adaptive lateral preview human driver model based on the adaptive predictive control framework. The optimal control is used to compute the steering angles that minimize the cost function including yaw error and lateral position error. It is assumed that an experienced driver may establish an internal model of lateral vehicle dynamics. The driver model uses the linear internal vehicle model to predict the future states. The outputs of the nonlinear vehicle are approximated and continuously update the internal model. The linear model is updated recursively to present the driver's capability in learning to a new car and adapting to the environment.

McAdam and Johnson [46] used the basic neuron network (NN) concepts to present the driver behavior. A sensor was assumed capable of detecting the lateral displacement of the path relative to the moving vehicle. The on-board sensor mounted in the vehicle provides the continuous information of the lateral offset between the longitudinal axis and road edge markers. The N measured points are presented to the NN which consists of two layers. The N neurons in the first layer process the N inputs. The only neuron in the second layer receives the outputs from the first layer. The output of the second layer is compared with the target road. The training process is performed to identify the NN weights in the first and second layers. The closed-loop system of driver and vehicle is considered as a NN with a specific set of NN weights. For a different vehicle, the values of weights may change. The model operates in the specific conditions as indicated by the authors.

Gou et al [47] proposed a preview optimal driver model based on the artificial neuron network. The simplest one consists of one single neuron with four inputs: preview path, lateral acceleration, lateral velocity and lateral position. The unknown weights must to be trained. The steering angle is the summation of the inputs after weighting. In order to present the neuromuscular property of a driver, the steering angle passes through the lag-delay block before providing to the vehicle model. In general, the structure of the model is similar to the preview model discussed in the previous work [31]. However the feedback gains are undetermined. They are tuned during the iterations with various maneuvers.

Lin et al [48] developed a NN model for a driver-vehicle-environment system. Two stages of the research were carried out. In the first stage, they constructed the mathematical model which includes three modules: environment input, vehicle dynamics and driver controller. The vehicle was required to follow a pre-defined route. The sequence of steering angles producing least lateral errors was computed. Three NN models were employed for the driver-vehicle-environment system. The NN learned to generate the similar steering angles profile with the same input. The NN with updated weights presents the driver model in lateral control. The experiments validated the model in the second stage. A good agreement was found between the simulations and experiments in terms of lateral position and steering angles. The study is restricted in lateral position control assuming constant forward speed.

Table 1.2: A summary of driver models

Authors	Model	Descriptions	Advantages	Disadvantages
Weir and McRuer (1970)	Quasi-linear compensatory	Driver's compensatory: lag, lead and time delay	Simplicity	No preview
Hess and Modjtahedzadeh (1990)	Structure model	Driver's response: the central nervous and neuromuscular system	Realistic representation	No preview
Sherian T. B. (1966)	Preview tracking	Lateral position preview	Preview effect	Only prediction of lateral position
McAdam (1981)	Optimal preview	To provide optimum steering input	Linear state space	No neuromuscular representation
Gou and Guan (1993)]	Optimal acceleration preview	Tracking of lateral position and orientation	Lateral position and acceleration preview	Complexity in evaluating driver parameters
Yang et al (1999)	Multi loops	Observing of lateral position, orientation, lateral acceleration, yaw rate and roll angle	Multi loops prediction	Complexity in evaluating driver parameters
Sharp and Valtetsiotis (2001)	Linear-quadratic regulator	Lateral and head angle feedback	Calculation of control gain	No neuromuscular representation
Pick and Cole (2003)	Linear-quadratic regulator	Built-in LQR and delays	Included neuromuscular	Difficulty in identification of parameters
Peng et al (2005)	Adaptive predictive control	Recursively update the linear internal model	Applying the nonlinear vehicle	No neuromuscular representation
McAdam and Johnson (1996), Gou et al (2004), Lin et al (2005)	Neural network	Trained NN presents driver behavior	Without knowledge of vehicle dynamics	Limit in several maneuvers

The studies of driver models may be summarized in the Table 1.2 where their advantages and disadvantages are also indicated. The chosen model depends on the control problem. The parameters in the compensatory model are easily identified. However it introduces a lag due to the lack of preview information. For the driving case, the preview path significantly improves the tracking problem. For the purpose of modeling of an impaired driver and designing a controller, the optimal preview control is used. This method represents an actual driver who can predict the future information of the vehicle and the environment. The control strategy also improves the performance of the controller when the vehicle follows a path with a suitable velocity. NN is also a potential application. Understanding the NN driver model may improve the design of autonomous vehicle controller.

1.2.3 Effects of alcohol on driving

The relation between alcohol and driving performance was reviewed by Moskowitz et al in 1988 and 2000 [49, 50]. The latter investigation covered 112 articles about the influence of various levels of blood alcohol concentration (BAC) on driving skills. There are the strong evidences to prove that alcohol impairs one or more driving skills even at very low BAC as of 0.01%. All drivers can be expected to experience impairment by BAC of 0.08% or less in terms of reaction time, tracking, concentrated attention, divided attention, information processing, visual function, perception, and psychomotor skill.

Fillmore et al [51] tested the cognitive performance of a group of social drinkers. The subjects were requested to press a key as rapidly as possible whenever they saw a triad of three consecutive even or odd digits on a screen. A correct response increases the

presentation rate of the digits; otherwise a failure slows the presentation rate. The presentation rate measures the rate of information processing. The evidence proved that alcohol impaired cognitive function by slowing the rate of information processing.

The cognitive performance of the alcohol affected-drivers with varying level of alcohol was also examined by Liu and Fu [52]. The effects of alcohol on performance of tasks involving information processing and short-term memory significantly deteriorated with the increase in alcohol level. The greater alcohol ingestion reduced the short-term memory and increased the duration of information processing thus prolonged reaction times for completion of tasks. They concluded that the cognitive faculty is the first to be impaired by drinking. The investigation by Linoila et al [53] revealed that both age and alcohol influenced the speed of the central processing of information by the brain and that the combination of two variables has an additive adverse effect on the rate of information processing.

Visual sensory is vitally important for driving. The effects of alcohol on contrast sensitivity, visual field and eye movement have been intensively studied. Andre et al [54] measured the contrast sensitivity of young males and females before and after ingestion of alcohol. The objects observed stationary gratings and gratings that traveled through a circle path. The alcohol consumption significantly reduces the contrast sensitivity for the moving gratings. This study led to the conclusion that alcohol impairs the ability to make pursuit eye movement. Hill and Toffolon [55] found that the subjects had a significant loss of visual field related to alcohol and the loss was more apparent for higher BAC levels. They explained that alcohol affects the central processing of visual information. The spatial vision pathway that processes the sensory and sensorimotor visual function is

impaired. Therefore, the visual field, accommodation and convergence of the objects are deteriorated.

The effect of alcohol intoxication on visual sustained attention was studied by Rohrbaugh et al [56]. It was established that alcohol consumption impairs the driving task that required continuous performance. The analysis of eye movements and blinks indicated that the impairment of peripheral visual function is negligible. The performance data were interpreted that alcohol disrupts central processes. The effect is found in the overall performance for the continuous task and the rate of increment increases over time.

1.2.4 Autonomous vehicles

Autonomous vehicles represent a type of automated machines that may operate in an arbitrary terrain by automatically finding feasible paths and choosing appropriate velocities. Such type of vehicles were implemented to fly (Unmanned Automated Vehicles) as the numbers of constrains for following a path in air are much less then ones on the ground. Planning the path of the ground autonomous vehicle is very complex problem, especially in the presence of obstacles. Frazzoli et al [57] proposed an algorithm that enables a robot to move from an original position to a desired position while avoiding stationary and moving obstacles. The randomized-planning method was presented to handle a broad variety of dynamic system. The research addressed the path-planning problem to find paths connecting the initial and final positions on the roadmap then to select an optimal sequence of paths.

A method for planning autonomous vehicles moving on general terrains was presented by Shiller and Gwo [58]. The research produced the optimal vehicle speeds and

the geometry path between given end points, considering vehicle dynamics, terrain topography, and surface mobility. The terrain and the optimal path were modeled by a continuous path and a spline curve respectively. A single velocity curve was formulated, representing the upper bound of vehicle speed along a given path.

The Intelligent Vehicle Highway Systems (IVHS) were extensively studied, especially in California PATH (Partners for Advanced Transit and Highways). Many research focused on the control of vehicle-follower in platoons [59-61]. The control law was derived to control the velocity of each vehicle following the lead vehicle. The velocity and acceleration of each vehicle is measured and transmitted to other vehicles. The onboard radar system produces the accurate distance between vehicles. The main objective of the research was to control the longitudinal velocity of the vehicles. The lateral control was based on special elements installed in the roadway instead of a vision system detecting the existing lane. Peng et al [62] developed the lateral control of a full-scaled vehicle. The experiments were conducted with two control algorithms: PID and optimal preview controllers. The lateral control system is based on the on-board sensors and the road reference system. The test results showed that the small lateral tracking errors can be achieved with the changes of load, speed and tire pressure. Pham et al [63] attempted to combine the longitudinal and lateral control for the IVHS. The surface control law was developed to integrate cornering and traction.

The Adaptive Cruise Control system (ACC) presented a partial automated vehicle that is able to automatically accelerate and decelerate its longitudinal speed [64, 65]. The goal is to relieve the driver workload in the highway routine. If a slower preceding vehicle is detected, the control system decelerates the vehicle to keep the safe distance.

The technique of lateral supervision integrated on the ACC was discussed by Holzmann et al [66]. The system checks the signals of important sensors to warn the driver if certain limits of safe and comfortable driving are reached.

The design of the controller for autonomous vehicles based on the driver model was introduced by Guo et al [67]. The controller combines the pure lateral and longitudinal driver models. The preview-follower theory was applied to both models. It was assumed that there are no interactions between the longitudinal and lateral dynamics of the vehicle. Therefore they are treated as independent processes. The model of autonomous vehicle performed good path-following and speed controlling. They recommended that the model may be implemented in an actual autonomous vehicle that faces uncertainties covering the environment in the full scale.

The attempts of designing a human-like controller for autonomous vehicles lead to the implementation of Artificial Neuron Networks (ANNs) [68]. The weights of neurons take initial values that have to be trained. At the training stage, the ANNs learn driving skills through the data recorded from the real driver. A video image provides an input to the network and the output is compared to the steering angle [69]. The back-propagation adjusts the weights to produce an appropriate steering response. An improved road-following system based on ANNs was developed by Rosenblum et al [70]. The optimization was used to train the networks. The experiments on a driving simulator and on an actual vehicle showed that the system may perform well with the changes of road conditions, road quality, light conditions and the presence of noise.

Work using Neural Networks (NNs) aims to process data from visual detectors and to produce a truly autonomous vehicle capable of navigating and speeding within realistic

environment [71]. NNs have shown promise in solving the nonlinear problem, especially coupling longitudinal and lateral vehicle dynamics. The performance of the autonomous vehicle with considering coupling effects is significantly improved when the maneuvers involve high acceleration and low road friction. Kumarawadu et al [72] proposed a NN adaptive control for a nonlinear model of an autonomous vehicle. The NN system quickly adapt to the desired road path without offline training. The robustness is guaranteed with parametric uncertainties and instantaneous road curvature changes. The model properly performs path-following while accelerating and decelerating.

1.3 SCOPE OF THE RESEARCH AND ORGANIZATION OF THE THESIS

The investigation focuses on developing a driver model that may present characteristics of an impaired driver and proposes an algorithm to control an autonomous vehicle. The research aims at neither proposing a novel vehicle model nor developing a control theory. Instead, it involves the careful studies in the current vehicle models and control theories in order to present the behavior of an impaired driver. The research also proposes a feasible control strategy for autonomous vehicle that is believed to improve its performance.

The specific objectives are summarized below:

a. Investigate a linear vehicle model and a non-linear vehicle model as controlled elements for driver models.

b. Develop an optimal preview model and a linear quadratic regulator control to represent a vehicle driver.

c. Propose methods to represent an impaired driver and determine the threshold for safe driving.

d. Propose an algorithm to integrate longitudinal and lateral control of an autonomous vehicle.

e. Develop a NN controller for an autonomous vehicle based on the driver model.

In Chapter 2, a linear vehicle model as the bicycle model with three DOF is investigated. Two important outputs of the model are lateral position and head angle. The driver model is developed from the optimal preview model introduced by MacAdam [27]. The driving performance is considered as the optimal process requires minimization of the cost function consisting of steering input and vehicle states. The root locus method is used to evaluate the closed-loop system of driver and vehicle models. To couple the linear driver model with a nonlinear vehicle model, the control gains are identified by initial tests. The impaired driver is presented by altering the optimal parameters.

In Chapter 3, the discrete LQR driver-vehicle model is derived. The delays in perception and action display the neuromuscular characteristic of the driver. The control law computes the steering angle based on the delayed states and input. The preview path is included into the system to improve the path-following task. The update mechanism is introduced to detect the discrete observed path. The impaired driver is modeled by increasing the reaction time, decreasing preview time and varying the control gains. Comparing the simulation results to the experiments yields a BAC level for the impaired driver model. The lateral performance of the impaired driver-vehicle model is investigated while changing the vehicle parameters.

In Chapter 4, the integration of the longitudinal and the lateral control for autonomous vehicles is performed. The derivation of a linear model for longitudinal vehicle motion is presented. The preview control theory is applied to design the controllers. The velocity profile for a desired path is computed with the reference of the experiments. The lateral position and the velocity profile of the preview path enhance the tracking problem. The linear longitudinal and lateral models of the vehicle are the approximation of the 8-DOF nonlinear model. The Kalman Filter eliminates the noises due to the environment and estimates the vehicle states for the linear model based on the nonlinear model.

In Chapter 5, NNs used to control an autonomous vehicle is discussed. The network weights the preview path before providing an additional steering angle and torque to the vehicle. The block diagram consisting of the longitudinal and lateral control is illustrated. The NN gains are updated by using the gradient descent algorithm. The gains are initiated in the similar manner that the driver model previews the path. A simulation with the Montreal F1 circuit is carried out to evaluate the capability of path-following and speed regulating.

In Chapter 6, the main contributions are highlighted. The future works on the experiments of impaired drivers and autonomous vehicles are discussed.

Chapter 2

AN OPTIMAL PREVIEW CONTROL REPRESENTING THE SYSTEM OF AN IMPAIRED DRIVER AND A NON-LINEAR VEHICLE

2.1 INTRODUCTION

Lateral handling of a vehicle is one of the most important tasks of a driver along with regulating the longitudinal speed. Understanding the mechanism of driver lateral handling improves not only the vehicle design towards minimizing traffic accidents due to direction tracking but also the driving assistance such as steer-by-wire and autonomous car. Control theory may quantify the driver behavior as a closed-loop system where the driver model is required to follow the path by continuously control the steering wheel.

Back in 1962, McRuer et al [16-20] performed experiments on human operators with various controlled elements. They concluded that the open-loop transfer function of the system including a human operator and a controlled element has the same pattern despite of the changing in transfer functions of the human and the controlled element. They proposed the "crossover model" which is also known as the compensation model, to identify the driver's parameters. For the driving task, compensation is not the only driver's duty. The future path provides essential information contributing to the decision upon the steering angle so that the driver manipulates the vehicle smoothly. MacAdam (1981) [26-29] applied the optimal preview control to a driver-vehicle system following a

path. The optimal steering angle is derived by minimizing the performance index which the lateral deviation is accounted for. Also considering the driving task as the optimal control, Cole et al (2006) [73] investigated the linear quadratic control where the future road path is incorporated with the vehicle state. The driver is assumed to observe the road path in finite lateral values at ahead of the vehicle equally spaced in the longitudinal direction.

The goal of modeling vehicle driver is to obtain the steering angle corresponding to an arbitrary path. Furthermore, the model's parameters must reflect a physical meaning of the driver's behavior which represents a considerable challenge given the human complexity. This chapter presents a driver model developed from modifying the model of MacAdam and attempts to relate its parameters to the reality circumstances. The steering cost is augmented to the cost function to compute the control input. The model is further implemented to various road inputs to find out the dependence of the parameters on the road configurations and their relationship.

The chapter also proposes a method to couple a linear driver model with a non-linear vehicle model. Feedback gains represent driver's abilities to predict the vehicle response. The gains are identified by applying initial condition tests that are similar to what a driver learns at an initial stage. A driver model with reduced parameters is introduced as an impaired driver model. It is widely accepted that an impaired driver needs longer time to react to an incident and may not accurately observe the road far from the vehicle. Therefore, longer reaction time and shorter preview time are used to model such conditions.

2.2 LINEAR VEHICLE MODEL

The driver acquainted with the vehicle responses is assumed to be skilful enough to handle driving tasks. He perceives the vehicle dynamics while performing driving. The experience acquired while driving the vehicle helps him to choose the appropriate action. In the control model, vehicle dynamics which is similar to that the driver acquired is described by the equations of motion. The driver, in fact, might not know the equations but he perceives with some approximation of the expected output (e.g. lateral displacement) to a known input (e.g. steering angle). A vehicle model that incorporates the non-linear components may adversely affect an attempt to apply the linear control theory in coupling the driver and the vehicle. This vehicle model may be used as a tool to quantify the driver's parameters indicated by the linear model. Thus a linear vehicle model which provides sufficient states but which reduces the complexity of the problem is used.

The linear bicycle model is considered by assuming that the vehicle is rigid and experiences negligible roll. The vehicle is travelling on a good road of equal coefficient of friction on the left and right sides and facing small differences in longitudinal forces [7-9]. Hence the left and right tires are lumped into an equivalent axle. The pair of tires on the axle is represented by a single tire with double the cornering stiffness. The lateral forces acting on the tires are also assumed to be equal in the left and right sides. The vehicle has longitudinal and lateral translation and yaw as shown in Figure 2.1. The linear vehicle model is derived in this section based on the references [22, 73].

Denote $\boldsymbol{R}$ as the position vector of the CG, then the transition velocity of vehicle is the time derivative of vector $\boldsymbol{R}$ described as:

$$\boldsymbol{v_B} = \dot{\boldsymbol{R}} = u\boldsymbol{i} + v\boldsymbol{j} \tag{2.1}$$

where u and v are the longitudinal and lateral velocity respectively, $\boldsymbol{i}$ and $\boldsymbol{j}$ are unit vectors. The acceleration of the vehicle is derived by differentiating its velocity:

$$\boldsymbol{a_B} = \dot{\boldsymbol{v}}_{\boldsymbol{B}} = \ddot{\boldsymbol{R}} = (\dot{u} - vr)\boldsymbol{i} + (\dot{v} + ur)\boldsymbol{j} \tag{2.2}$$

where r is the yaw velocity. The equations of motion for the rigid vehicle are:

$$\begin{aligned} F_x &= m(\dot{u} - vr) \\ F_y &= m(\dot{v} + ur) \\ M_z &= \dot{r} I_z \end{aligned} \tag{2.3}$$

where F_x is the total longitudinal force acting on the vehicle, F_y the lateral force, M_z the yaw moment, and I_z the inertial about z axis. Assuming the steering angle δ_f is small, the equations of motion may be written as:

$$\begin{aligned} m(\dot{u} - vr) &= F_{xf} + F_{xr} \\ m(\dot{v} + ur) &= F_{yf} + F_{yr} \\ \dot{r} I_z &= l_f F_{yf} - l_r F_{yr} \end{aligned} \tag{2.4}$$

When the vehicle is negotiating a curve, the centrifugal force acting at the center of gravity will develop appropriate slip angles on tires. Refer to Figure 2.1, the slip angle of front and rear tire are:

$$\alpha_f = \delta_f - \frac{v + l_f r}{u} \text{ and } \alpha_r = \frac{l_r r - v}{u} \tag{2.5}$$

where the steering angle δ_f relating to steering wheel angle δ_{sw} as:

$$\delta_f = \frac{1}{n_{sw}} \delta_{sw} \tag{2.6}$$

The relationship between cornering force and slip angle is a complex one depending on normal load, tire properties and road condition. For a small angle and constant normal load, this relationship is considered linear as the following expressions:

$$\begin{aligned} F_{yf} &= 2C_{\alpha f}\alpha_f \\ F_{yr} &= 2C_{\alpha r}\alpha_r \end{aligned} \tag{2.7}$$

where $C_{\alpha f}$ and $C_{\alpha r}$ are the cornering stiffness of the front and rear tire.

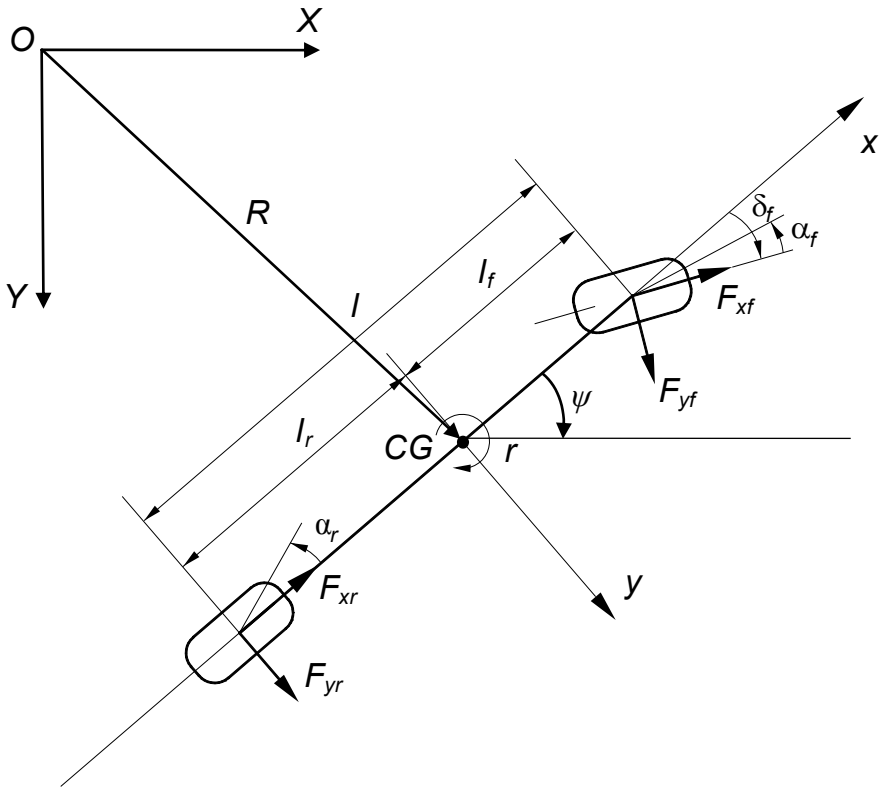

Figure 2.1: The 3 DOF linear vehicle model

If the vehicle is not accelerated or decelerated, the equation of motion in longitudinal direction will be neglected. Hence, the motion of the vehicle is described as:

$$
\begin{aligned}
m\dot{v} + \left(\frac{2C_{\alpha f} + 2C_{\alpha r}}{u}\right)v + \left(mu + \frac{2l_f C_{\alpha f} - 2l_r C_{\alpha r}}{u}\right)r &= \frac{2C_{\alpha f}}{n_{sw}}\delta_{sw}(t) \\
I_z\dot{r} + \left(\frac{2l_f C_{\alpha f} - 2l_r C_{\alpha r}}{u}\right)v + \left(\frac{2l_f^2 C_{\alpha f} + 2l_r^2 C_{\alpha r}}{u}\right)r &= \frac{2l_f C_{\alpha f}}{n_{sw}}\delta_{sw}(t)
\end{aligned}
\tag{2.8}
$$

where m denotes the total mass of the vehicle, I_z the yaw moment of inertia. v is the lateral vehicle velocity, u the longitudinal vehicle velocity, r the yaw rate. l_f and l_r stand for the distances from the center of gravity to the front and rear axle, $C_{\alpha f}$ and $C_{\alpha r}$ the front and rear tire cornering coefficients. δ_{sw} is the steering wheel angle, n_{sw} the steering ratio.

In the path following control, the lateral and yaw deviation of the vehicle from the road path may be incorporated into a cost function. To obtain the optimal steering angle for the driver model, the cost function is minimized. The yaw displacement is the angle between the global and vehicle system and its rate of change is the yaw velocity:

$$
\dot{\psi}(t) = r(t) \tag{2.9}
$$

The vehicle's position in the global system is *X(t)* and *Y(t)* and its velocity is $\dot{X}(t)$ and $\dot{Y}(t)$. The relationship of velocities between global and vehicle system is represented by:

$$
\begin{Bmatrix} \dot{X}(t) \\ \dot{Y}(t) \end{Bmatrix} = \begin{bmatrix} \cos\psi(t) & -\sin\psi(t) \\ \sin\psi(t) & \cos\psi(t) \end{bmatrix} \begin{Bmatrix} \dot{x}(t) \\ \dot{y}(t) \end{Bmatrix} \tag{2.10}
$$

where $\dot{x}(t)$ and $\dot{y}(t)$ are vehicle coordinate system's velocities. Without loss of generality, the global coordinate system is set as the X-axis aligned with the direction of the road path so that the vehicle has a small yaw displacement $\psi(t)$. The reasonable assumption is $\dot{x}(t) >> \dot{y}(t)$ when the vehicle is cornering with a small steering angle. The equation (2.10), then, is rewritten as:

$$\begin{aligned} \dot{X}(t) &= u \\ \dot{Y}(t) &= u\psi(t) + v(t) \end{aligned} \tag{2.11}$$

where u denotes the constant forward speed of the vehicle and $u = \dot{x}(t) = \dot{X}(t)$ if the small angles are assumed, and $v(t) = \dot{y}(t)$ the lateral velocity.

In the path following control, the lateral deviation of the vehicle from the road path represents a clue for the driver. A linear relationship between the lateral position and the vehicle states is obtained by assuming that the longitudinal velocity is much larger than the lateral velocity and the vehicle is cornering with a small steering angle [22, 73]. Then, the vehicle motion is represented as:

$$\begin{Bmatrix} \dot{v}(t) \\ \dot{r}(t) \\ \dot{Y}(t) \\ \dot{\psi}(t) \end{Bmatrix} = \begin{bmatrix} -\left(\frac{2C_{\alpha f} + 2C_{\alpha r}}{mu}\right) & -\left(u + \frac{2l_f C_{\alpha f} - 2l_r C_{\alpha r}}{mu}\right) & 0 & 0 \\ -\left(\frac{2l_f C_{\alpha f} - 2l_r C_{\alpha r}}{I_z u}\right) & -\left(\frac{2l_f^2 C_{\alpha f} + 2l_r^2 C_{\alpha r}}{I_z u}\right) & 0 & 0 \\ 1 & 0 & 0 & u \\ 0 & 1 & 0 & 0 \end{bmatrix} \begin{Bmatrix} v(t) \\ r(t) \\ Y(t) \\ \psi(t) \end{Bmatrix} + \begin{Bmatrix} \frac{2C_{\alpha f}}{m} \\ \frac{2l_f C_{\alpha f}}{I_z} \\ 0 \\ 0 \end{Bmatrix} \frac{\delta_{sw}(t)}{n_{sw}} \tag{2.12}$$

where *Y(t)* denotes the vehicle position in the global system, and *ψ(t)* stands for the head angle of the vehicle. In the compact form, equation (2.12) may be written as:

$$\begin{aligned} \dot{\boldsymbol{x}}(t) &= \boldsymbol{A}\boldsymbol{x}(t) + \boldsymbol{B}\frac{\delta_{sw}(t)}{n_{sw}} \\ y(t) &= \boldsymbol{C}\boldsymbol{x}(t) \end{aligned} \tag{2.13}$$

where *y(t)* is the scalar output related to the state vector ***x(t)*** by the matrix $\boldsymbol{C} = \begin{bmatrix} 0 & 0 & 1 & 0 \end{bmatrix}$. Equation (2.13) represents a linear bicycle model of the vehicle. It provides a lateral displacement output corresponding to a steering input. The vehicle

modeling using equation (2.13) is carried out with the parameter values indicated in reference [34].

Table 2.1: Vehicle parameters [34]

Parameter	Symbol	Value
Vehicle total mass (kg)	m	1200
Vehicle moment of inertia about z axis (kg.m^2)	I_z	1500
Distance from vehicle CG to front axle (m)	l_f	0.92
Distance from vehicle CG to rear axle (m)	l_r	1.38
Wheel base (m)	l	2.3
Cornering stiffness for front tires (N/rad)	$C_{\alpha f}$	60000
Cornering stiffness for rear tires (N/rad)	$C_{\alpha r}$	40000
Steering ratio	n_{sw}	16
Forward velocity (m/s)	u	25.9

2.3 OPTIMAL PREVIEW MODEL OF DRIVER

The lateral controlling of a vehicle involves the driver observing the path and processing the preview information in the context of current motion to yield the appropriate steering input [35]. For the frequent driving circumstances, the driver achieves sufficient future path information before initiating the maneuver. For instance, before taking the double-lane-change, the geometry of the requiring path is anticipated and previewed. The next double-lane-change is far and may not account for generating the current steering angle. The vehicle performs single tasks subsequently such as double-lane-change, maintaining straight line, lane-change and so on.

Figure 2.2 illustrates a single task as the curve defined by its coordinates of the path that the driver must overcome. The strategy of driving is the single-point preview. The

driver captures the road path by several peak points in the view of the moving-vehicle framework [34]. The nearest point within the preview distance is processed for the steering input. In Figure 2.2, *G* represents that point. The driver may not observe every point forming the continuous curve but approximately generates the path based on the points *F* and *G*, where *F* is the beginning of the curve. Therefore, the path consisting of line segments (which is used in the simulations in Figure 2.6 and Figure 2.7) is the input to driver. Another consideration is that the lateral distance of the path seen by the driver is relative to the longitudinal axis *x* of the vehicle instead of the absolute axis *X*. For instance, they are y_F, y_G, and y_H.

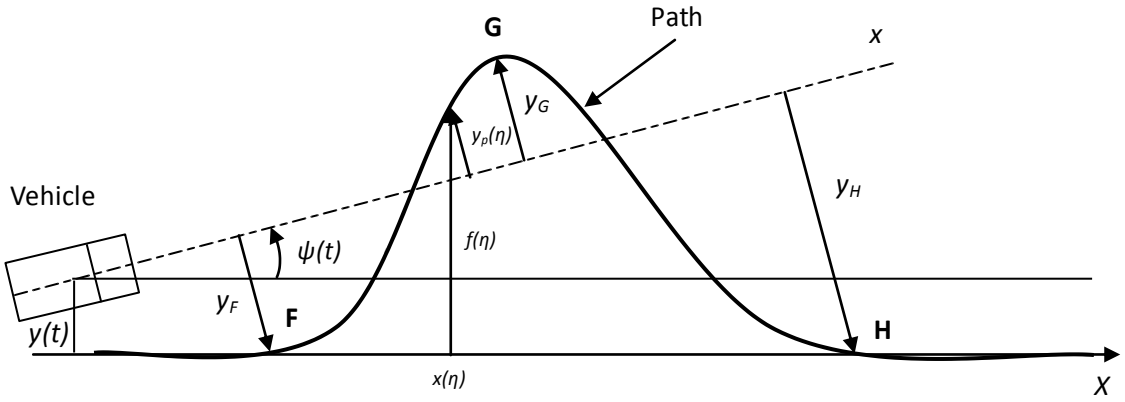

Figure 2.2: The preview path

The current lateral position and head angle of the vehicle are *y(t)* and *ψ(t)* respectively. Let $\eta=t+T_p$ be the anticipated future time where T_p is the preview time derived from the preview distance depending on the driver's capability. The preview time is the ratio of preview distance to vehicle speed assumed constant. By assuming the head angle small, absolute lateral path at the time η ahead the vehicle *f(η)* may be represented as:

$$f(\eta) = f(t) + x(\eta)\psi(t) + y_p(\eta) \tag{2.14}$$

where $y_p(\eta)$ is the relative lateral path at the time η. $x(\eta)$ stands for the longitudinal distance as shown in Figure 2.2. If the head angle at the time t is small and neglected and the vehicle center coincides with the path center, the absolute lateral path will be $f(\eta) = y_p(\eta)$, the relative path observed by the driver. This investigation uses the absolute lateral path $f(\eta)$ as the input to the driver with the assumption discussed above.

The lateral position of the vehicle is required to follow the desired path with minimizing lateral deviation. Then, the driver-vehicle system is represented by the optimal tracking problem where the performance index or the cost function is associated with the mean square of the error and the input [74]. For the driving case, the experienced driver follows the best path defined by the least energy consumed. The cost function is introduced to the driving task as:

$$J = \frac{1}{T}\int_t^{t_f} \left\{ [f(\eta) - y(\eta)]^2 R_1 + \left[\frac{\delta_{sw}(\eta)}{n_{sw}} \right]^2 R_2 \right\} d\eta \tag{2.15}$$

where $f(\eta)$ is the previewed path at the time η, $y(\eta)$ represents the previewed output of the vehicle and R_1, R_2 are the weighting factors of the lateral deviation and the steering input. The values of R_1 and R_2 are chosen so that the lateral error and steering angle equally contribute to the total cost. For various performances, they are selected as $R_1 = \frac{1}{(\Delta y)^2}$ and $R_2 = \left(\frac{n_{sw}}{\Delta \delta_{sw}} \right)^2$, where Δy=0.5m and $\Delta \delta_{sw}$= 0.15rad [75, 76].

The previewed output, $y(\eta)$, is derived from the state equation (2.13) as:

$$y(\eta) = \boldsymbol{C}e^{\boldsymbol{A}(\eta-t)}x(t) + \int_t^{\eta} \boldsymbol{C}e^{\boldsymbol{A}(\eta-\xi)}\boldsymbol{B}\frac{\delta_{sw}(\xi)}{n_{sw}}d\xi \tag{2.16}$$

where the matrix exponential is defined as $e^{\boldsymbol{A}t} = \sum_{n=0}^{\infty}\frac{\boldsymbol{A}^n t^n}{n!}$. The preview output is the prediction of the driver including the estimation of the current initial condition and the response of the system to the steering input after the *(η-t)* time. Assuming that the steering input $\delta_{sw}(t)$ is constant during the preview interval, then, the preview output is rewritten as:

$$y(\eta) = \boldsymbol{C}e^{\boldsymbol{A}(\eta-t)}x(t) + \frac{\delta_{sw}(t)}{n_{sw}}\int_t^{\eta} \boldsymbol{C}e^{\boldsymbol{A}(\eta-\xi)}\boldsymbol{B}d\xi \tag{2.17}$$

Substitution of $y(\eta)$ to the cost function yields:

$$J = \frac{1}{T}\int_t^{t_f}\left\{\left[f(\eta) - \boldsymbol{C}e^{\boldsymbol{A}(\eta-t)}x(t) - \frac{\delta_{sw}(t)}{n_{sw}}\int_t^{\eta}\boldsymbol{C}e^{\boldsymbol{A}(\eta-\xi)}\boldsymbol{B}d\xi\right]^2 R_1 + \left[\frac{\delta_{sw}(t)}{n_{sw}}\right]^2 R_2\right\}d\eta \tag{2.18}$$

In equation (2.18), *f(η)* represents the function of the future path and is previewed. *x(t)* is the state of the vehicle at the current time *t* that the driver is aware of. Therefore, the function *J* is depending only on the steering input $\delta_{sw}(t)$. To investigate the variation of *J*, its first derivative with respect to steering input $\delta_{sw}(t)$ is derived as:

$$\frac{dJ}{d\delta_{sw}(t)} = \frac{2}{T}\int_t^{t_f}\left\{\left[f(\eta) - \mathbf{C}e^{\mathbf{A}(\eta-t)}x(t) - \frac{\delta_{sw}(t)}{n_{sw}}\int_t^{\eta}\mathbf{C}e^{\mathbf{A}(\eta-\xi)}\mathbf{B}d\xi\right]\left[-\frac{1}{n_{sw}}\int_t^{\eta}\mathbf{C}e^{\mathbf{A}(\eta-\xi)}\mathbf{B}d\xi\right]R_1 + \frac{\delta_{sw}(t)}{(n_{sw})^2}R_2\right\}d\eta \tag{2.19}$$

The necessary condition to satisfy the minimum value of the cost function is $\frac{dJ}{d\delta_{sw}(t)} = 0$.

The optimal steering function is:

$$\delta_{sw}^{*}(t)=\left[f(\eta)-\boldsymbol{C}e^{\boldsymbol{A}(\eta-t)}x(t)\right]K_2 \tag{2.20}$$

where $K_2=\dfrac{K_1R_1}{K_1^2R_1+\dfrac{R_2}{(n_{sw})^2}}$ and $K_1=\dfrac{1}{n_{sw}}\int_t^{\eta}\boldsymbol{C}e^{\boldsymbol{A}(\eta-\xi)}\boldsymbol{B}d\xi$.

For the single-point preview control, the preview time η represents the instants at which the driver perceives the lateral deviation of the path. The optimal preview interval, then, is $T^{*}=\eta-t$. Computation of the constants K_1 by applying the exponential expansion yields:

$$K_1=\frac{1}{n_{sw}}\int_t^{t+T^{*}}\boldsymbol{C}\left(\sum_{n=0}^{\infty}\frac{\boldsymbol{A}^n\left[\left(t+T^{*}\right)-\xi\right]^n}{n!}\right)\boldsymbol{B}d\xi=\frac{1}{n_{sw}}\boldsymbol{C}\left(\sum_{n=0}^{\infty}\frac{\boldsymbol{A}^n\left(T^{*}\right)^{n+1}}{(n+1)!}\right)\boldsymbol{B} \tag{2.21}$$

In fact, there is a delay for processing data due to the human operator. The steering input to the vehicle is the non-optimal $\delta_{sw}(t)$ instead of the optimal $\delta_{sw}^{*}(t)$. The pure delay $e^{-\tau s}$ is inserted between the optimal and non-optimal steering input. The block diagram of the driver-vehicle system based on equations (2.17) and (2.21) and the delay property of human operator is illustrated in Figure 2. 3. This is a closed-loop system where the input is the desired path *f(η)* and the output is the prediction of vehicle lateral position *y(η)*.

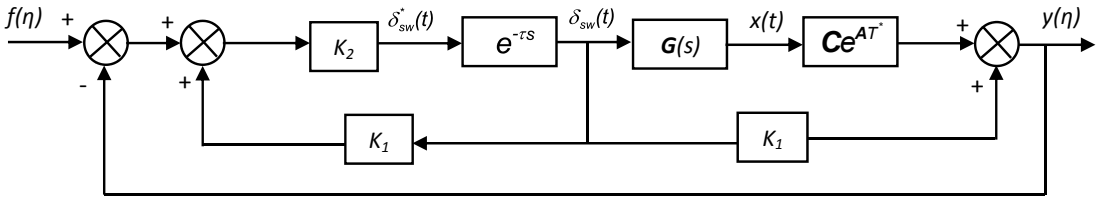

Figure 2.3: The block diagram of the driver-vehicle system

To evaluate the suitability of the driver model in conjunction with that of the vehicle, the system performance is assessed while maintaining a straight line and performing lane-change and double lane-change maneuvers.

2.4 DRIVER-VEHICLE RESPONSE

Maintaining the straight line path represents the most frequent driving task. The driver often adjusts the steering wheel to eliminate the lateral deviation due to road fluctuation and wind disturbance. The system is stable if it recovers its states after a disturbance. The stability of the system is assessed by the root locus of the closed-loop system. The open-loop transfer function of the system is obtained from Figure 2.3 as:

$$H(s) = \frac{K_2 e^{-\tau s}}{1 - K_1 K_2 e^{-\tau s}} \left(K_1 + \boldsymbol{C} e^{\boldsymbol{A} T^*} G(s) \right) \tag{2.22}$$

Two un-determined parameters are the preview time T^* and the delay time τ. Various experiments were performed to identify the values of these parameters [77, 78]. Depending on the method and experiment set-up, the results may considerably differ.

To implement the values to the model, initial tests were conducted. Each value of τ is accompanied by an optimal value of T^* where a minimum value of the cost function is obtained. When the driver model has a larger delay time, the preview time must be larger in order to minimize the cost function. The relation of the preview time, delay time and cost function is illustrated in Figure 2.4.

Five values of delay time varying from 0.3s to 0.7s are implemented to the driver model. The optimal preview time achieved at τ=0.7s is 2.22s that is larger than 1.46s at

τ=0.3s. The value of cost function at τ=0.7s (C=0.86) is also higher than that at τ=0.3s (C=0.67). The smaller delay time introduces the lower value of the cost function resulting in better performance. However, the delay time of the driver model represents the ability of the driver to cope with the information processing, decision and reaction. The driver needs a sufficient delay time to perform a proper response. For the purpose of modeling the driver, the delay time is taken at 0.4s and higher [71]. Assume that the driver is in a good condition for driving, then, T^*=1.6s and τ=0.4s have been chosen as the moderate values.

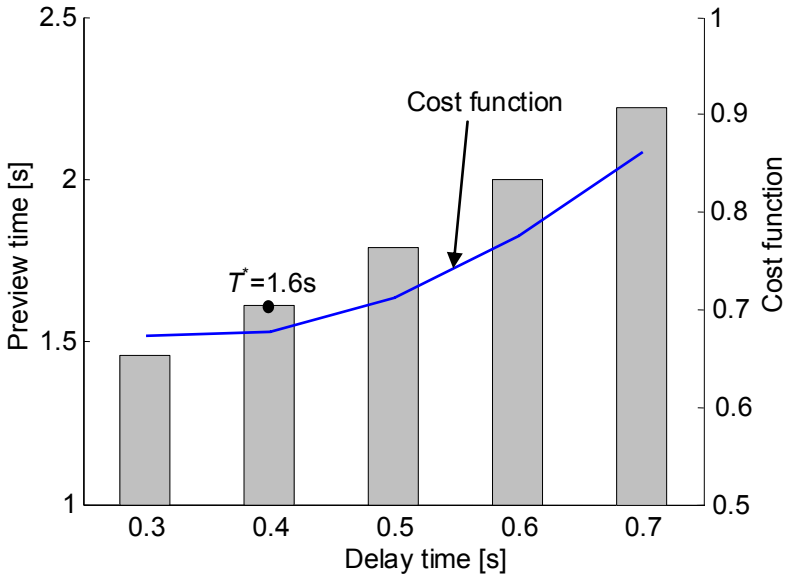

Figure 2.4: The relation of the preview time, delay time and cost function

The root locus of the closed-loop system with varying T_p and τ are shown in Figure 2.5 where the conjugated parts are removed. T_p denotes the preview time of the driver model including the optimal preview time T^*. Figure 2.5(a) illustrates the roots of the system when the preview time changes from 1.2s to 0.45s for the constant delay time

τ=0.4s. The arrow indicates the trend of roots when the preview time is decreased. The dominant complex root passes through the imaginary axis and locates in the right plane when the preview time approaches 0.85s.

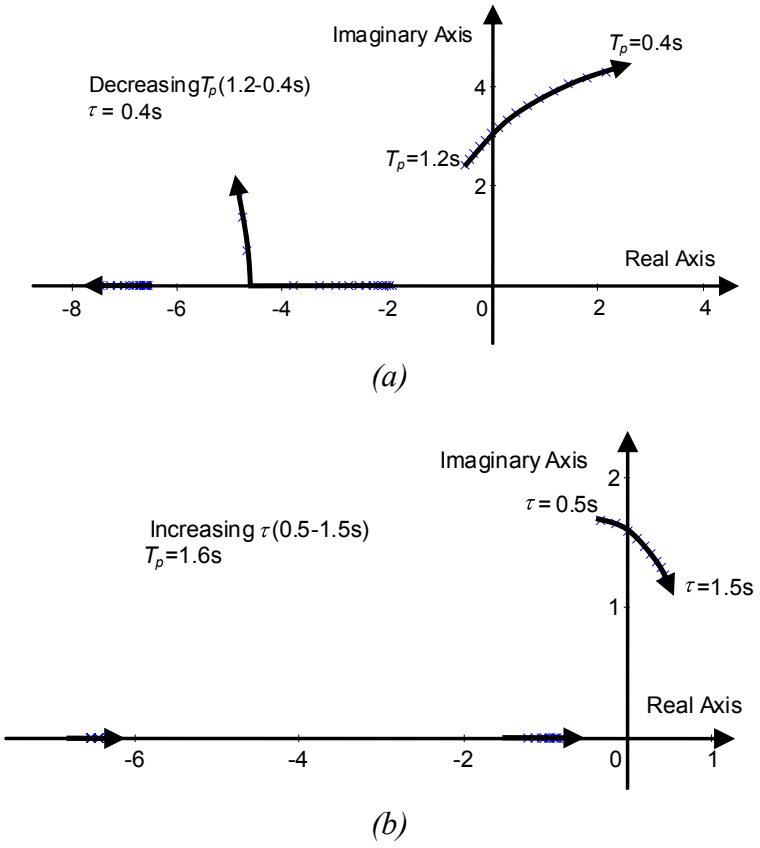

Figure 2.5: The root locus of the closed-loop system with *a)* varying T_p and *b)* varying τ

Figure 2.5(b) presents the roots of the driver-vehicle system with the delay time τ varies in range 0.5-1.5s while T_p=1.6s. When τ is increased, the dominant roots translate to the right plane at τ=0.8s. The system is unstable whenever there is a root in the right plane. These parameters physically relate to the human driver. The driver is capable of driving if he has sufficiently a large preview time and a short reaction time.

Figure 2.6 illustrates the time history of the dynamic response of the driver-vehicle system to a double lane-change maneuver. The model performs a tracking to the path defined by the previewed path depicted as in Figure 2.6(a). The modified model is compared with the model of MacAdam [27]. The peak value of the lateral acceleration, yaw rate and steering angle for the modified model slightly reduce. The peak lateral acceleration of the modified driver-vehicle model is 0.21g which means a reduction by 12%. The peak yaw rate of the modified driver-vehicle model is 0.086 rad/s, which is 11% lower than that of the MacAdam model. The peak steering angle is also reduced 12.5%, 0.12 rad for the modified model comparing to 0.16rad for the model of MacAdam. The performance index is computed for both models from the below formulation:

$$J = \frac{1}{T}\int_{t}^{t_f}\left[\left(\frac{f(t)-y(t)}{\Delta y}\right)^2 + \left(\frac{\delta_{sw}(t)}{\Delta\delta_{sw} n_{sw}}\right)^2\right]dt \tag{2.23}$$

The result is J_m=0.628 for the modified model while that of MacAdam model is J_M=0.663 which are the minimum values of the cost function at the preview time T_p=1.65s and reaction time τ=0.4s. By including the steering angle to the cost function, the vehicle needs less effort while ensuring the good path following. The smaller effort of the modified driver-vehicle model is expressed as the smaller required steering control and thus, the lower lateral acceleration and yaw rate.

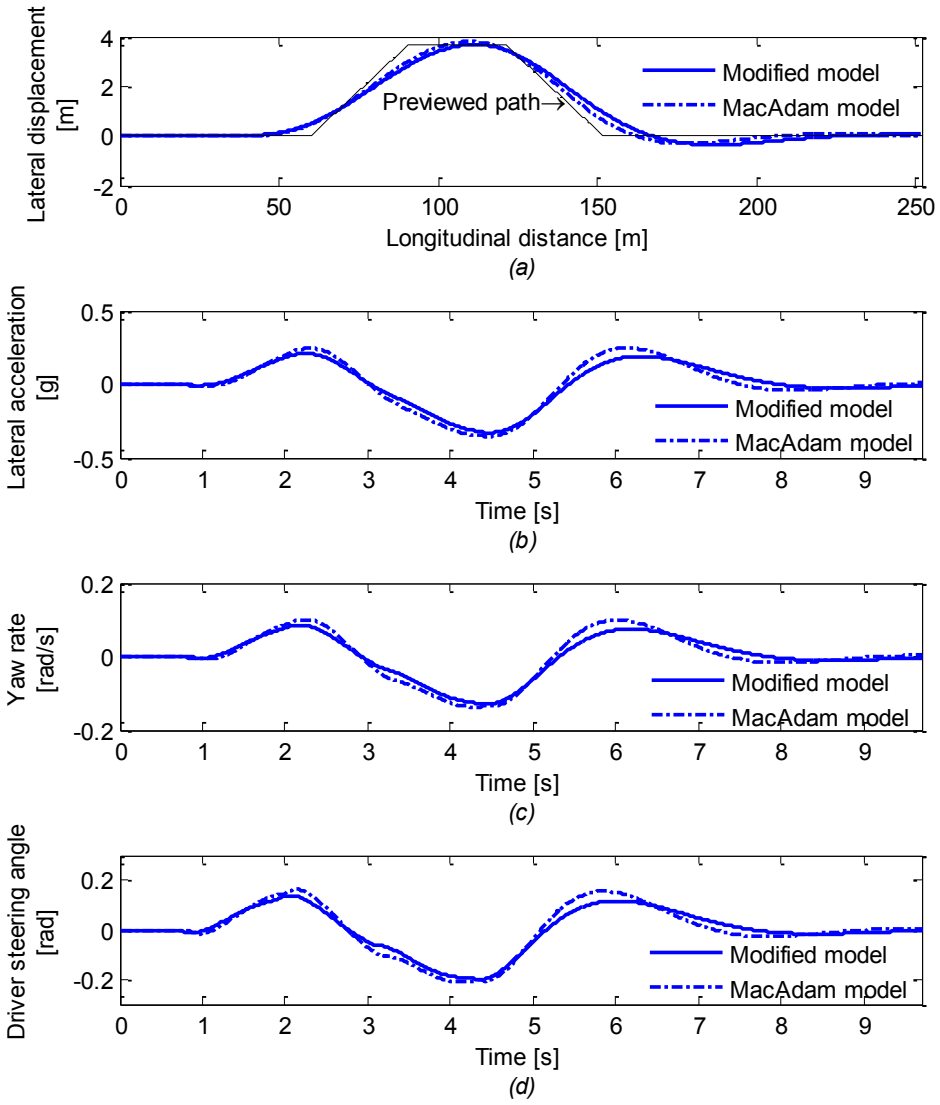

Figure 2.6: The dynamic response of the modified driver-vehicle model comparing to that of MacAdam model

The vehicle model with the parameters in Table 2.1 exhibits neutral steer properties. The following simulations identify the influence of the understeer coefficient (K_{us}) on the performance of the driver model. Depending on the values of the front and rear cornering stiffness and the normal load distribution on front and rear tires, K_{us} may take three possible values. In Figure 2.6, the vehicle exhibits neutral steer (K_{us}=0) when $C_{\alpha f}$=60000

N/rad and $C_{\alpha r}$=40000 N/rad. The comparison of neutral steer (K_{us}=0), understeer (K_{us}>0 when $C_{\alpha f}$=50000 N/rad and $C_{\alpha r}$=40000 N/rad) and oversteer (K_{us}<0 when $C_{\alpha f}$=70000 N/rad and $C_{\alpha r}$=40000 N/rad) vehicle models is illustrated in Figure 2.7.

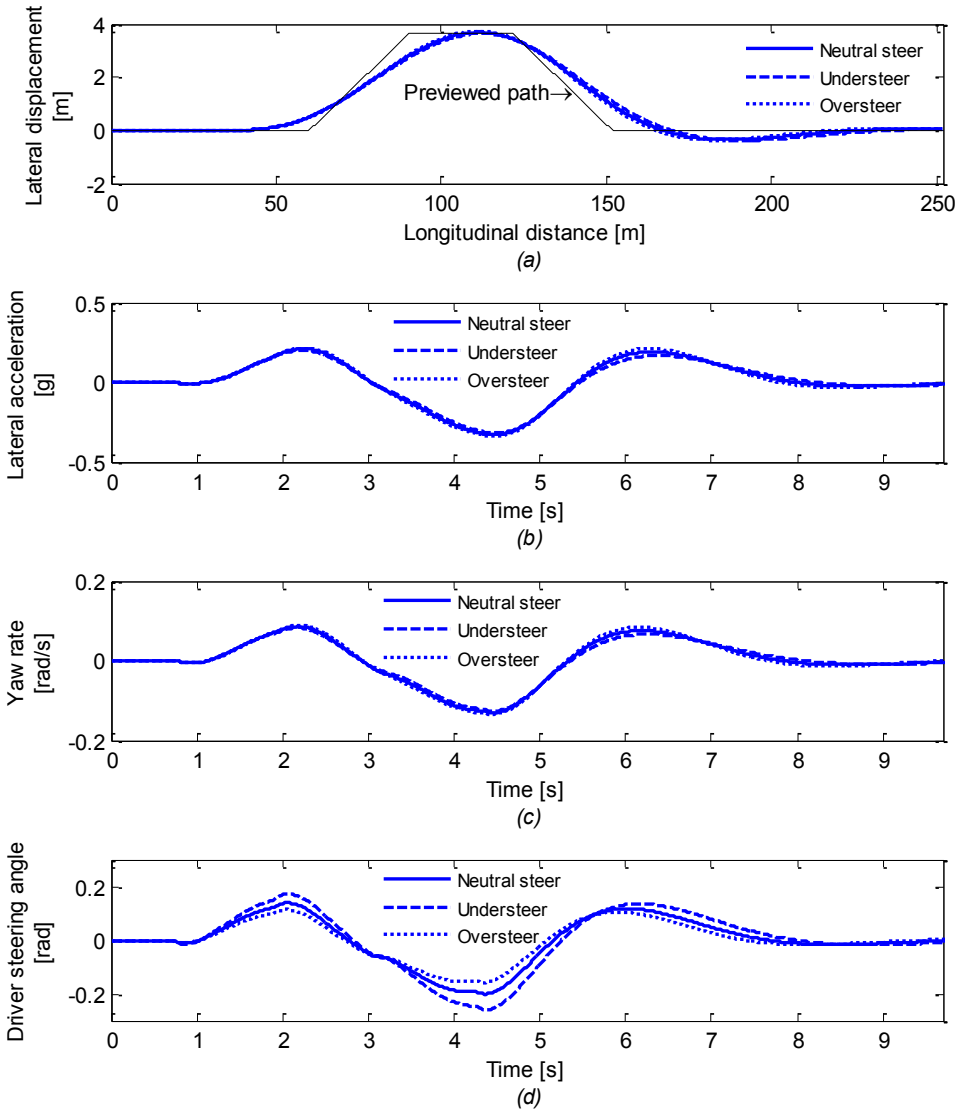

Figure 2.7: The effect of understeer coefficient (K_{us}) on the performance of the driver model

Although the vehicle parameters are changed, the differences in the lateral displacement, lateral acceleration and yaw rate for three vehicle models are negligible. The driver model adapts to the vehicle by generating appropriate steering angles. For the understeer vehicle, the maximum steering angle is 0.17 rad which is higher than that of neutral steer vehicle (δ_{sw}=0.14 rad). For the oversteer vehicle, the maximum steering angle is 0.11 rad, which is reduced by 21% comparing to that of neutral steer vehicle. The driver model may adjust the control input to minimize the effect of changes from the vehicle handling characteristic.

The modified model performs three lane-changes with different curvature as depicted in Figure 2.8(a). The lane-change 1 corresponds to the largest curvature where the lane-change angle is 20^0. The lane-change angle for lane-change 2 and 3 are 5.2^0 and 2.3^0 respectively. The cost associated with each lane-change is shown in Figure 2.8(b) where the reaction time fixed at 0.4s and the preview time varying from 1.1s to 2.1s. With the restricted lane-change (denoted by lane-change 1), the system hardly follows the path resulting the large cost function value of C_1=0.678. Comparing to the easy lane-change (denoted by the lane-change 3), the cost C_3=0.033 proves that the system needs little effort to pass the task while achieving least lateral deviation. Figure 2.8(b) also shows that the system meets the optimal performance at different T_p corresponding to different lane-changes, T_{p1}=1.61s, T_{p2}=1.59s and T_{p3}=1.54s for lane-change 1, 2, 3 respectively. Relating to the driving reality, the larger curvature of road, the larger preview time the driver has. The driver needs to obtain more future path to deal with such challenges.

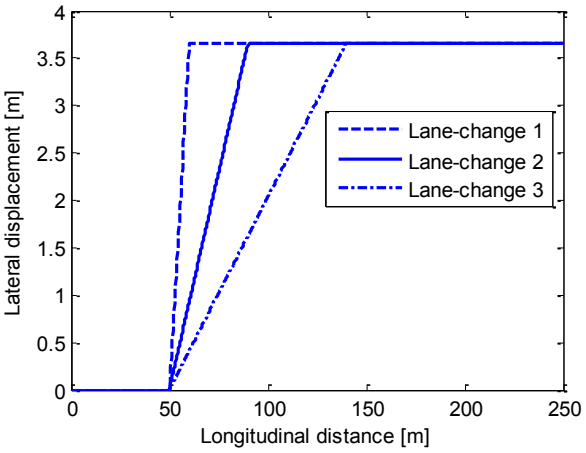

(a)

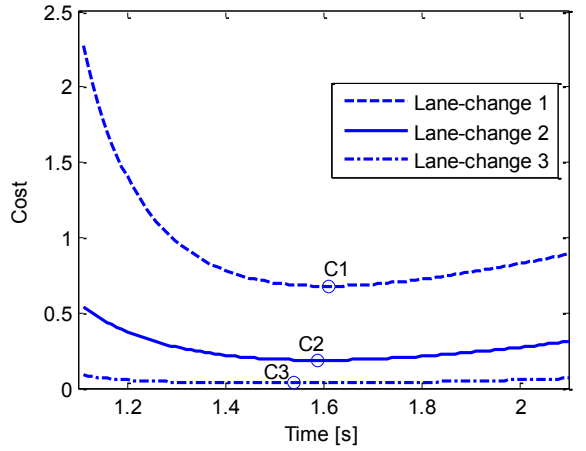

(b)

Figure 2.8: Three levels of lane-change and their cost

The driver-vehicle responses show that the incorporated steering input to the cost function introduces better performance of the driver-vehicle system. The values of parameters found via simulations reflect the behavior of the driver. The good driver is capable of reacting quickly to the unexpected disturbance and observing far ahead of the vehicle. The driver is suitable for driving if he has sufficiently small delay in reaction and large preview time. The driver model also frequently adapts its parameters to the road.

2.5 THE COUPLING OF DRIVER MODEL AND NON-LINEAR VEHICLE AND THE PRESENTATION OF DETERIORATED DRIVING SKILLS

Investigating the driver-vehicle system as in Figure 2.3 reveals that the system comprises the delay function $e^{-\tau s}$, the vehicle transfer function $G(s)$ and the gains. The delay function and gains characterize the driver's performance by the factors that are the effect delay time τ in $e^{-\tau s}$ and the optimal preview time T^* in K_1, K_2 and $\boldsymbol{C}e^{\boldsymbol{A}T^*}$. The gain K_1 and K_2 only depend on T^* and are computed as in equations (2.20) and (2.21). The terms K_1 and $\boldsymbol{C}e^{\boldsymbol{A}T^*}$ are mentioned in equation (2.17) as the preview gains. K_1 represents the preview gain in steering input with zero states. The matrix (1×4) of gains $\boldsymbol{C}e^{\boldsymbol{A}T^*}$ expresses the driver's preview in the current vehicle states with zero steering input. It means that the lateral position of vehicle after a duration T^* is the summation of previewed components: steering input $\delta_{sw}(t)$, lateral velocity $v(t)$, yaw rate $r(t)$, lateral position $y(t)$ and yaw angle $\psi(t)$.

There is the only transfer function $G(s)$ in Figure 2.3 representing vehicle states that lead to the attempt of modeling the system of driver and non-linear vehicle. It is expected that the driver uses the same scheme as the one in Figure 2.3 to manipulate the non-linear vehicle as illustrated in Figure 2.9.

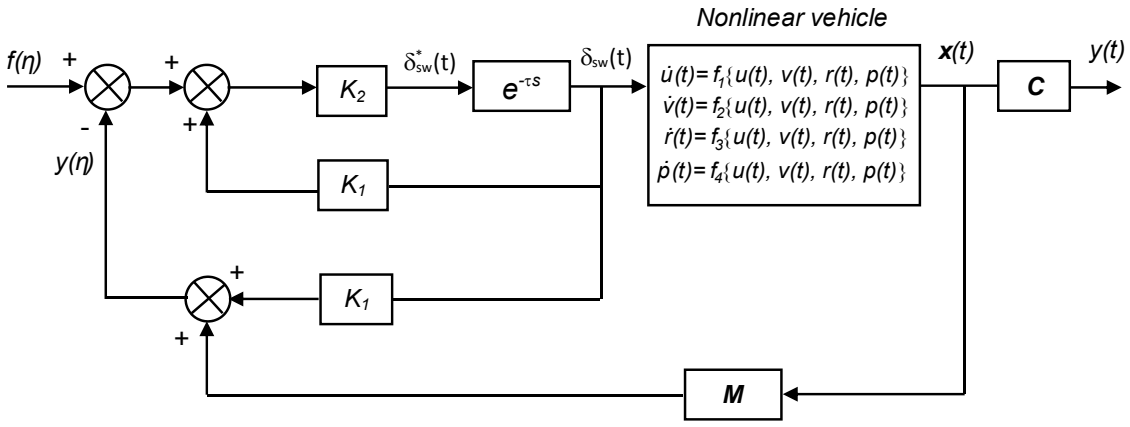

Figure 2.9: The system of driver and non-linear vehicle

Hence, the linear vehicle is replaced by the non-linear model. The equations of motion are derived in section 4.3. This non-linear vehicle model was investigated in references [79-81] including the longitudinal, lateral, yaw, roll motion and the rotation of the four wheels. The chosen outputs are lateral velocity *v(t)*, yaw rate *r(t)*, lateral position *y(t)* and yaw angle $\psi(t)$. The occurring issue is the identification of gains K_1, K_2 and $\boldsymbol{M}$ corresponding to the non-linear vehicle. As discussed above, K_1 and $\boldsymbol{M}$ are preview gains for steering input and vehicle states respectively. K_2 is computed from K_1 by applying equation (2.20). For the non-linear vehicle, K_1 is the ratio of lateral position output to steering input while states are set to zero. M_v of $\boldsymbol{M}$=[M_v M_r M_y M_ψ] is the ratio of lateral position output to current lateral velocity while steering input and other states are zero. M_r, M_y and M_ψ are identified by the similar method. The gains of non-linear and linear vehicle are illustrated in Figure 2.10. These values are calculated at T_p=1.6s and τ=0.4s.

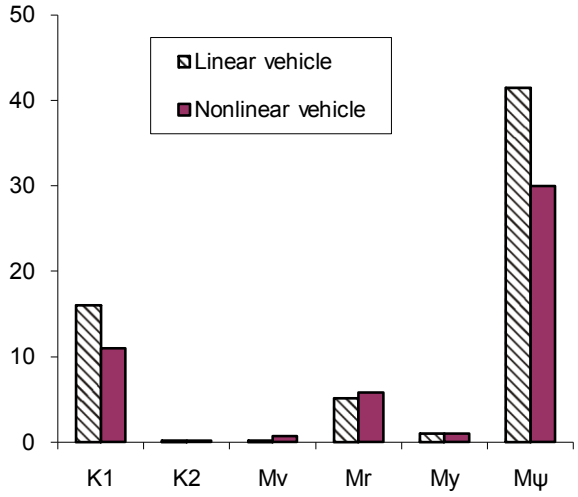

Figure 2.10: Preview gains of linear vehicle and non-linear vehicle

The preview gains of a vehicle are unique and different from those of other vehicles. For instance, the yaw gain M_r of the linear vehicle is 5.12 (m·sec) while that of non-linear vehicle is 5.8 (m·sec). The preview gains for outputs of the non-linear vehicle are also significantly different. For instance, the lateral velocity gain M_v of the non-linear vehicle is 0.7 (sec) while the head angle gain M_ψ is 30 (m). These preview gains are dependent on the characteristics of the vehicle such as the center of gravity, wheel base and tires. The driver is considered to be capable of predicting the future states of the vehicle based on the feedback of lateral velocity, yaw velocity, lateral position and heading angle. The feedback gains are assumed to be equal to the preview gains above calculated.

Parameter sensitivity analyses are performed to identify the effect of driver model parameters and vehicle parameters on the driver-vehicle system. The normalized mean square value of the lateral deviation is defined as:

$$J_y(\boldsymbol{\beta}) = \frac{1}{T}\int_0^T \left(\frac{f(t) - y(t,\boldsymbol{\beta})}{\Delta y} \right)^2 dt \tag{2.24}$$

where T is the length of simulation time and $\boldsymbol{\beta}$ denotes the parameter vector with a nominal value $\bar{\boldsymbol{\beta}}$. A variation in β_k of $\boldsymbol{\beta}$ results in a variation in J_y. However with various β_k, the variations in J_y are different. The sensitivity coefficient is defined as:

$$S_{Jy,k} = \left.\frac{\partial J_y(\boldsymbol{\beta})}{\partial \beta_k}\right|_{\boldsymbol{\beta}=\bar{\boldsymbol{\beta}}} \tag{2.25}$$

Figure 2.11 illustrates the sensitivity of the lateral performance to the variations in lateral position gain M_y, head angle gain M_ψ, roll stiffness k_p, and height of C.G, denoted by h. For the driver model's parameters, the results show that variations in both M_y and M_ψ primarily affect the lateral performance. Since the signs of the value $S_{Jy,My}$ indicate an increase (+) or decrease (-) in lateral response, Figure 2.11(a) shows that variations in M_y yield an increase and decrease in lateral performance for M_y>1 and M_y<1 respectively. It means that when M_y<1, an increase in M_y yields a decrease in J_y. When M_y>1, an increase in M_y yields an increase in J_y. M_y=1 is considered the optimal lateral position gain. The lateral performance will become worse if the gain is smaller or greater than 1. The effect of M_ψ on J_y is similar as in Figure 2.11(b). M_ψ=31 is considered the optimal head angle gain. A comparison of response sensitivity to variations in M_y and M_ψ reveals that the lateral response of vehicle is relatively more sensitive to variations in M_y.

For the vehicle's parameters, the results show that variations in h and k_p also affect the lateral performance as in Figure 2.11(c) and 2.11(d). An increase in h results in an increase in J_y while an increase in k_p yields a decrease in J_y. It means that a larger C.G. height introduces a worse lateral performance while a larger roll-stiffness introduces a better lateral performance. The further investigation as illustrated in Figure 2.11 reveals a method to reduce the lateral position error. If the driver model parameters are not at the

optimal values ($M_y \neq 1$ and $M_\psi \neq 31$) the lateral performance may be improved by decreasing the C.G. height and increasing the roll-stiffness.

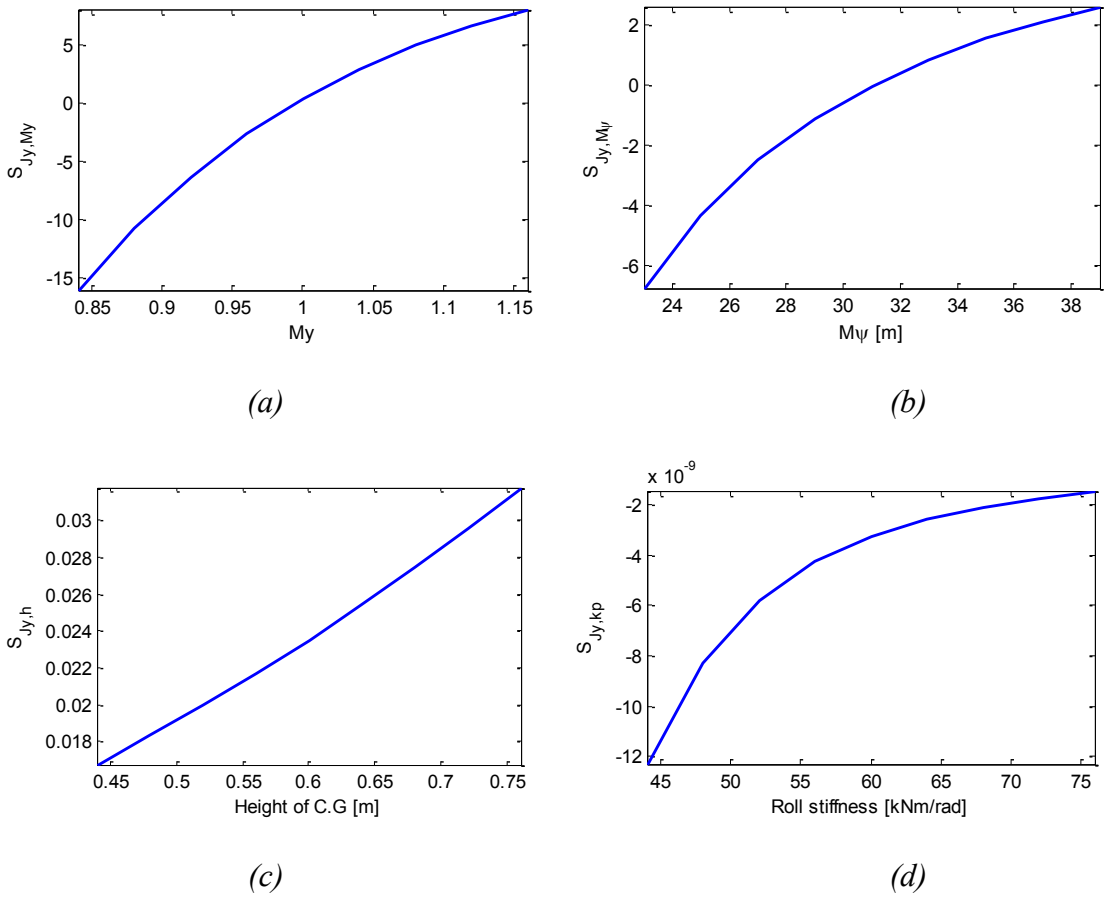

Figure 2.11: Sensitivity of lateral performance to variations in M_y, M_ψ, h and k_p

The coupling of driver and non-linear vehicle model, then, performs a lane-change test as in Figure 2.12. The parameters of the driver model for a specific vehicle model are identified by applying the initial tests. They are the gains used to predict the future state of the vehicle in order to minimize the lateral error. The lateral displacement is computed while applying three values of the preview time. The shorter preview time introduces the larger over-shoot.

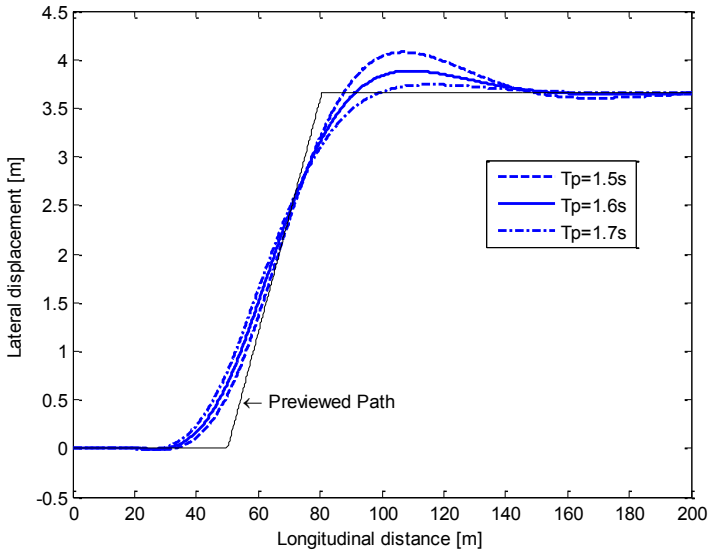

Figure 2.12: Lateral position of the non-linear vehicle with three values of preview time

The advantage of non-linear vehicle model is to achieve more details on vehicle response such as the roll angle, roll rate, load transfer, and force distributed on the wheels. The roll angle of the non-linear vehicle as shown in Figure 2.13 is not available for the linear vehicle. The roll angle was measured when the driver and non-linear vehicle performed a lane-change as in Figure 2.12. Three values of the preview time are implemented, T_p=1.5s, 1.6s and 1.7s while the constant delay time is τ=0.4s. The vehicle roll depends not only on the path required but also on the driver's performance identified by the parameters. For this case, the driver-vehicle system with the preview time T_p=1.7s introduces lower roll comparing to the system with T_p=1.5s. The driver model with larger preview time increased the stability of the vehicle against a roll-over situation. Therefore, the non-linear vehicle coupling to the driver model provides the specific information aiding the vehicle design.

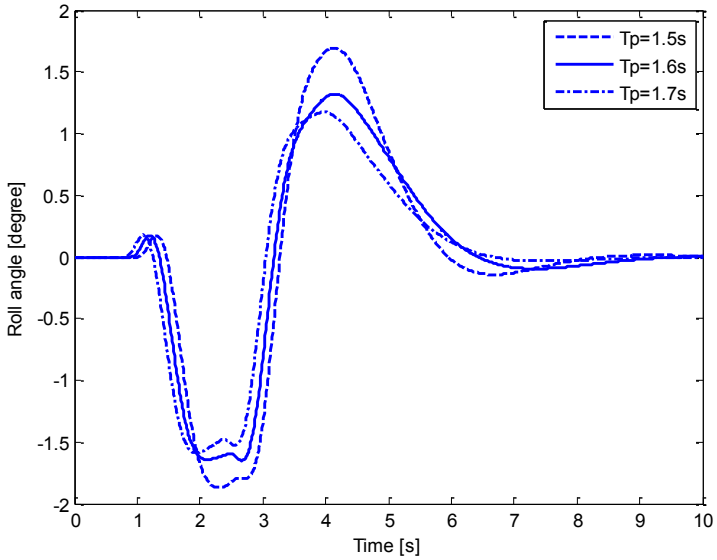

Figure 2.13: Roll angle of the non-linear vehicle with three values of preview time

The further discussion is on an arbitrary-selected non-linear vehicle model which is described by the system of equations of motion. The method presented above provides a driver model to vehicle models. The unknown gains are easy to be evaluated by applying few initial tests. The tests determine the future lateral position of the vehicle with separate initial conditions. The steering angle gain K_1 is obtained by applying as a step steering angle while states are zero. The lateral velocity gain M_v is obtained by applying an initial lateral velocity while steering angle and other states are zero. The other gains M_r, M_y, and M_ψ may be identified by the same scheme. The resulting coefficients are considered as the driver's preview gains with the assumption that the driver may perceive the future states of the vehicle.

The preview gain which is the ratio of the lateral position to the initial state depends on the preview time. Therefore, the preview time defines the performance of the model of

the driver and non-linear vehicle. Corresponding to a delay time, there is a preview time where the performance index is obtained at a minimum value. The optimal preview time is identified by implementing varying preview times to the model. The optimal preview time is achieved at the point that the performance index increases when the preview time either increases or decreases. For instance, the above non-linear vehicle achieves the best performance at the preview time T_p=1.55s while the delay time τ=0.4s. The optimal path following is illustrated in Figure 2.14 as the bold curve. The lateral position of the vehicle is represented by the position of its C.G.

The parameters of the driver model are obtained under the assumption that the driver was trained and he is in good condition for driving. The driver's performance, however, depends on other factors such as the environment, mood, condition of vehicle and the influence of alcohol and drugs. The driver-vehicle system may be at the severe condition if the driving skill deteriorates. Three levels of deterioration of 25%, 50%, and 70% are represented in Figure 2.14. The deterioration of 50% means the preview time is shorter by 50% and the delay time longer by 50% than the optimal ones. Then, the deteriorated preview time and delay time are T_p=0.78s and τ=0.6s. The preview gains also change due to change of the preview time. If the lane exceeding Δy=0.5m is used as the critical lateral deviation, the maneuvers of the 50% and 70% deterioration may not satisfy this requirement. For this case, the maximum allowed reduction of driving skills is of 46% corresponding to T_p=0.84s and τ=0.58s. It is considered the vehicle remains within the lane as long as the deviation of the C.G. from the axis of the path would not exceed 0.5m. A deviation larger than 0.5m is associated with an interference of the vehicle with the adjacent lane and thus, a significant higher risk of a collision.

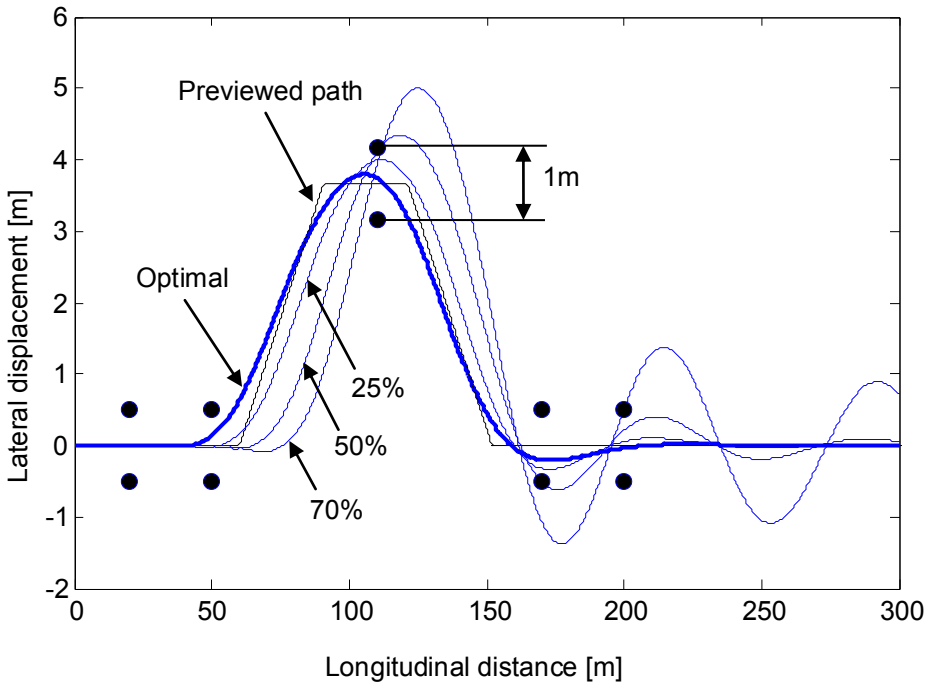

Figure 2.14: The performance of the non-linear vehicle model with levels of deterioration

The driver model with deteriorated parameters exhibits the higher lateral deviation and lateral oscillation. After performing a curved path, the vehicle is unable to return the straight path without an oscillation. As seen in Figure 2.14, the optimal driver model takes about 50m to return to a straight path while the 25% deterioration model takes about 100m. The longer distance is required for the model with 50% and 70% deterioration. This characteristic relates to the performance of an alcohol-affected driver where the weaving car is characterized for this type of impairment. The driver may not maintain the lane due to the road excitation or wind disturbance. By changing the parameters, the driver model may represent an impaired driver.

2.6 CONCLUSION

The proposed model provides another useful tool for quantifying the human performance in driving a specific vehicle. The model consists of the coupling of the linear vehicle model and the optimal preview driver model through the predicted lateral error and steering angle that introduces the good performance with various path inputs. The parameters express a good physical correlation to the driver's behavior. The driver model is out of control of the vehicle if the preview time smaller than 0.85s and the reaction time larger than 0.8s. The driver model also adapts its parameters to the changing path curvature.

The modified driver model has a potential application to a non-linear vehicle where the preview gains are determined by initial tests. The feedback gains of lateral velocity, yaw velocity, lateral position and head angle vary significantly. The driver-nonlinear vehicle system performs successfully a lane-change maneuver as the linear system does. The non-linear vehicle provides various outputs that depend on the driver's parameters. For an arbitrary non-linear vehicle, the proposed model may be applied as a virtual driver for vehicle design.

The parameters of the driver model may change to represent the driver with deteriorated skills. The performance of the driver model exhibits a larger lateral deviation. The level of impairment when the driver model is considered still suitable for driving the vehicle model is obtained by applying the safe driving criteria. The impaired driver model may contribute to road safety research. The further application of the impaired driver model is on the adapting the vehicle to a driver. The response of the

vehicle with the impaired driver becomes better if changing the vehicle parameters. A tire pressure control system is capable of adjusting the air pressure in the pneumatic tire in order to change the cornering stiffness of the tire. An active suspension control may regulate the hydraulic pressure in dampers that may change not only the damping ratio but also the suspension stiffness and the height of center of gravity. The parameters are adjusted to reduce the impact of the amplification of the driver impairment by the vehicle and improve the driver-vehicle safety.

Chapter 3

AN IMPAIRED DRIVER MODEL AND THE CONTROL OF VEHICLE PARAMETERS

3.1 INTRODUCTION

An impaired driver is a person who is unable to optimally drive a motor vehicle due to the effect induced by the consumption of alcohol or drugs, excessive fatigue or old age related inabilities. This chapter focuses on the alcohol-affected driver as drunk driving represents one of the most significant causes of automobile accidents [1]. It is widely accepted that alcohol has negative effects on driving performance. In 1988, a review of Moskowitz and Robinson [49] covered studies on the effects of low level of alcohol consumption on driving behaviour including reaction time, tracking, concentrated attention, divided attention, information processing, visual function, perception, and psychomotor skill. They used more than 500 studies from sampling of the open literature. 158 studies reported impairment of one or more driving skills at the blood alcohol concentration (BAC) ranging from 0.01% to 0.1%. The specific actions due to impairment should be considered in conjunction with the vehicle design in order to improve the vehicle safety. This chapter investigates the deterioration of driving performance of the impaired driver based on the linear control theory.

The control theory contributed to quantify the driver behaviour into simple transfer functions. The variety of driver models was reviewed by Plochl and Edelmann (2007) [25]. Focusing on the vehicle applications, the driver model is considered as a

controller where the controlled element is the vehicle model. The simple transfer functions may represent the driving strategy for diminishing the lateral deviation and previewing the desired path. The cross-over model [16-20] was used to identify the driver's parameters such as the reaction time representing the neuromuscular properties and gains, time lead and lag associating with the controlled vehicle. Another approach to the closed-loop driver-vehicle system was the application of the optimal preview control [26-29]. The steering angle is obtained by the steering control strategy that can be viewed as a time-lagged optimal control process. The multi-point preview was introduced to incorporate the future path information as the system states [32, 35]. Two components of gains, the vehicle prediction and path preview, are determined by the linear quadratic regulator method.

These models are successful in simulation the driver based on the assumption that he/she was trained and he/she is in good condition for driving. The driver performance, however, depends on other factors such as the environment, mood, the influence of alcohol and drugs. This chapter utilizes the linear control method to present the variation of driving skill under the influence of alcohol. The linear vehicle model is coupled to the linear quadratic regulator (LQR) driver model.

3.2 LINEAR QUADRATIC REGULATOR (LQR) CONTROL MODEL OF DRIVER AND VEHICLE

In this section, the driver-vehicle model is derived from the LQR control theory where the linear vehicle model is the controlled element. The 3-DOF vehicle model providing

necessary feedback for the path following was discussed in Chapter 2. In the matrix notation, equation (2.13) may be written as:

$$\dot{\boldsymbol{x}}(t) = \boldsymbol{A}_c \boldsymbol{x}(t) + \boldsymbol{B}_c \delta_{sw}(t) \tag{3.1}$$

This is a continuous equation representing the vehicle dynamics. Solving the equation yields the vehicle states such as lateral velocity, yaw rate, lateral position and head angle depending on time.

The input to the vehicle system as in equation (3.1) is the steering angle that represents the output of the coupled driver model. The input to the driver is the path information which is arbitrary. It is preferred to present the lateral position of the path by discrete data as such formulation is more realistic than a pre-determined function. In the next section, the lateral path is included to the vehicle system to improve its path following. It is necessary thus to discretize the continuous vehicle system in form of lateral path. The discrete version using a sampling period of *T* is:

$$\boldsymbol{x}(k+1) = \boldsymbol{A}_d \boldsymbol{x}(k) + \boldsymbol{B}_d \delta_{sw}(k) \tag{3.2}$$

where $\boldsymbol{A}_d = e^{\boldsymbol{A}T}$, and $\boldsymbol{B}_d = \int_0^T e^{\boldsymbol{A}\tau} \boldsymbol{B} d\tau$. The discretization process assumes that the steering angle input $\delta_{sw}(t)$ to the continuous vehicle is adjusted only at times *kT*, and that it is held constant (zero-order hold) between switchings.

The lateral controlling of a vehicle involves the driver observing the path and processing the preview information and the current vehicle states to yield the appropriate steering input [30]. The driver captures the road path by several peak points in the view of the moving-vehicle framework. The path is represented as in Figure 3.1(a). Two points

defining the curved path are *F* and *G*. The driver may not precisely know every lateral distance of the path but may interpret it as line segments based on the selected points. Figure 3.1(b) illustrates the lateral position of the peak points *F* and *G* and the intermediate points providing the path input to the driver.

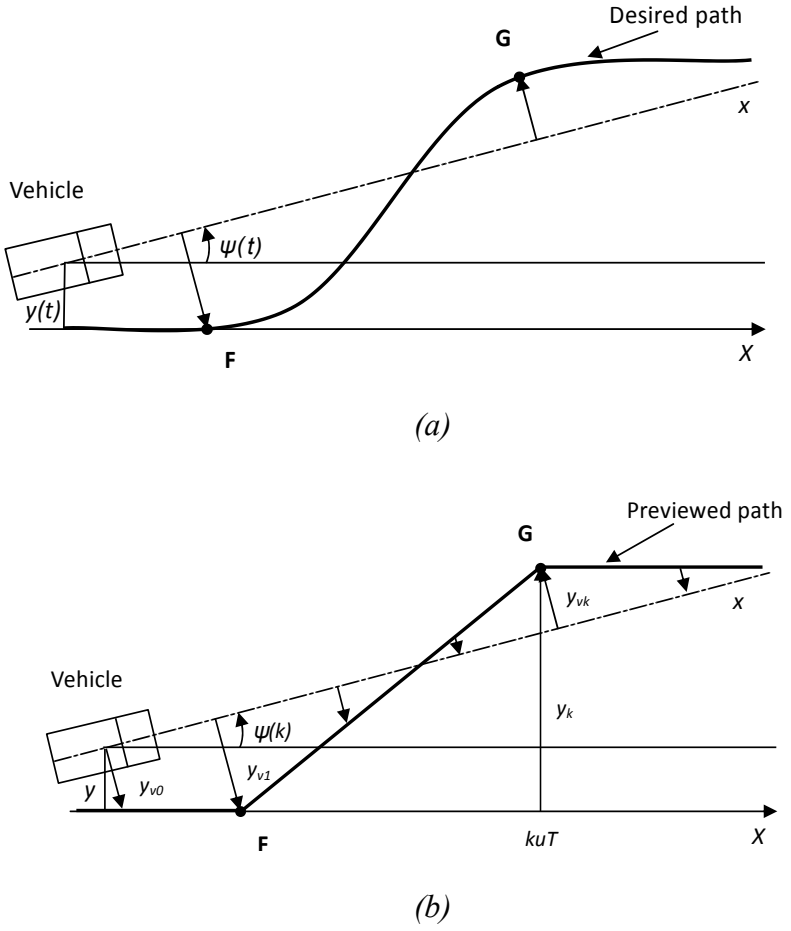

Figure 3.1: (a) The absolute path and (b) the path planned by the driver

The convenient way to describe the arbitrary path is to discrete it into *(N+1)* lateral values equally spaced in the longitudinal direction, $\boldsymbol{y}_v = [y_{v0}\ y_{v1}\ y_{v2}\ \ldots\ y_{vN}]^T$ with the interval uT, where T is the simulation step. The vehicle is at the current instant k. If

the vehicle proceeds to the next instant, $k+1$, the driver will achieve the same set of $\boldsymbol{y}_v$ where y_{v1} shifts to y_{v0}, y_{v2} shifts to y_{v1} and so on. The new value of path information y_{vN+1} enters the set at y_{vN}. Then, the lateral profile of the road path is described as:

$$\boldsymbol{y}_v(k+1) = \boldsymbol{D}_y \boldsymbol{y}_v(k) + \boldsymbol{E}_y y_{vi}(k) \tag{3.3}$$

where y_{vi} is considered as the single scalar external input. $\boldsymbol{D}_y$ represents the matrix of size $(N+1)\times(N+1)$ while $\boldsymbol{E}_y$ stands for the vector $(N+1)\times 1$ as follows:

$$\boldsymbol{D}_y = \begin{bmatrix} 0 & 1 & 0 & \dots & 0 \\ 0 & 0 & 1 & \dots & 0 \\ . & . & . & & . \\ . & . & . & & . \\ . & . & . & & . \\ 0 & 0 & 0 & \dots & 1 \\ 0 & 0 & 0 & \dots & 0 \end{bmatrix}, \quad \boldsymbol{E}_y = \begin{bmatrix} 0 \\ 0 \\ . \\ . \\ . \\ 0 \\ 1 \end{bmatrix}$$

It is assumed that the driver is aware through position of his location in the absolute system and of the head angle of the vehicle. Further, he is capable of deriving the absolute position based on the relative one. The driver uses the absolute lateral position as path input instead of the lateral path observed relatively to the longitudinal axis of the vehicle. Assuming the small head angle, the lateral path of the previewed point k in the absolute system may be calculated in the vehicle system as:

$$y_k = y + kuT\psi + y_{vk} \tag{3.4}$$

The vehicle motion on the road forms a closed-loop system with the driver, where the primary input to the vehicle is determined by the driver. The driver controls the lateral position of the vehicle based on previewed path information that is available. The performance of the driver-vehicle system in the path following problem is greatly

improved by introducing the future path information as system states. This approach corresponds to the actions of an experimented driver. Combining the discrete time equation (3.2) for the vehicle and the equation (3.3) for the road path yields:

$$\begin{bmatrix} \mathbf{x}(k+1) \\ \mathbf{y}_v(k+1) \end{bmatrix} = \begin{bmatrix} \mathbf{A}_d & \mathbf{0} \\ \mathbf{0} & \mathbf{D}_y \end{bmatrix} \begin{bmatrix} \mathbf{x}(k) \\ \mathbf{y}(k) \end{bmatrix} + \begin{bmatrix} \mathbf{B}_d \\ \mathbf{0} \end{bmatrix} \delta_{sw}(k) + \begin{bmatrix} \mathbf{0} \\ \mathbf{E}_y \end{bmatrix} y_i(k) \tag{3.5}$$

In the compact form, equation (3.5) may be written as:

$$\mathbf{z}(k+1) = \mathbf{A}\mathbf{z}(k) + \mathbf{B}\delta_{sw}(k) + \mathbf{E}y_i(k) \tag{3.6}$$

where $z(k)$ denotes the vector $(N+5)\times 1$, $\mathbf{z}(k) = \begin{bmatrix} \mathbf{x}(k) \\ \mathbf{y}_v(k) \end{bmatrix}$. $\boldsymbol{A}$, the matrix $(N+5)\times(N+5)$, $\boldsymbol{A} = \begin{bmatrix} \boldsymbol{A}_d & \boldsymbol{0} \\ \boldsymbol{0} & \boldsymbol{D}_y \end{bmatrix}$. $\boldsymbol{B}$, the vector $(N+5)\times 1$, $\boldsymbol{B} = \begin{bmatrix} \boldsymbol{B}_d \\ \boldsymbol{0} \end{bmatrix}$. $\boldsymbol{E}$, the vector $(N+5)\times 1$, $\boldsymbol{E} = \begin{bmatrix} \boldsymbol{0} \\ \boldsymbol{E}_y \end{bmatrix}$.

The steering angle $\delta_{sw}(k)$ in equation (3.6) is provided by the driver who is considered as a controller. One of the characteristics of human operators is the transport delay derived from the perceptual and neuromuscular mechanisms [27]. It is required a sufficient time to process information from the plant and transport a command to the plant. For driving a vehicle, the driver perceives the vehicle states and the path to decide the appropriate action and then manipulates the steering wheel. It is assumed that there are equal delays in perception and action. The linear system with equal delays in state and input is presented as:

$$\mathbf{z}(k+1) = \mathbf{A}\mathbf{z}(k-n_\tau) + \mathbf{B}\delta_{sw}(k-n_\tau) + \mathbf{E}y_i(k-n_\tau) \tag{3.7}$$

where $n_\tau = \frac{\tau}{2T}$, with τ denotes the effective time delay.

The associated performance index is defined as the quadratic function [82]:

$$J_{k0} = \frac{1}{2}\mathbf{z}^T(N)\mathbf{S}(N)\mathbf{z}(N) + \frac{1}{2}\sum_{k=k0}^{N-1}\left\{\mathbf{z}^T(k)\mathbf{Q}\mathbf{z}(k) + \delta_{sw}^T(k)R\delta_{sw}(k)\right\} \tag{3.8}$$

where $\boldsymbol{Q} = \boldsymbol{C}^{\boldsymbol{T}}\boldsymbol{Q}_v\boldsymbol{C}$. $\boldsymbol{Q}_v = \begin{bmatrix} q_y & 0 \\ 0 & q_\psi \end{bmatrix}$, with q_y and q_ψ represent the weighting factors of lateral path and head angle, respectively. $\boldsymbol{C}$ denotes the matrix $2\times(N+5)$, $\boldsymbol{C} = \begin{bmatrix} 0 & 0 & 1 & 0 & -1 & 0 & 0 & 0 & \dots & 0 \\ 0 & 0 & 0 & 1 & \frac{1}{uT} & -\frac{1}{uT} & 0 & 0 & \dots & 0 \end{bmatrix}$.

By changing the weighting factors q_y and q_ψ, the priorities in the cost function are defined. The control law for the delay system is derived in this section based on the reference [83-87].

The optimal problem is described by the performance index as equation (3.8) and the constraint as equation (3.7). Solving the problem is to determine the optimal control sequence $\delta_{sw,k0}$, $\delta_{sw,k0+1}$, …, $\delta_{sw,N-1}$ to minimize J_{k0}. Using the Lagrange-multiplier theory by adding the constraint to the performance index converts the optimization with constraint to without constraint. The augmented performance index, then, is:

$$\begin{aligned} J_a &= \frac{1}{2}\mathbf{z}^T(N)\mathbf{S}(N)\mathbf{z}(N) \\ &+ \sum_{k=1}^{N-1}\left[\frac{1}{2}\left\{\mathbf{z}^T(k)\mathbf{Q}\mathbf{z}(k) + \delta_{sw}^T(k)R\delta_{sw}(k)\right\} + \boldsymbol{\lambda}^T(k+n_\tau+1)\left\{\mathbf{A}\mathbf{z}(k-n_\tau) + \mathbf{B}\delta_{sw}(k-n_\tau) - \mathbf{z}(k+1)\right\}\right] \end{aligned} \tag{3.9}$$

The Hamiltonian function is defined as:

$$\mathbf{H}(k)=\frac{1}{2}\left\{\mathbf{z}^T(k)\mathbf{Q}\mathbf{z}(k)+\delta_{sw}^T(k)R\delta_{sw}(k)\right\}+\boldsymbol{\lambda}^T(k+n_\tau+1)\left\{\mathbf{A}\mathbf{z}(k-n_\tau)+\mathbf{B}\delta_{sw}(k-n_\tau)\right\} \quad (3.10)$$

Substituting the Hamiltonian function (3.10) into the performance index (3.9) and rearranging yields:

$$J_a=\frac{1}{2}\mathbf{z}^T(N)\mathbf{S}(N)\mathbf{z}(N)-\boldsymbol{\lambda}^T(N+n_\tau)\mathbf{z}(N)+\mathbf{H}(1)+\sum_{k=2}^{N-1}\left[\mathbf{H}(k)-\boldsymbol{\lambda}^T(k+n_\tau)\mathbf{z}(k)\right] \quad (3.11)$$

where ***H(1)*** denotes the Hamiltonian function at the initial state. The minimum of the performance index is achieved when its increment dJ_a is equal to zero. The increment of J_a is obtained as:

$$\begin{aligned} dJ_a &= \left\{\mathbf{S}(N)\mathbf{z}(N)-\boldsymbol{\lambda}(N+n_\tau)\right\}^T d\mathbf{z}(N)+\left\{\frac{\partial\mathbf{H}(1)}{\partial\mathbf{z}(1)}\right\}^T d\mathbf{z}(1)+\left\{\frac{\partial\mathbf{H}(1)}{\partial\delta_{sw}(1)}\right\}^T d\delta_{sw}(1) \\ &+\sum_{k=2}^{N-1}\left[\left\{\frac{\partial\mathbf{H}(k)}{\partial\mathbf{z}(k)}-\boldsymbol{\lambda}(k+n_\tau)\right\}^T d\mathbf{z}(k)+\left\{\frac{\partial\mathbf{H}(k)}{\partial\delta_{sw}(k)}\right\}^T d\delta_{sw}(k)\right]+\sum_{k=2}^{N}\left[\left\{\frac{\partial\mathbf{H}(k-1)}{\partial\boldsymbol{\lambda}(k+n_\tau)}-\mathbf{z}(k)\right\}^T d\boldsymbol{\lambda}(k+n_\tau)\right] \end{aligned} \quad (3.12)$$

The conditions for a minimum of J_a are given by:

$$\mathbf{z}(k+1)=\frac{\partial\mathbf{H}(k)}{\partial\boldsymbol{\lambda}(k+n_\tau+1)}=\mathbf{A}\mathbf{z}(k-n_\tau)+\mathbf{B}\delta(k-n_\tau) \quad (3.13a)$$

$$\boldsymbol{\lambda}(k+n_\tau)=\frac{\partial\mathbf{H}(k)}{\partial\mathbf{z}(k)}=\mathbf{Q}\mathbf{z}(k)+\mathbf{M}_1(k)\mathbf{A}^T\boldsymbol{\lambda}(k+n_\tau+1) \quad (3.13b)$$

$$\frac{\partial\mathbf{H}(k)}{\partial\delta_{sw}(k)}=R\delta_{sw}(k)+\mathbf{M}_2(k)\mathbf{B}^T\boldsymbol{\lambda}(k+n_\tau+1)=0 \quad (3.13c)$$

where $\mathbf{M}_1(k)=\frac{\partial\mathbf{z}(k-n_\tau)}{\partial\mathbf{z}(k)}$ and $\mathbf{M}_2(k)=\frac{\partial\delta_{sw}(k-n_\tau)}{\partial\delta_{sw}(k)}$. The initial condition ***z(1)*** is fixed and the final state ***z(N)***is free. This is required that:

$$\boldsymbol{\lambda}(N+n_\tau)=\mathbf{S}(N)\mathbf{z}(N) \tag{3.13d}$$

When the simulation step k is sufficient large, the delay step n_τ is considered very small comparing to k. It is assumed that:

$$\boldsymbol{\lambda}(k)=\mathbf{S}(k)\mathbf{z}(k) \tag{3.14}$$

From the equation (3.13c), the steering angle is derived as:

$$\delta_{sw}(k)=-R^{-1}\mathbf{M}_2(k-n_\tau)\mathbf{B}^T\boldsymbol{\lambda}(k+n_\tau+1) \tag{3.15}$$

Substituting the control $\delta_{sw}(k)$ achieved in equation (3.15) to equation (3.13a) gives:

$$\mathbf{z}(k+1)=\mathbf{A}\mathbf{z}(k-n_\tau)+\mathbf{B}\left\{-R^{-1}\mathbf{M}_2(k-n_\tau)\mathbf{B}^T\boldsymbol{\lambda}(k+1)\right\} \tag{3.16}$$

Applying the relation in equation (3.14) to equation (3.16) and then rearranging yields:

$$\mathbf{z}(k+1)=\left\{\mathbf{I}+\mathbf{B}R^{-1}\mathbf{M}_2(k-n_\tau)\mathbf{B}^T\mathbf{S}(k+1)\right\}^{-1}\mathbf{A}\mathbf{z}(k-n_\tau) \tag{3.17}$$

Substituting equation (3.17) to equation (3.13b) yields:

$$\mathbf{S}(k)=\mathbf{Q}+\mathbf{A}^T\mathbf{M}_1(k)\mathbf{S}(k+1)\left\{\mathbf{I}+\mathbf{B}R^{-1}\mathbf{M}_2(k-n_\tau)\mathbf{B}^T\mathbf{S}(k+1)\right\}^{-1}\mathbf{A} \tag{3.18}$$

or, using the matrix inversion lemma

$$\mathbf{S}(k)=\mathbf{A}^T\left[\mathbf{M}_1(k)\mathbf{S}(k+1)-\mathbf{M}_1(k)\mathbf{S}(k+1)\mathbf{B}\left\{\mathbf{B}^T\mathbf{S}(k+1)\mathbf{B}+R\right\}^{-1}\mathbf{M}_2(k-n_\tau)\mathbf{B}^T\mathbf{S}(k+1)\right]\mathbf{A}+\mathbf{Q} \tag{3.19}$$

For the value of $\mathbf{M}_1(k)=\dfrac{\partial\mathbf{z}(k-n_\tau)}{\partial\mathbf{z}(k)}$, if $k\in[k_0,k_0+n_\tau)$, $\mathbf{M}_1(k)=\mathbf{0}$. If $k\geq k_0+n_\tau$, then, $\mathbf{M}_1(k)=\mathbf{I}$ [78]. The value of $\mathbf{M}_2(k)=\dfrac{\partial\delta_{sw}(k-n_\tau)}{\partial\delta_{sw}(k)}$ is always equal to $\mathbf{I}$ when $k\geq k_0$. Therefore, if $k\geq k_0+n_\tau$, the quasi-Riccati equation becomes as:

$$\mathbf{S}(k) = \mathbf{A}^T \left[\mathbf{S}(k+1) - \mathbf{S}(k+1)\mathbf{B} \left\{ \mathbf{B}^T \mathbf{S}(k+1)\mathbf{B} + R \right\}^{-1} \mathbf{B}^T \mathbf{S}(k+1) \right] \mathbf{A} + \mathbf{Q} \tag{3.20}$$

The optimal control at the time *k* is:

$$\delta_{sw}(k) = -\mathbf{K}(k)\mathbf{z}(k - n_\tau) \tag{3.21}$$

where $\mathbf{K}(k) = \left\{ \mathbf{B}^T \mathbf{S}(k+1)\mathbf{B} + R \right\}^{-1} \mathbf{B}^T \mathbf{S}(k+1)\mathbf{A}$

The system state then is:

$$\mathbf{z}(k+1) = \left\{ \mathbf{A} - \mathbf{B}\mathbf{K}(k) \right\} \mathbf{z}(k - n_\tau) + \mathbf{E} y_i (k - n_\tau) \tag{3.22}$$

The driver model as LQR optimal control derives the steering angle from the vehicle states, the characteristic of vehicle and the path. It is assumed that the driver perceived all information of the path before performing the manoeuver. The steering angle, therefore, is obtained as the subsequent angles must be taken in order to drive through the path. The path which is out of the preview will not affect to the driver's judgment. The driver performs a single task such as lane-change depicted as the previewed path in Figure 3.2(a). The driver turns the vehicle to the left lane and then maintains the straight path.

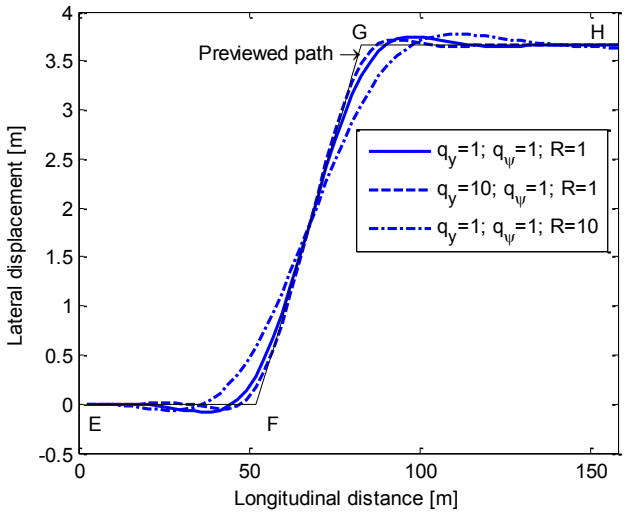

(a)

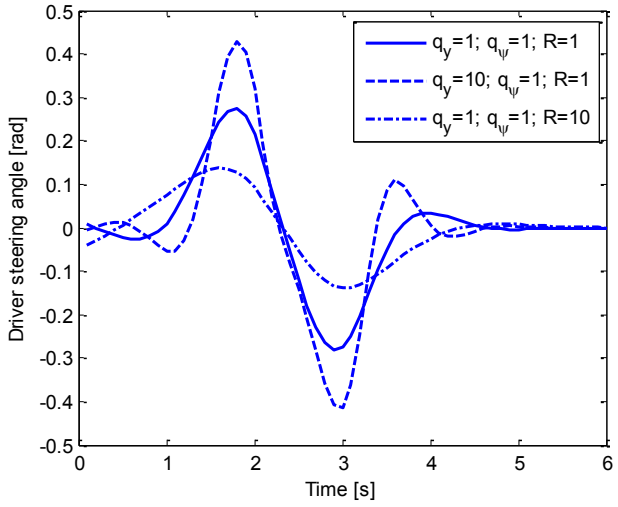

(b)

Figure 3.2: (a) Lateral displacement and (b) driver steering angle of the driver-vehicle system with a lane-change

Figure 3.2 illustrates the lateral position and the steering angle when the transport delay is ignored (n_τ=0). The shape of lateral displacement and the magnitude of driver steering angle depend on the weighting factors q_y, q_ψ and R. The priority is on lateral displacement if the set of q_y=10, q_ψ=1and R=1 is chosen. The vehicle follows the path

tightly as the dash line in Figure 3.2(a). The driver needs more effort required by fast accelerating the steering wheel and producing thus larger steering angle in a short time. If the control priority is on the steering angle such that q_y=1, q_ψ=1and R=10, the driver would spend less effort represented by small steering angle as the dash-dot line in Figure 3.2(b). As a result, the vehicle follows the path with a lager deviation. Change in the weighting factors could yield a very accurate path following that requires a significant demand on the steering angle of the driver model.

The effect of delay time on path following is illustrated in Figure 3.3. It is obvious that the vehicle follows the path with a larger deviation. After performing a lane-change, the vehicle weaves along the straight path. It is required a longer time to set the straight moving comparing to the case without delay time. The trajectory of the vehicle is presented in Figure 3.3(a) while the delay time is set as 0.5s and the preview time is varied. The shorter preview time results in the larger over-shoot and longer oscillation. In Figure 3.3(b), when the preview time is set as 5s and the delay time is 0.4s, 0.5s and 0.6s, the larger delay time introduces the larger weaving and deviation.

The driving strategy for a lane-change discussed above is only applied to the single task. The driver model is imposed to perform a task in order to test its compatibility and reliability with various vehicle models and road paths. However, the driver usually takes series of tasks while driving such as lane-change, turning, straight line and double lane-change. The information of the path is not available if it is out of the preview distance. The driver may not know every detail of the path before driving. Even while performing a single task, he may not entirely know the lateral position of the path

due to the conditions of the environment. The driver must continuously preview the path to acquire sufficient clues.

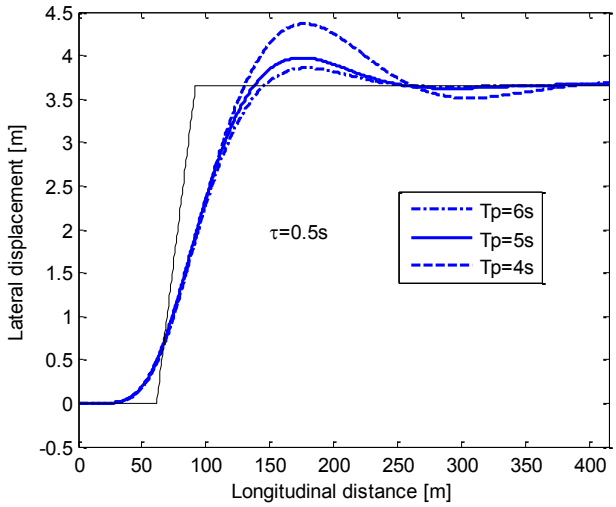

(a)

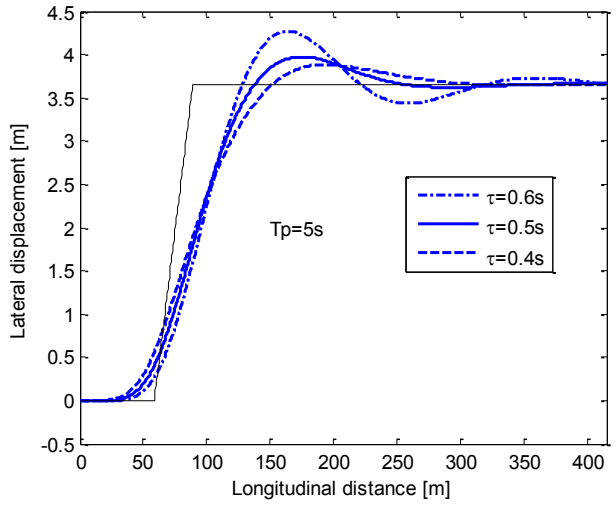

(b)

Figure 3.3: Path following with (a) varying preview time and (b) varying delay time

While the vehicle proceeds, the covered section of the path is revealed as illustrated in Figure 3.4. The driver frequently updates this information and re-calculates

the steering angle based on the latest clues. With this preparation, the vehicle will move smoothly without any abrupt adjustment. Figure 3.4 illustrates the path seen by the driver where the shadowed region indicates the unknown section. When the vehicle is moving forward, the driver retrieves new information from the path. For instance, the path within the bold line rectangle represents to the next update. The update mechanism allows the driver model work online with an arbitrary path of unlimited length.

The updating procedure is applied to the LQR driver model. The computation for every update is required since the lateral path is considered within the states. Therefore, the states of the diver-vehicle system update whenever the new information of path is available. As a result, the control gain $\boldsymbol{K}_k$ also changes inciting the deviation in steering angle. In the case that the driver model knows the path, the steering angle varies smoothly as seen in Figure 3.2(b). With the update of the new path, the steering angle fluctuates slightly since the driver model must adjust the lateral position after performing the correction.

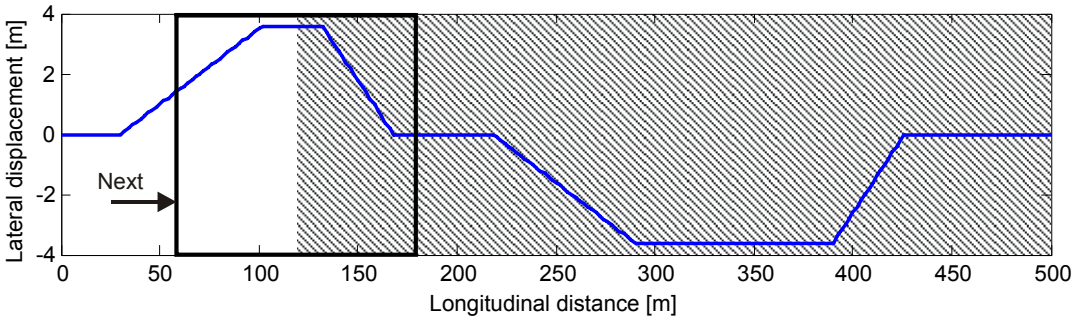

Figure 3.4: The road path and the segment seen by the driver

Figure 3.5 illustrates the time history of the simulation of driver-vehicle model with the update procedure. The path position is provided as in Figure 3.4. The driver-vehicle model followed the path defined by the arbitrary series of tasks with the forward

velocity of u=20m/s. Two values of preview time are considered for the model, T_p=2s and T_p=5s. The delay time is ignored, τ=0. The model successfully maintained along with the previewed path. The lateral displacement for T_p=2s mostly coincides with the one for T_p=5s as seen in Figure 3.5(a). The steering angle for T_p=5s exhibits little fluctuation. The steering angle for T_p=2s introduces the abrupt changes while the path is updated. The control priority is chosen as q_y=1, q_ψ=1and R=10. The update interval is the random value in the range of 0.5s to 1s.

Instead of abrupt changes in the steering angle when the preview time is reduced, steering oscillations are observed when the delay time is increased as in Figure 3.6(b). In this simulation, the performance of the driver-vehicle model with update mechanism and delay is compared to the model with update mechanism and without delay. There is a small difference between two trajectories as seen in Figure 3.6(a) where the preview is 5s. The variation of the steering angle for the delay system is higher than that the one for the system without delay.

The steering angle abruptly changes and highly oscillates when the preview time is decreased and the delay time is increased. In Figure 3.7(b), when T_p=2s and τ=0.7s, the driver model generates an unusual steering as the one performed by a good human driver. There are sudden changes and high oscillations. For the human driver, it may be interpreted as when the driver achieves insufficient preview path and the reaction time is significantly deteriorated. The worst case is encountered when the vehicle is out of control.

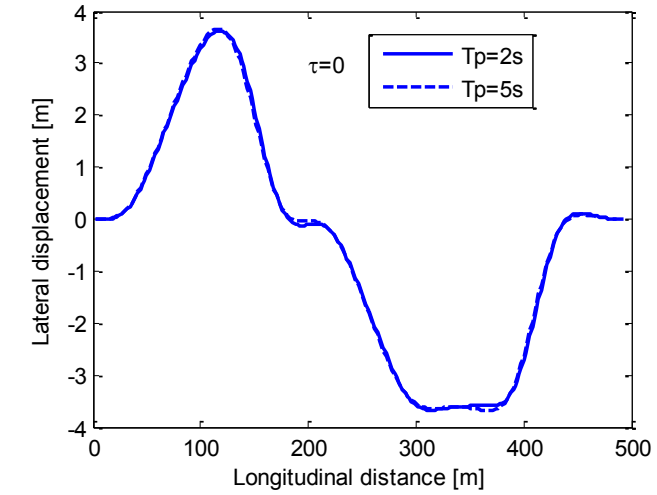

(a)

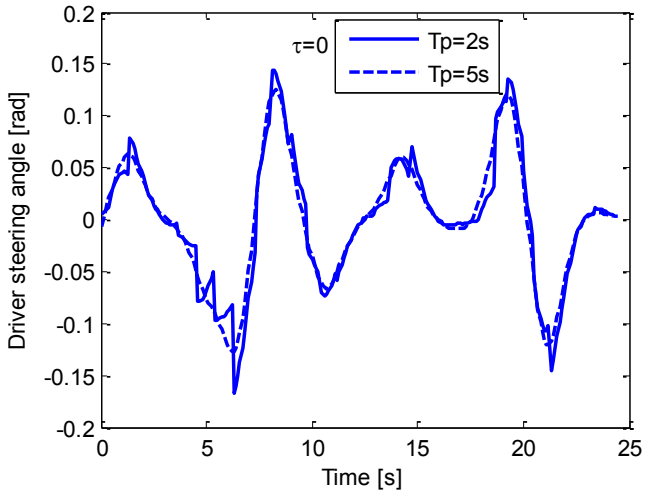

(b)

Figure 3.5: Time history of (a) lateral displacement and (b) driver steering angle for the simulation of driver-vehicle model with the path update mechanism

When the preview time increases and the delay time is neglected (τ=0), the fluctuation of steering angle decreases. The best steering input is achieved as whole information of the path corresponding to the maximum preview time T_{pmax} is available for preview. If the lateral response for this case is set as the best lateral performance, then there is a difference between the best lateral performance and the performance at the

decreased preview time. The lateral deviation of the vehicle from the desired path is measured and presented in Figure 3.8.

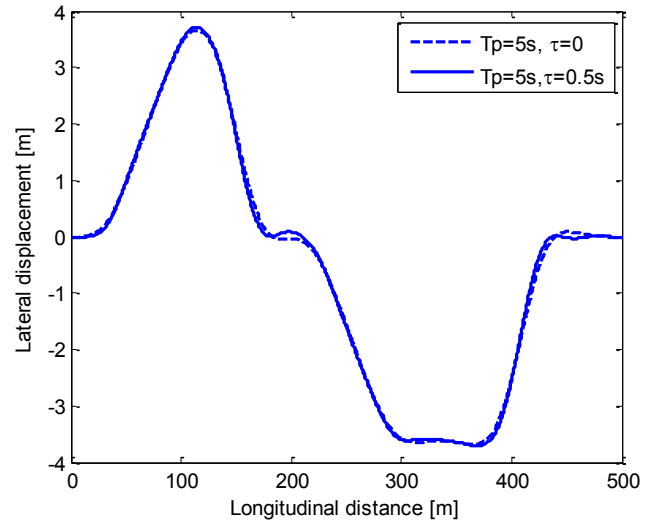

(a)

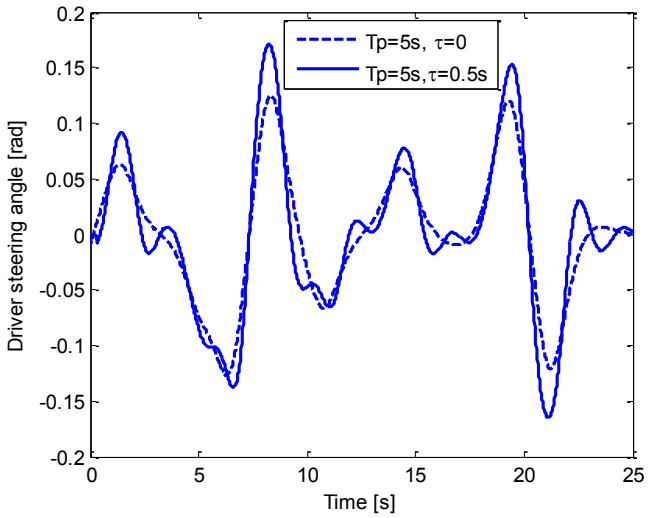

(b)

Figure 3.6: The performance of the delay system comparing to the system without delay

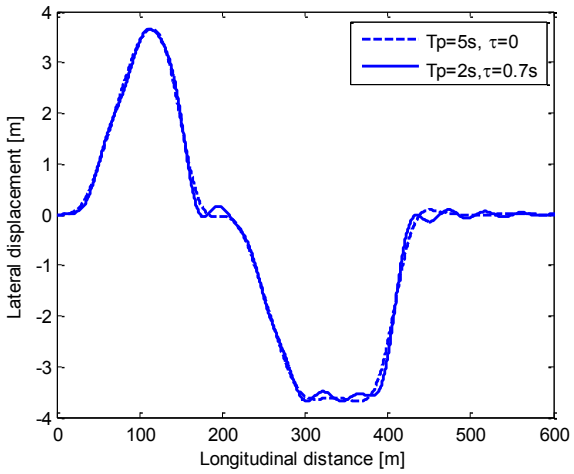

(a)

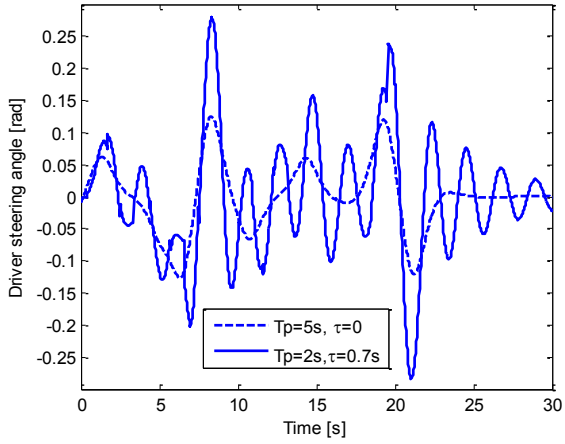

(b)

Figure 3.7: The performance of the driver-vehicle system with the decreased preview time and increased delay time

When the preview time varies from 2s to 6s, the deviation denoted as the standard lateral deviation decreases. Comparing to the small preview time, T_p=2s, the lateral deviation is quickly reduced when the preview time increases. The rate of change at that point is 6.9cm s^{-1}. If the preview time is higher than 5s, the rate of change is smaller than 0.35cm s^{-1} which presents about 5.1% of that found at T_p=2s. The lateral performance is

imposed as identical to the best performance. Therefore, T_p=5s is chosen as the good vision for the driver model.

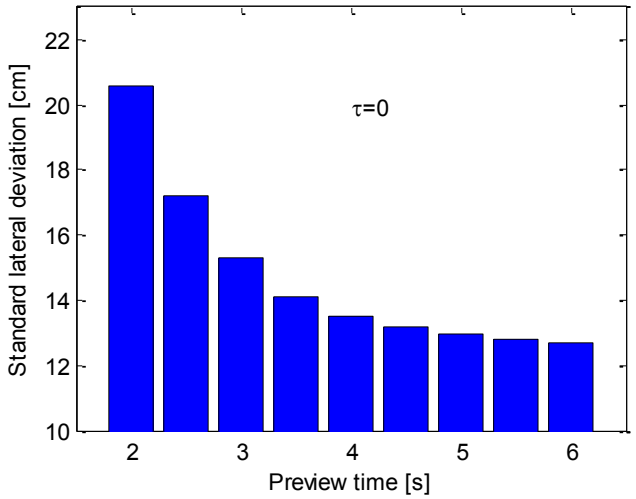

Figure 3.8: The relation of standard lateral deviation and preview time

Figure 3.9 illustrates the lateral deviation when T_p=5s, and τ increases from 0.35s to 0.8s. The system with delay time introduces larger lateral error. For instance, the deviation at 0.35s is 14.1cm which is larger than 12.95cm by about 9% for the system without delay. When the reaction time increases, the lateral deviation rapidly increases. The reaction time of 0.5s is chosen for modelling a normal driver [88].

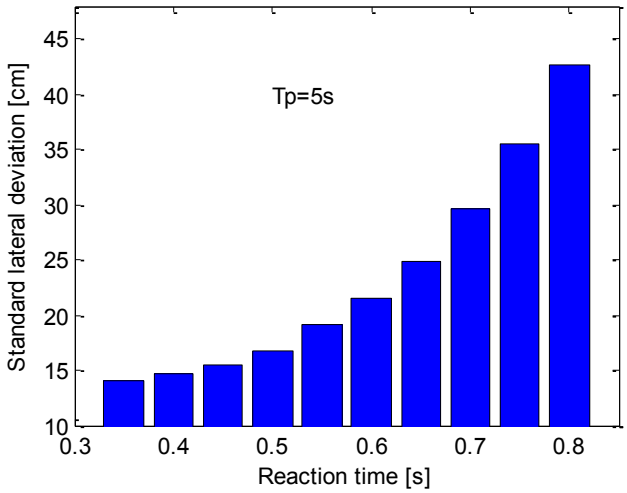

Figure 3.9: The standard lateral deviation with changing reaction time

The LQR driver model coupled with the linear vehicle model is capable of presenting a human driver in lateral position control. The model provides a good path following when the preview time T_p=5, the reaction time τ=0.5s, and the control priority q_y=1, q_ψ=1and R=10 are assigned. The driver model frequently updates the information from the road so that it can work with the unknown path out of the preview. The update mechanism and delay time also introduces the fluctuation in steering input that is similar to the adjustment performance by the human driving.

3.3 THE IMPAIRED DRIVER MODEL AND THE CONTROL OF VEHICLE PARAMETERS

The driving performance of a driver easily deteriorates after alcohol consumption [89]. Alcohol is well-known to affect driver state that it is related to driver impairment and performance decrement. Depending on the health state and alcohol consumption in the recent history of the driver, the driving performance may be affected at very low BAC as

0.01%. Studies on divided attention and recognition reaction time proved that complex tasks are more vulnerable to error than simple tasks. The measurement of performance parameters of a driver under the influence of alcohol is still a challenge since driving is a complex process that involves many functions. The record of a separate parameter may be different under diverse circumstances. Two parameters that have been intensively studied are visual function and tracking ability that are believed to be sensitive to the matter of alcohol [90].

The effect of alcohol on drivers' vision is most significant. Alcohol causes abnormal eye movements, difficulty in accurate eye tracking of moving objects, and even temporary blindness [91]. Alcohol slows processing of visual information requiring longer time to observe and perceive an object. Consequently, fewer potential incidents can be noticed and predicted by the impaired driver. Drivers perceive fewer details or they are under the trend to overlook certain clues as the visual estimation takes longer when under the influence. Alcohol-affected drivers are unable to recognize the path or traffic signs until they are close to them. As a controller, the parameters of preview distance and preview time are therefore decreased to model such condition.

Tracking ability of the alcohol-affected driver was one of the earliest performance measures studied [92] since vehicle weaving is the most recognizable hint of an alcohol impaired driver. Path tracking involves observing the difference between the desired path and the vehicle position and action performed with the intention to reduce the error. The impaired driver produces the large errors that may be out of the safety margin. The capability of path following is interpreted as the precision of lateral perception and the consistency of control priority. The impaired driver may not accurately predict the lateral

position. He also may alter the control priority while updating the new information on the path.

Reaction time of the driver is another parameter affected by alcohol. Reaction time measured during experiments of real driving involving complex tasks tends to amplify when complex tasks are performed rather than when simple tasks are carried out. Thus the reaction time required to perform more complex tasks is higher than the one for simple tasks [90]. Hindmarch [88] performed the alcohol test on nine male and nine female subjects and found that complex tasks are more vulnerable than simple tasks. The data showed that the recognition reaction time (RRT) is affected much more than the motor reaction time (MRT). The RRT of subjects before and after consuming a dose of alcohol at 0.5g per kg of bodyweight are 379ms and 401ms respectively.

The impaired driver is modelled in this work by assuming that the preview time, reaction time, lateral perception and control priority equally deteriorate. The preview time of the impaired driver is shorter than that of a normal driver while the reaction time is larger. The lateral perception and the control priorities vary within a range depending on the level of impairment. The lateral position error value increases with the level of impairment. The previewed lateral path varies about the actual path. The impaired driver may apply the random value of control priority for each update. The larger deviation in priority reflects the worse impairment. The deterioration is then applied to the LQR driver model derived in the previous section. The measurement of the model is compared to that of experiments and the results were analysed.

The standard deviation of lateral position (SDLP) is a primary parameter to measure the influence of alcohol on driving. O'Hanlon et al (1982) [92] proved that the

ability of the driver to control weaving of the vehicle sensitively deteriorates with a dose of drug ingestion. Using the driving simulator, Mets et al (2011) [93] measured the SDLP for three levels of BAC, 0.05%, 0.08%, and 0.11%. They concluded that the driving impairment depends on the BAC where the SDLP was significantly increased with the increasing of alcohol dose. The mean SDLPs are recorded as 29.7 cm, 33.8 cm and 36.3 cm for BAC 0.05%, 0.08% and 0.11% respectively.

To identify the impairment in driving skill of the driver model, the varying values of parameters are applied. The simulation is performed with the same percentage of decrement in preview time, reaction time, lateral perception and control priority for each calculation. Let the percentage increase from that represent the normal driver. The SDLP, then, was calculated as the error between the current lateral displacement and the desired path where T_p=5, τ=0.5s, q_y=1, q_ψ=1and R=10. The SDLP was increased while the parameters deteriorated. The percentages when the SDLP met 29.7cm, 33.8cm and 36.3cm were recorded.

Figure 3.10 illustrates the time history of the lateral performance for 16 tests that generates the SDLP around 29.7cm. The driver model used the path input as in Figure 3.4. For each test, the preview time was taken at 3.95s that is 21% below the optimal preview time at 5s. The reaction time was taken at 0.4s that is 21% higher the reaction time at 0.5s. The lateral path and control priority were taken at the variation within ±21% of the optimal values. For the SDLP 33.8cm and 36.3cm, the percentages of deterioration were ±26% and ±30% respectively.

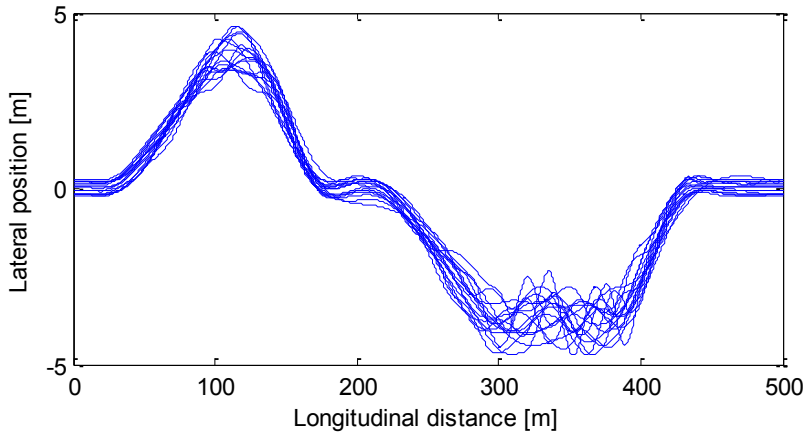

(a)

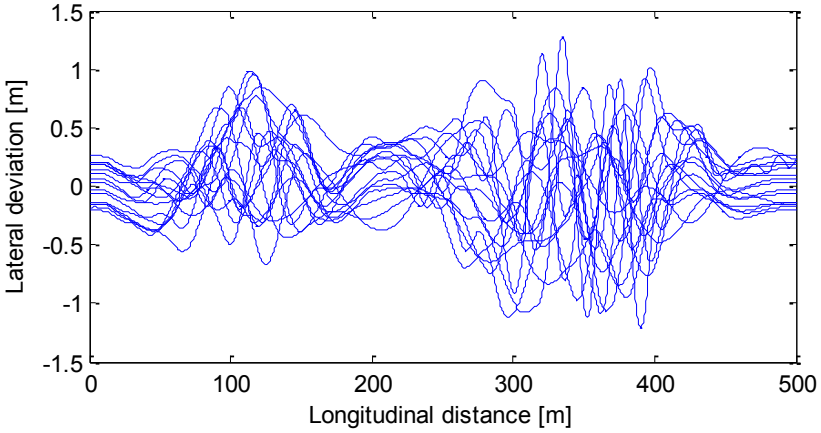

(b)

Figure 3.10: (a) Lateral position and (b) lateral deviation of the vehicle model with the driver model impairment of 21%

Figure 3.11 summarized the simulation results for three levels of impairment. The mean of standard lateral deviation and its standard error (SE) in each condition were 29.6±1.5 (impaired 21%), 33.9±1.7 (impaired 26%) and 36.5±2.3 (impaired 30%). The result are correlated to the experiment conducted by Mets et al [84] that leads to implement BAC level to the driver model. The performance of the impaired driver model

with BAC of 0.05%, 0.08% and 0.11% correspond to the deterioration of 21%, 26% and 30% in driving skill respectively. The model with high BAC produces large lateral deviation.

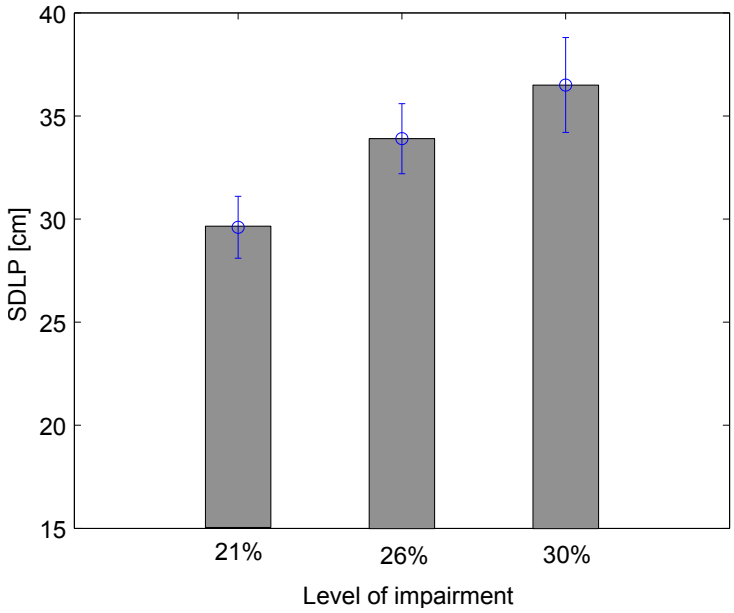

Figure 3.11: Mean (SE) standard deviation of lateral position for three levels of impairment.

The performance of the driver model under the influence of other BAC levels is approximated by assuming that there is a linear relationship between the BAC and the impairment within the identified range. For instance, BAC of 0.06% is between BAC 0.05% and 0.08%. The deterioration should be ranging from 21% to 26%. By linear interpolation, the deterioration is obtained at 22.7%.

The further investigation is carried out to evaluate the influence of vehicle parameters on the performance of the vehicle model coupled with the impaired driver model. With the same steering input, the response of the vehicle is different if its

parameters change. When the vehicle is driven by an impaired driver, the adjustment of vehicle parameters may improve the dynamic response for an input expected from an impaired driver. Figure 3.12 illustrates the SDLPs with varying values of the cornering stiffness.

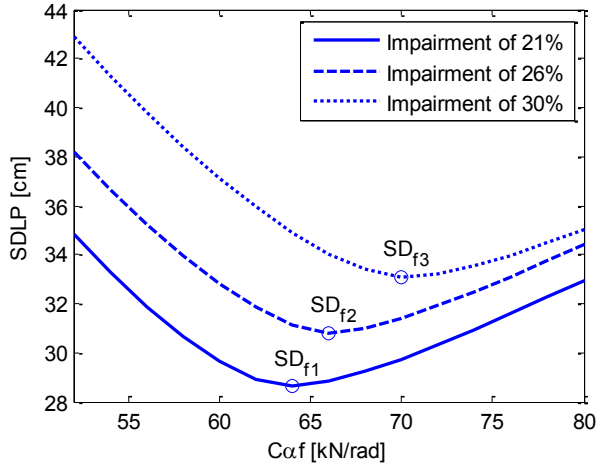

(a)

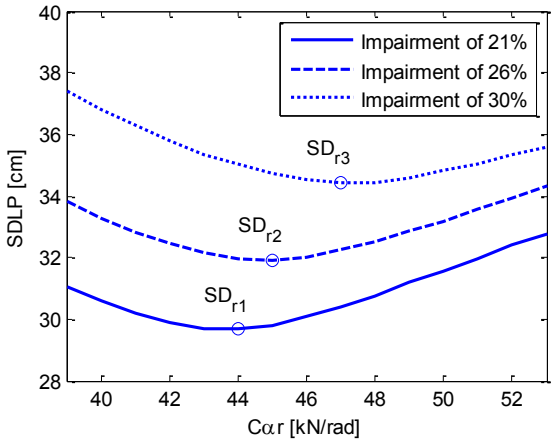

(b)

Figure 3.12: The SDLPs when (a) $C_{\alpha f}$ changes and (b) $C_{\alpha r}$ changes

The lateral performance of the vehicle is represented in Figure 3.12(a) when the cornering stiffness of the front tires ($C_{\alpha f}$) increases from 52kN/rad to 80kN/rad. The cornering stiffness of the rear tires remains constant, $C_{\alpha r}$=40kN/rad. The results show that the SDLPs for three levels of impairment decrease first after which increase. With a level of impairment, there is a circumstance where the minimum value of SDLP is achieved. For instance, at the impairment of 21%, SDLP=28.9cm when $C_{\alpha f}$=64kN/rad. The minimum values of SDLP are 31.2cm ($C_{\alpha f}$=66kN/rad) and 33.8cm ($C_{\alpha f}$=70kN/rad) for the impairments of 26% and 30% respectively. The SDLPs are smaller than that summarized in Figure 3.11.

Figure 3.12(b) illustrates the variations in SDLP when the cornering stiffness of rear tires increase from 39kN/rad to 53kN/rad. The cornering stiffness of the front tires remain constant, $C_{\alpha f}$=60kN/rad. The minimum values of SDLP are 28.7cm ($C_{\alpha r}$=44kN/rad), 31.9cm ($C_{\alpha r}$=45kN/rad) and 34.1cm ($C_{\alpha r}$=47kN/rad) for the impairments of 21%, 26% and 30% respectively. By modifying $C_{\alpha r}$, the smaller SDLPs are also obtained. The simulation results prove that the lateral deviation of the vehicle model driven by an impaired driver model is reduced by increasing the cornering stiffness of the front tires and the rear tires. The amount of increase is identified as optimum based on the level of impairment.

3.4 CONCLUSION

The impaired driver model was derived from the LQR with the update mechanism and delay. The model simulates properly the alcohol-affected driver for various BAC levels. Under the influence of alcohol, the driving is impaired since vision, reaction time, lateral

perception, and tracking ability deteriorate. The model represented the driver by reducing the preview time, increasing the reaction time and introducing the error in lateral preview and control gains. The standard deviation of lateral position is the criterion used to evaluate the level of impairment for both model and real driver. The performance of the driver with BAC of 0.05%, 0.08% and 0.11% corresponds to that of the model with 21%, 26%, and 30% deterioration.

In most countries, the BAC of 0.08% is a typical threshold over which is forbidden to operate a vehicle. The model with deterioration of 26% is considered the threshold for safe driving. Road accidents likely occur while the vehicle is weaving. The driver model may not follow the path within the safe lateral deviation. These characteristics reflect the behaviour of the alcohol-affected driver. The impaired model, then, may be utilized in vehicle design as a virtual driver to improve vehicle safety.

The proposed model may be used to fine-tune the gains to adaptively control the vehicle. The vehicle may change its parameters to reduce the negative impact of the impaired driver. The cornering stiffness of the tires is one of these parameters. A tire pressure control system is capable of adjusting the air pressure in the pneumatic tire in order to change its cornering stiffness. The driving of such a vehicle by an impaired driver may be made safer on the roads than the vehicle-driver running at the present time.

Chapter 4

LATERAL AND LONGITUDINAL PLANNING FOR AUTONOMOUS VEHICLES

4.1 INTRODUCTION

Autonomous ground vehicles have recently been revealed to the public. They represent an attractive subject that is intensively investigated and tested. The autonomous vehicles running on road reduce accidents caused by human errors and improve the traffic flow on highway [3]. The design of an autonomous vehicle involves many challenges. In the control aspect, strategies to regulate vehicle speed and to follow a path are critical important.

Falcone et al (2007) [95, 96] proposed a model predictive controller (MPC) for an active steering system. Two different MPC were presented and compared. The first one used a nonlinear vehicle model to compute the future states of the system. The second one was the linear time-varying (LTV) MPC based on the online linearization of the nonlinear vehicle. The LTV MPC of low order overcame the difficulty in computational time and yielded good performance.

Another approach to path following control was carried out by Cole et al [36]. The predictive and linear quadratic controllers were used to model the driver steering control. Road path was previewed relative to the vehicle longitudinal axis and it contributed to generating the steering input. The controllers are based on the previewed control theory that incorporating the future information to improve the vehicle performance.

A vehicle longitudinal control algorithm was developed by Han et al [97]. First, the experiments were conducted to obtain the time gap and range clearance during vehicle following for human drivers. Further, the desired acceleration was calculated from the time to collision, the speed of the preceding vehicle and the controlled vehicle. The focus to maintain a safe distance while following the preceding vehicle speed was attained.

The combination of longitudinal and lateral control represents a challenge due to the nonlinear dynamics of the vehicle. Rajamani et al [3, 94] developed a longitudinal and lateral strategy to control vehicles in platoons. The longitudinal control system determined the desired acceleration for each car and the commands required to accelerate or decelerate. The lateral control system ensured the lane-keeping or automatically steered the vehicle to an adjacent lane. The lateral and longitudinal controls were treated as decoupled processes. The integrated longitudinal and lateral control has been very little reported in the literature.

In this chapter, a novel strategy to integrate the lateral and longitudinal control for an autonomous vehicle is presented. The design of linear lateral and longitudinal controllers is based on the preview control theory. The future information of the path is included to enhance the performance of the system. The nonlinear vehicle model that represents the real vehicle is treated as a black-box exposed to noise. Kalman filter estimates the vehicle states and provides feedback to the linear controllers. The simulations are performed under the assumption that the necessary path information is already obtained. The research attempts to develop a comprehensive controller that may be implemented to automated vehicles.

4.2 DESIGN OF LONGITUDINAL AND LATERAL CONTROLLERS

4.2.1 Velocity profile of the path

Road is designed to ensure the continuity of its curvature [98]. The maximum curvature is determined by the centrifugal force that is related to the recommended speed. Figure 4.1 illustrates a method to create the curvature for an observed path that includes line segments.

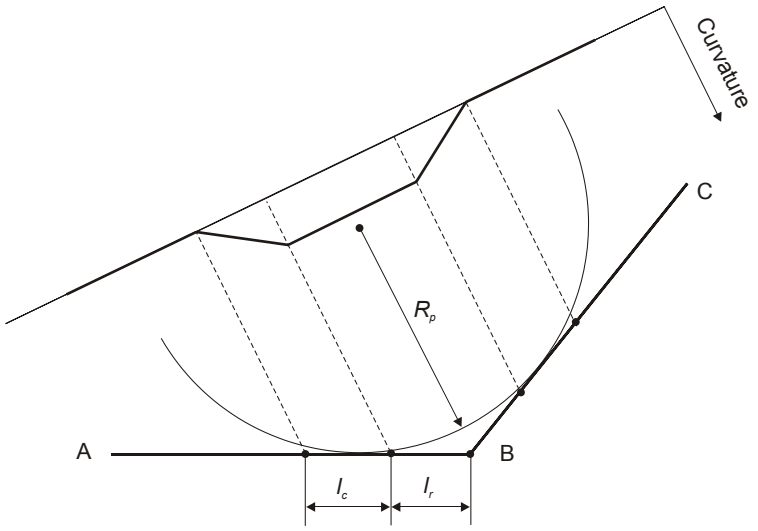

Figure 4.1: The observed path and the curvature

The curvature of a straight line is zero *(κ_l=0)* while the curvature of a circle is constant *($\kappa_c = \frac{1}{R_p}$)*. To create a smooth transition between the line and the circle, a clothoid is used. The clothoid curvature increases from zero to κ_c for the entrance of the curve or decreases from κ_c to zero for the exit of the curve. The lengths *(l_c and l_r)* of the

path with varying curvatures and constant curvatures are chosen with the consideration of the speed limitation.

The speed of the vehicle is determined by the path curvature. The experiments conducted by Lee et al [100] reveal that usually, the speed of the vehicle is not taken as the maximum speed corresponding to the limit of the centrifugal force. The drivers tend to choose the most comfortable speeds for their own that may be lower than the limitation. In general, the lower the curvature, the higher speed is taken. For instance, the vehicle generic speed profile for the observed path is constructed as in Figure 4.2. For the longitudinal control, the acceleration is used as the preview information. The acceleration profile is computed from the speed profile.

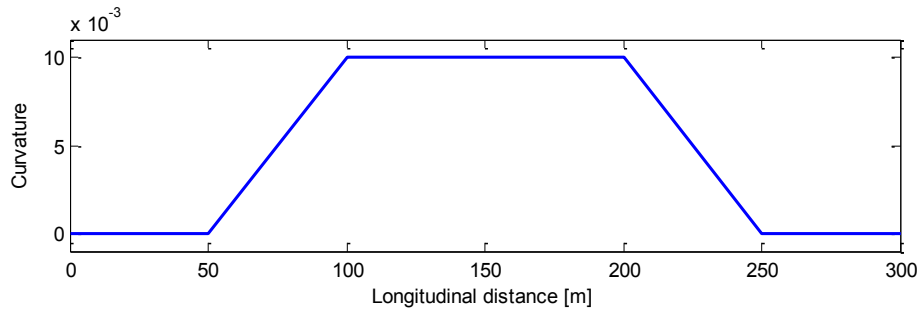

(a)

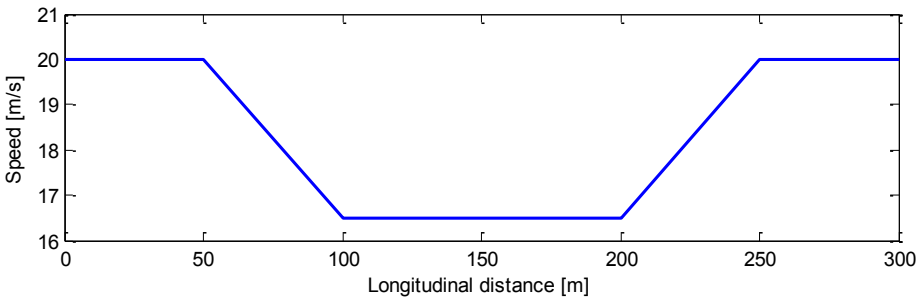

(b)

Figure 4.2: The velocity profile of the path

When new information of the path is available, the acceleration profile is updated as:

$$\boldsymbol{a}(k+1) = \boldsymbol{M}_d \boldsymbol{a}(k) + \boldsymbol{N}_d a_i(k) \tag{4.1}$$

where $a_i(k)$ is considered as the single scalar input. $\boldsymbol{M}_d$ represents the matrix $(N+1)\times(N+1)$ while $\boldsymbol{N}_d$ stands for the vector $(N+1)\times 1$ as follows:

$$\boldsymbol{M}_d = \begin{bmatrix} 0 & 1 & 0 & \dots & 0 \\ 0 & 0 & 1 & \dots & 0 \\ \cdot & \cdot & \cdot & & \cdot \\ \cdot & \cdot & \cdot & & \cdot \\ \cdot & \cdot & \cdot & & \cdot \\ 0 & 0 & 0 & \dots & 1 \\ 0 & 0 & 0 & \dots & 0 \end{bmatrix}, \quad \boldsymbol{N}_d = \begin{bmatrix} 0 \\ 0 \\ \cdot \\ \cdot \\ \cdot \\ 0 \\ 1 \end{bmatrix} \tag{4.2}$$

4.2.2 Linear model of the vehicle and the preview control for longitudinal direction

The linear model of a vehicle for the longitudinal motion is illustrated in Figure 4.3. The three degrees of freedom are the motion in the forward direction and the rotations of two wheels. The forces, F_{xf} and F_{xr} that drive the vehicle with a velocity V are applied at the contact patch of the tires and the road surface. These forces are generated due to the slips between the wheels and the ground. For the simplicity, the longitudinal forces are approximated as the linear relationship to the difference of the vehicle velocity and wheel velocity as follows:

$$\begin{aligned} F_{xf} &= C_{\lambda f}\left(R\omega_f - V\right) \\ F_{xr} &= C_{\lambda r}\left(R\omega_r - V\right) \end{aligned} \tag{4.3}$$

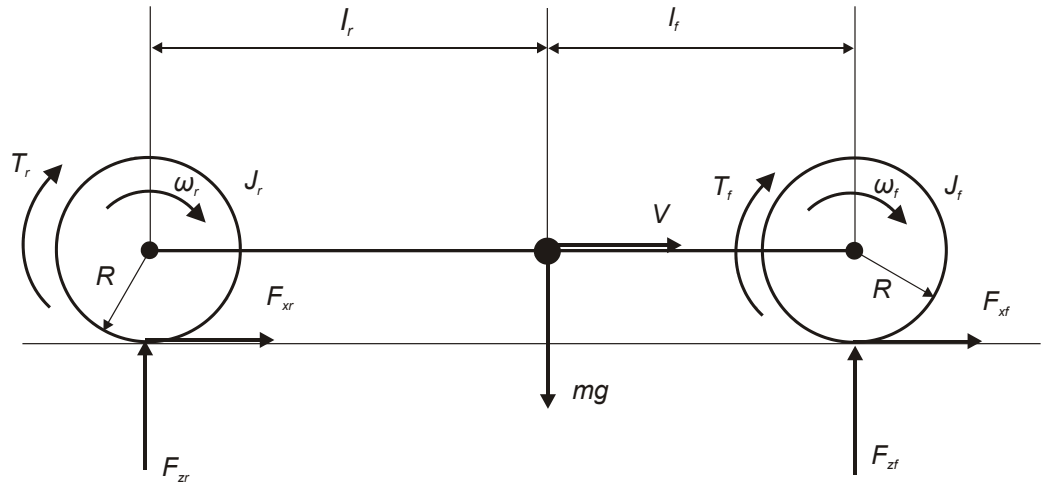

Figure 4.3: The longitudinal vehicle model

Assuming the front-drive vehicle configuration, the tracking torque is only applied on the front wheels while the braking torque is applied on both front and rear wheels. When the vehicle is accelerating, the wheel velocity is higher than the vehicle velocity, $R\omega_f > V$, that results in $F_{xf} > 0$. If the vehicle is braking, both braking force on front and rear wheels are negative, $F_{xf} < 0$ and $F_{xr} < 0$.

The vehicle velocity is dominated by the Newton second law as:

$$m\dot{V} = F_{xf} + F_{xr} \tag{4.4}$$

The motions of two wheels are represented by the equations:

$$\begin{aligned} I_{wf}\dot{\omega}_f &= -F_{xf}R + T_f \\ I_{wr}\dot{\omega}_r &= -F_{xr}R + T_r \end{aligned} \tag{4.5}$$

Combining equations (4.4) and (4.5) and rearranging yields:

$$\begin{Bmatrix} \dot{V} \\ \dot{\omega}_f \\ \dot{\omega}_r \end{Bmatrix} = \begin{bmatrix} a_{11} & a_{12} & a_{13} \\ a_{21} & a_{22} & 0 \\ a_{31} & 0 & a_{33} \end{bmatrix} \begin{Bmatrix} V \\ \omega_f \\ \omega_r \end{Bmatrix} + \begin{bmatrix} 0 & 0 & 0 \\ 0 & b_{22} & 0 \\ 0 & 0 & b_{33} \end{bmatrix} \begin{Bmatrix} 0 \\ T_f \\ T_r \end{Bmatrix} \tag{4.6}$$

where:

$$a_{11} = -\frac{\left(C_{\lambda f} + C_{\lambda r}\right)}{m},\ a_{12} = \frac{C_{\lambda f} R}{m},\ a_{13} = \frac{C_{\lambda r} R}{m}$$

$$a_{21} = \frac{C_{\lambda f} R}{I_{wf}},\ a_{22} = -\frac{C_{\lambda f} R^2}{I_{wf}}$$

$$a_{31} = \frac{C_{\lambda r} R}{I_{wr}},\ a_{33} = -\frac{C_{\lambda r} R^2}{I_{wr}}$$

$$b_{22} = \frac{1}{I_{wf}},\ b_{33} = \frac{1}{I_{wr}}$$

In the matrix notation, equation (4.6) may be written as:

$$\dot{\boldsymbol{\xi}}(t) = \boldsymbol{F}_c \boldsymbol{\xi}(t) + \boldsymbol{G}_c \boldsymbol{T}_{wh}(t) \tag{4.7}$$

The discrete version of equation (4.7) using a sampling period of T is:

$$\boldsymbol{\xi}(k+1) = \boldsymbol{F}_d \boldsymbol{\xi}(k) + \boldsymbol{G}_d \boldsymbol{T}_{wh}(k) \tag{4.8}$$

To apply the preview control in the longitudinal direction, the acceleration profile is incorporated to the vehicle states. The system can be represented as:

$$\begin{bmatrix} \boldsymbol{\xi}(k+1) \\ \boldsymbol{a}(k+1) \end{bmatrix} = \begin{bmatrix} \boldsymbol{F}_d & \boldsymbol{0} \\ \boldsymbol{0} & \boldsymbol{M}_d \end{bmatrix} \begin{bmatrix} \boldsymbol{\xi}(k) \\ \boldsymbol{a}(k) \end{bmatrix} + \begin{bmatrix} \boldsymbol{G}_d \\ \boldsymbol{0} \end{bmatrix} \boldsymbol{T}_{wh}(k) + \begin{bmatrix} \boldsymbol{0} \\ \boldsymbol{N}_d \end{bmatrix} a_i(k) \tag{4.9}$$

In the compact form, equation (4.9) may be written as:

$$\boldsymbol{s}_{k+1} = \boldsymbol{F}\boldsymbol{s}_k + \boldsymbol{G}\boldsymbol{T}_{wh,k} + \boldsymbol{N}a_{ik} \tag{4.10}$$

where $\boldsymbol{s}_k$ denotes the vector $(N+4)\times 1$, $\boldsymbol{s}_k = \begin{bmatrix} \boldsymbol{\xi}(k) \\ \boldsymbol{a}(k) \end{bmatrix}$. $\boldsymbol{F}$, the matrix $(N+4)\times(N+4)$, $\boldsymbol{F} = \begin{bmatrix} \boldsymbol{F}_d & \boldsymbol{0} \\ \boldsymbol{0} & \boldsymbol{M}_d \end{bmatrix}$. $\boldsymbol{G}$, the matrix $(N+4)\times(N+4)$, $\boldsymbol{G} = \begin{bmatrix} \boldsymbol{G}_d & \boldsymbol{0} \\ \boldsymbol{0} & \boldsymbol{0} \end{bmatrix}$. $\boldsymbol{N}$, the vector $(N+4)\times 1$, $\boldsymbol{N} = \begin{bmatrix} \boldsymbol{0} \\ \boldsymbol{N}_d \end{bmatrix}$.

The associated performance index is defined as the quadratic function [101, 102]:

$$J_{si} = \frac{1}{2}\boldsymbol{s}_N^T \boldsymbol{P}_N \boldsymbol{s}_N + \frac{1}{2}\sum_{k=i}^{N-1}\left(\boldsymbol{s}_k^T \boldsymbol{Q}_s \boldsymbol{s}_k + \boldsymbol{T}_{wh,k}^T \boldsymbol{R}_{wh} \boldsymbol{T}_{wh,k}\right) \tag{4.11}$$

where $\boldsymbol{Q}_s$ is the matrix $(N+4)\times(N+4)$, $\boldsymbol{Q}_s = \begin{bmatrix} \boldsymbol{Q}_{sa} & \boldsymbol{0} \\ \boldsymbol{0} & \boldsymbol{0} \end{bmatrix}$,

$$\boldsymbol{Q}_{sa} = \begin{bmatrix} a_{11}^2 & a_{11}a_{12} & a_{11}a_{13} & 0 & -a_{11} \\ a_{11}a_{12} & a_{12}^2 & a_{12}a_{13} & 0 & -a_{12} \\ a_{11}a_{13} & a_{12}a_{13} & a_{13}^2 & 0 & -a_{13} \\ 0 & 0 & 0 & 0 & 0 \\ -a_{11} & -a_{12} & -a_{13} & 0 & 1 \end{bmatrix}.$$

The torque applying to the front wheels is:

$$\boldsymbol{T}_{wh,k} = -\boldsymbol{K}_{s,k}\boldsymbol{s}_k \tag{4.12}$$

where $\boldsymbol{K}_{s,k}$ is the optimal gain for the longitudinal control.

4.2.3 Lateral controller design

The path following problem was discussed in Chapter 3 based on the LQR with delay and update mechanism. The driver model observes the path and computes the appropriate steering angle to minimize the lateral errors. The similar technique is used to design the

lateral controller where the delay is neglected. The computational time is assumed much smaller than the transport delay characterizing a human operator and thus it is ignored. The system without delay is represented by equation (3.6) as:

$$\mathbf{z}(k+1) = \mathbf{A}\mathbf{z}(k) + \mathbf{B}\delta_{sw}(k) + \mathbf{E}y_i(k)$$

The cost function used to evaluate the lateral performance is:

$$J_{yi} = \frac{1}{2}\boldsymbol{z}_N^T \boldsymbol{P}_N \boldsymbol{z}_N + \frac{1}{2}\sum_{k=i}^{N-1}\left(\boldsymbol{z}_k^T \boldsymbol{Q}_y \boldsymbol{z}_k + \delta_{swk}^T R_{sw} \delta_{swk}\right) \tag{4.13}$$

Using the optimal criteria, the steering angle is obtained as:

$$\delta_{swk} = -\boldsymbol{K}_{yk}\boldsymbol{z}_k \tag{4.14}$$

where $\boldsymbol{K}_{yk} = \left(\boldsymbol{B}^T \boldsymbol{P}_{k+1}\boldsymbol{B} + R_{sw}\right)^{-1}\boldsymbol{B}^T \boldsymbol{P}_{k+1}\boldsymbol{A}$. The Riccati difference equation is computed backward as:

$$\boldsymbol{P}_k = \boldsymbol{A}^T\left[\boldsymbol{P}_{k+1} - \boldsymbol{P}_{k+1}\boldsymbol{B}\left(\boldsymbol{B}^T \boldsymbol{P}_{k+1}\boldsymbol{B} + R_{sw}\right)^{-1}\boldsymbol{B}^T \boldsymbol{P}_{k+1}\right]\boldsymbol{A} + \boldsymbol{Q}_y \tag{4.15}$$

4.3 THE NONLINEAR VEHICLE MODEL

In this section, a nonlinear model representing the real vehicle is derived. The derivation of equations is based on the reference [9-10, 80-81, 105]. The model is capable of providing necessary states of the vehicle for integrating longitudinal and lateral control. The nonlinear model is more accurate than the linear one when both steering and accelerating are applied at the same time. The steering affects not only on the lateral position but also on the vehicle speed. Accelerating and decelerating the vehicle also requires a re-calculation of the steering angle when the vehicle follows a curve.

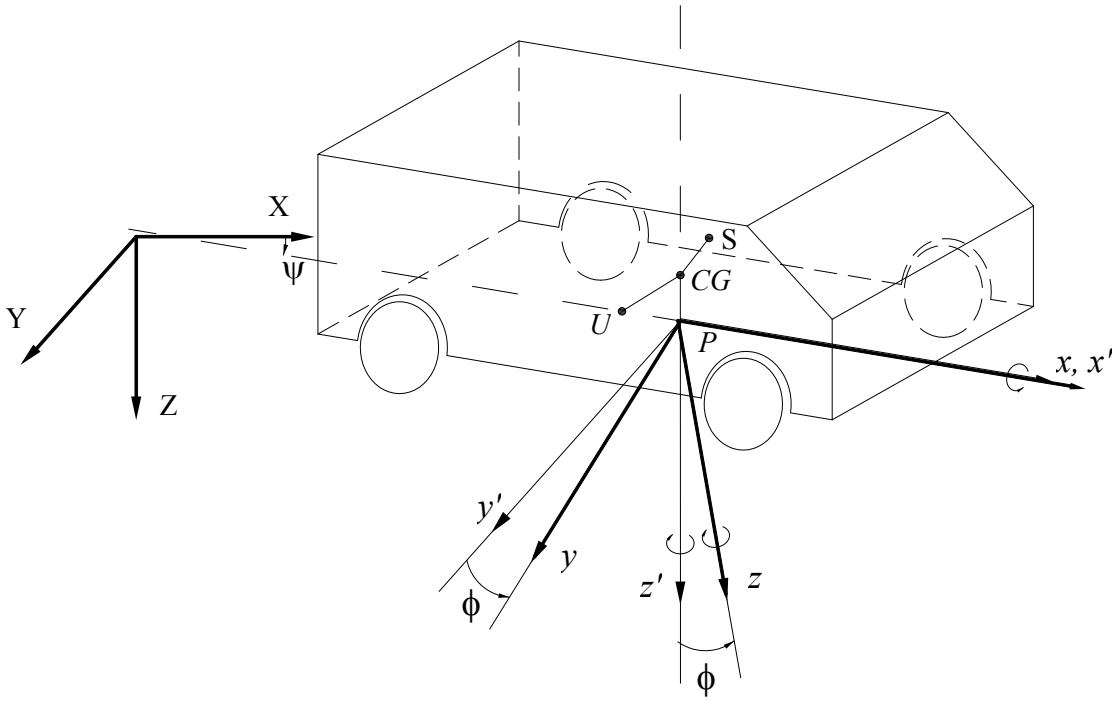

Figure 4.4: Vehicle coordinate systems

Coordinate systems of the vehicle are shown as the Figure 4.4 where the absolute coordinate *XYZ* is fixed to the ground. A coordinate system *xyz* is fixed to the sprung mass of vehicle, and the *x'y'z'* for the un-sprung mass. *P* is the origin of *xyz* and *x'y'z'*. *S* is the center of gravity of the sprung mass while *U* is that of the un-sprung mass. *CG* is the mass center of the whole vehicle and lies on the *z* axis. The longitudinal direction of the vehicle is the *x* axis, the lateral direction is *y* axis and *z* axis is in the vertical direction. The same rule is applied for *x'y'z'* coordinate system. The sprung mass rolls around the *x* axis while roll angle of un-sprung mass is neglected. The sprung mass has the yaw motion about the *z* axis while the un-sprung mass rotates about the z' axis. Assuming the height of the point *U* is small that can be neglected therefore the *x* axis goes through point

P and *U*. $\boldsymbol{i}$, $\boldsymbol{j}$, $\boldsymbol{k}$ are the unit vectors of *x, y, z* direction and $\boldsymbol{i}'$, $\boldsymbol{j}'$, $\boldsymbol{k}'$ are unit vectors of *x', y', z'* direction.

A simplified vehicle coordinate system is shown in the Figure 4.5. Position vectors of the point *P*, *S*, and *U* in the *XYZ* coordinate system are $\boldsymbol{R}$, $\boldsymbol{r}_S$ and $\boldsymbol{r}_U$ respectively.

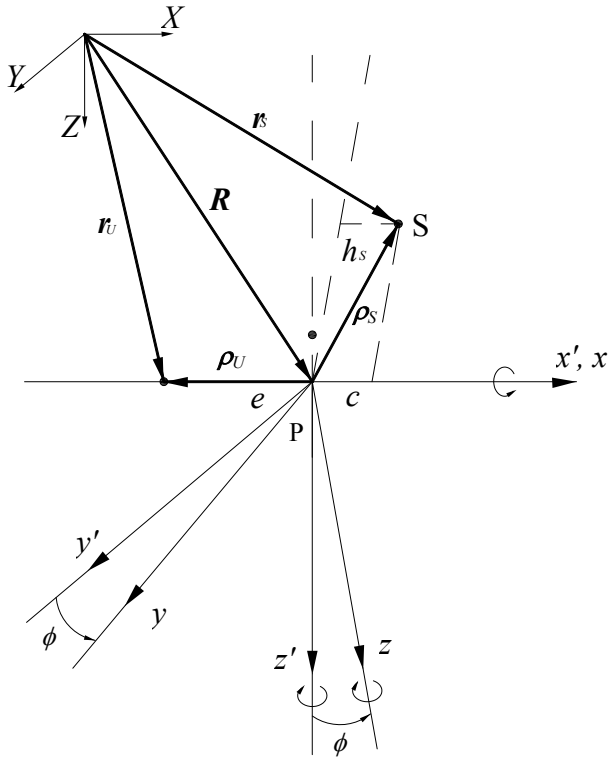

Figure 4.5: The simplified vehicle coordinate system.

If the point S and U are described by position vectors $\boldsymbol{\rho}_S$ and $\boldsymbol{\rho}_U$ in the *xyz* coordinate system, then

$$\boldsymbol{r}_S = \boldsymbol{R} + \boldsymbol{\rho}_S \tag{4.16}$$

$$\boldsymbol{r}_U = \boldsymbol{R} + \boldsymbol{\rho}_U \tag{4.17}$$

The *xyz* and *x'y'z'* have a translation velocity $\dot{\boldsymbol{R}}$ relative to the *XYZ* coordinate system and also a rotation with a angular velocity of $\boldsymbol{\omega}$. Thus

$$\dot{\boldsymbol{r}}_S = \dot{\boldsymbol{R}} + \boldsymbol{\omega} \times \boldsymbol{\rho}_S \tag{4.18}$$

$$\dot{\boldsymbol{r}}_U = \dot{\boldsymbol{R}} + \boldsymbol{\omega} \times \boldsymbol{\rho}_U \tag{4.19}$$

If *u* and *v* are the longitudinal and lateral velocity of the point *P*, then

$$\dot{\boldsymbol{R}} = u\boldsymbol{i} + v\boldsymbol{j} \tag{4.20}$$

The *xyz* coordinate system fixed to the sprung mass has a yaw motion (*r)* about *z* axis and roll motion (*p)* about *x* axis, hence

$$\boldsymbol{\omega}_S = p\boldsymbol{i} + r\boldsymbol{k} \tag{4.21}$$

The *x'y'z'* coordinate system fixed to un-sprung mass has only the yaw motion about *z* axis, hence

$$\boldsymbol{\omega}_U = r\mathbf{k}' \tag{4.22}$$

The projections of $\boldsymbol{\rho}_S$ and $\boldsymbol{\rho}_U$ on their coordinate axis are

$$\boldsymbol{\rho}_S = c\boldsymbol{i} - h_S\boldsymbol{k} \tag{4.23}$$

$$\boldsymbol{\rho}_U = -ei' \tag{4.24}$$

Substituting equations (4.20) to (4.24) into equations (4.18) and (4.19) gives

$$\boldsymbol{v}_S = \dot{r}_S = u\boldsymbol{i} + \left(v + h_S p + cr\right)\boldsymbol{j} \tag{4.25}$$

$$\boldsymbol{v}_U = \dot{r}_U = u\boldsymbol{i}' + \left(v - er\right)\boldsymbol{j}' \tag{4.26}$$

Acceleration vectors of point S and P are derived by differentiating equations (4.25) and (4.26) as following:

$$\boldsymbol{a}_S = \ddot{r}_S = \left(\dot{u} - vr - h_S pr - cr^2\right)\boldsymbol{i} + \left(\dot{v} + ur + h_S\dot{p} + c\dot{r}\right)\boldsymbol{j} + \left(vp + h_S p^2 + cpr\right)\boldsymbol{k} \tag{4.27}$$

$$\boldsymbol{a}_U = \ddot{\boldsymbol{r}}_U = \left(\dot{u} - vr + er^2\right)\boldsymbol{i}' + \left(\dot{v} + ur - e\dot{r}\right)\boldsymbol{j}' \tag{4.28}$$

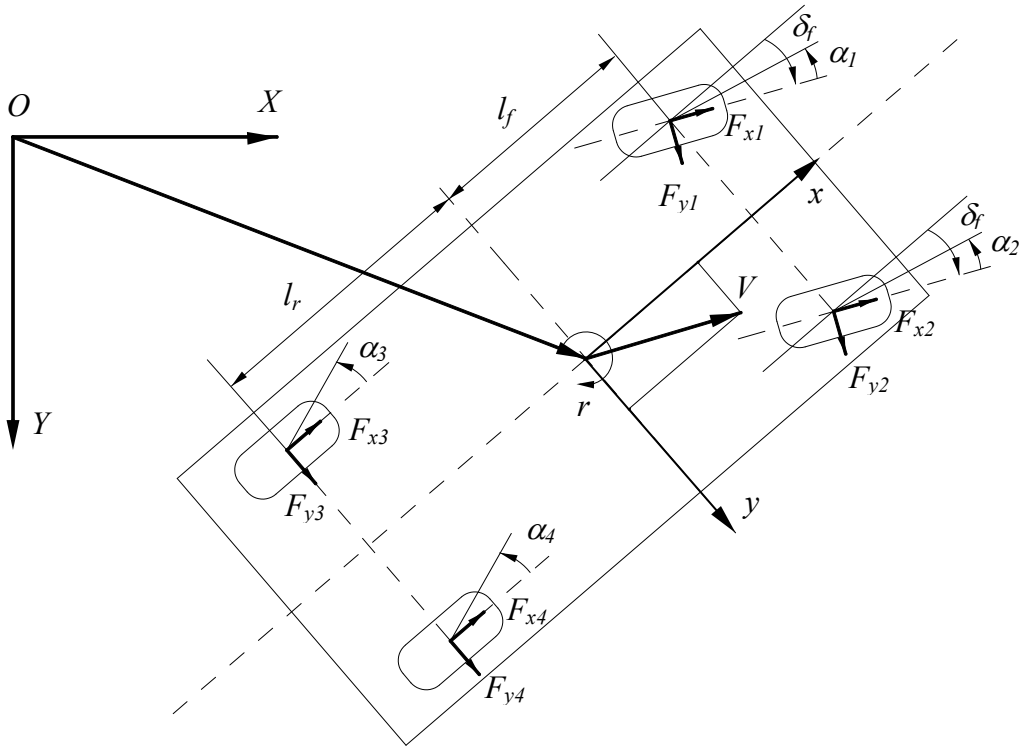

Figure 4.6: Forces acting on the planar vehicle.

Assuming that yaw angle of the vehicle in the *xy* plane is small, the total force in the longitudinal direction is $\sum_{i=1}^{4} F_{xi}$, the vehicle on this direction is described:

$$m_S a_{Sx} + m_U a_{Ux} = \sum_{i=1}^{4} F_{xi} \tag{4.29}$$

where a_{Sx} and a_{Ux} are derived from equations (4.27) and (4.28) as

$$a_{Sx} = \dot{u} - vr - h_S pr - cr^2 \tag{4.30}$$

$$a_{Ux} = \dot{u} - vr + er^2 \tag{4.31}$$

Substituting equations (4.30) and (4.31) to equation (4.29) gives

$$m(\dot{u} - vr) - m_S h_S rp = \sum_{i=1}^{4} F_{xi} \tag{4.32}$$

where, $m_S + m_U = m$, and $m_{Sc} = m_U e$.

Lateral equation of motion is

$$m_S a_{Sy} + m_U a_{Uy} = \sum_{i=1}^{4} F_{yi} \tag{4.33}$$

where a_{Sy} and a_{Uy} are derived from equations (4.27) and (4.28) as

$$a_{Sy} = \dot{v} + ur + h_S \dot{p} + c\dot{r} \tag{4.34}$$

$$a_{Uy} = \dot{v} + ur - e\dot{r} \tag{4.35}$$

Substituting equations (4.34) and (4.35) to equation (4.33) yields:

$$m(\dot{v} + ur) + m_S h_S \dot{p} = \sum_{i=1}^{4} F_{yi} \tag{4.36}$$

Considering a vehicle with two rigid bodies connected by the suspension system, the moment of momentum of the sprung mass is

$$\boldsymbol{H}_S = \boldsymbol{I}_S \times \boldsymbol{\omega}_S \tag{4.37}$$

Assuming that *xz* plane is the symmetrical plane of the sprung mass, hence $\boldsymbol{I}_{yxS} = 0$ and $\boldsymbol{I}_{yzS} = 0$. The inertia tensor matrix, I_S, is

$$\boldsymbol{I}_S = \begin{bmatrix} I_{xxS} & 0 & I_{xzS} \\ 0 & I_{yyS} & 0 \\ I_{xzS} & 0 & I_{zzS} \end{bmatrix} \tag{4.38}$$

Combining equations (4.21), (4.37) and equation (4.38) gives

$$\boldsymbol{H}_S = (I_{xxS} p + I_{xz} r)\boldsymbol{i} + (I_{xzS} p + I_{zzS} r)\boldsymbol{k} \tag{4.39}$$

Differentiating equation (4.31) with respect to time gives

$$\dot{\boldsymbol{H}}_S = \left(I_{xxS}\dot{p} + I_{xz}\dot{r}\right)\boldsymbol{i} + \left(-I_{zzS}p^2 + \left(I_{xxS} - I_{zzS}\right)pr + I_{xzS}r^2\right)\boldsymbol{j} + \left(I_{xzS}\dot{p} + I_{zzS}\dot{r}\right)\boldsymbol{k} \quad (4.40)$$

Similarity, the un-sprung mass has

$$\boldsymbol{H}_U = I_{zzU}\boldsymbol{k}' \quad (4.41)$$

$$\dot{\boldsymbol{H}}_U = I_{zzU}\dot{r}\boldsymbol{k}' \quad (4.42)$$

The equation of yaw motion is expressed as:

$$\sum M_z = I_{xzS}\dot{p} + I_{zzS}\dot{r} + m_S a_{Sy}c - m_U a_{Uy}e = I_{zz}\dot{r} + I_{xz}\dot{p} \quad (4.43)$$

Hence,

$$I_{zz}\dot{r} + I_{xz}\dot{p} = \sum M_z \quad (4.44)$$

The external moment acting on the vehicle about z axis is:

$$\sum M_z = l_f\left(F_{y1} + F_{y2}\right) - l_r\left(F_{y3} + F_{y4}\right) + \frac{d_f}{2}\left(F_{x1} - F_{x2}\right) + \frac{d_r}{2}\left(F_{x3} - F_{x4}\right) + \sum_{i=1}^{4} M_{zi} \quad (4.45)$$

Substituting equation (4.44) to equation (4.45) gives:

$$I_{zz}\dot{r} + I_{xz}\dot{p} = l_f\left(F_{y1} + F_{y2}\right) - l_r\left(F_{y3} + F_{y4}\right) + \frac{d_f}{2}\left(F_{x1} - F_{x2}\right) + \frac{d_r}{2}\left(F_{x3} - F_{x4}\right) \quad (4.46)$$

The equation of roll motion is:

$$\sum M_x = I_{xxS}\dot{p} + I_{xzS}\dot{r} + m_S a_{Sy}h_s = I_{xx}\dot{p} + I_{xz}\dot{r} + m_S h_S\left(\dot{v} + ur\right) \quad (4.47)$$

Hence,

$$I_{xx}\dot{p} + I_{xz}\dot{r} + m_S h_S\left(\dot{v} + ur\right) = \sum M_x \quad (4.48)$$

As shown in Figure 4.7, the total moment acting on the sprung mass about x axis is

$$\sum M_x = m_S g h_S - \left(k_{\phi f} + k_{\phi r}\right)\phi - \left(c_{\phi f} + c_{\phi r}\right)p \quad (4.49)$$

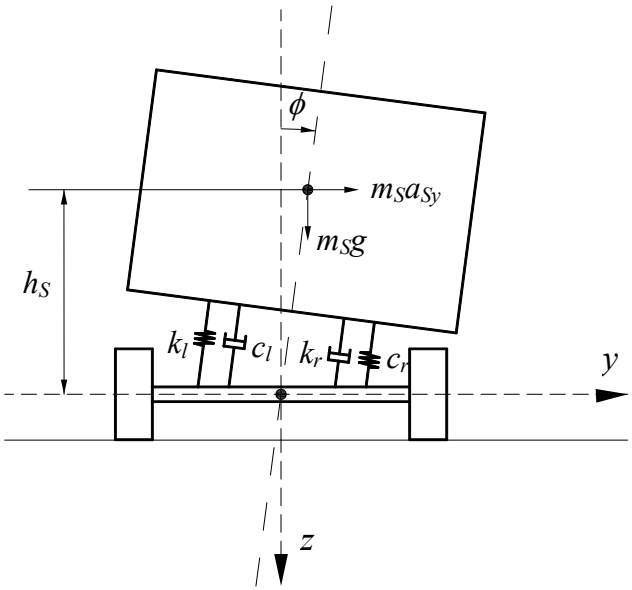

Figure 4.7: Vehicle roll in plane model

Substituting equation (4.49) to equation (4.48) gives

$$I_{xx}\dot{p} + I_{xz}\dot{r} = -m_S h_S(\dot{v} + ur) + m_S g h_S \phi - (k_{\phi f} + k_{\phi r})\phi - (c_{\phi f} + c_{\phi r})p \tag{4.50}$$

When the vehicle is moving and maneuvering, the normal force on each tire is different and varies to time. The resultant force is the combination of static part and the load transfer in longitudinal, lateral and roll motion. They are expressed as:

$$F_{z1} = \frac{mgl_r}{2l} - ma_x\frac{h}{2l} - \frac{ma_y l_r h}{ld_f} + \frac{M_{\phi f}}{d_f} \qquad F_{z2} = \frac{mgl_r}{2l} - ma_x\frac{h}{2l} + \frac{ma_y l_r h}{ld_f} - \frac{M_{\phi f}}{d_f}$$

$$F_{z3} = \frac{mgl_f}{2l} + ma_x\frac{h}{2l} - \frac{ma_y l_f h}{ld_r} + \frac{M_{\phi r}}{d_r} \qquad F_{z4} = \frac{mgl_f}{2l} + ma_x\frac{h}{2l} + \frac{ma_y l_f h}{ld_r} - \frac{M_{\phi r}}{d_r} \tag{4.51}$$

The Figure 4.6 shows the angles on each tire, considering the relationship among the lateral velocity *v*, the longitudinal velocity *u* and the yaw velocity *r*, the tire slip angle can be calculated as:

$$\alpha_1 = \delta_f - \tan^{-1}\left(\frac{v + l_f r}{u + \frac{d_f}{2} r}\right) \qquad \alpha_2 = \delta_f - \tan^{-1}\left(\frac{v + l_f r}{u - \frac{d_f}{2} r}\right)$$

$$\alpha_3 = \tan^{-1}\left(\frac{v - l_f r}{u - \frac{d_r}{2} r}\right) \qquad \alpha_4 = \tan^{-1}\left(\frac{v - l_f r}{u + \frac{d_r}{2} r}\right) \tag{4.52}$$

The contact surface between the vehicle and the road is not perfect and there is always a slip. In the case of braking, the forward vehicle velocity is larger than the velocity of the wheel. The wheel slip ratio is defined:

$$\lambda_i = \frac{R_i w_i - V}{V} \tag{4.53}$$

Four wheels of the vehicle rotate independently, the rotation of wheels are represented by the equation of motion:

$$I_w \dot{w}_i = -R_i F_{xi} + T_{wh} \tag{4.54}$$

Where I_w is the moment of inertia of the wheel about its axis of rotation, R_i is the wheel effective rolling radius, F_{xi} is the braking force acting on the tire in x direction, and T_{wh} is the braking torque applied to the wheel as shown in Figure 4.8.

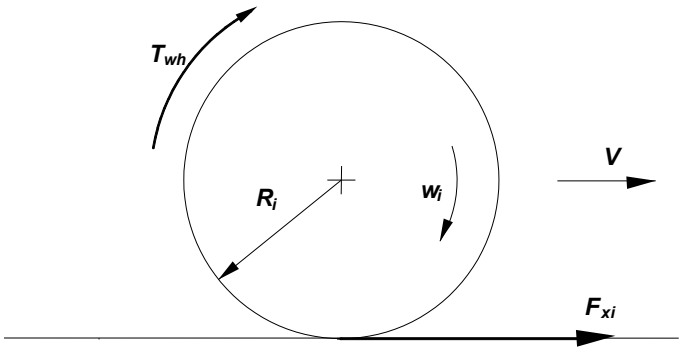

Figure 4.8: Forces acting on the wheel

Table 4.1: Vehicle parameters [80]

Parameter	Symbol	Value
Vehicle total mass (kg)	m	1070
Sprung mass (kg)	m_s	900
Height of vehicle Center of Gravity (CG) (m)	h	0.6
Distance from roll axis to sprung mass (m)	h_s	0.55
Vehicle moment of inertia about z axis (kg.m^2)	I_z	2100
Vehicle moment of inertia about x axis (kg.m^2)	I_x	500
Vehicle moment of inertia about x and z axis (kg.m^2)	I_{xz}	47.5
Distance from vehicle CG to front axle (m)	l_f	1.1
Distance from vehicle CG to rear axle (m)	l_r	1.3
Wheel base (m)	l	2.4
Front track width (m)	d_f	1.4
Rear track width (m)	d_r	1.41
Roll stiffness (Nm/rad)	$k_{\phi f}$, $k_{\phi r}$	32250
Roll damping (Nms/rad)	$c_{\phi f}$, $c_{\phi r}$	1050
Wheel moment of inertia (kg.m^2)	I_w	0.9
Effective rolling radius of wheels (m)	R	0.28

The Magic Formula [13, 106] is used in the vehicle model for the tires. In general form, the formula is

$$y(x) = D\sin\{C\tan^{-1}[Bx - E(Bx - \tan^{-1} Bx)]\} \tag{4.55}$$

$$Y(X) = y(x) + S_{vx}$$

$$x = X + S_{hx}$$

where $Y(X)$ is either the braking force F_x with X the wheel slip ratio λ or cornering force, F_y with X the tire slip angle α or self-aligning moment M_z with X is slip angle. S_{vx} and S_{hx} allow a shift in the horizontal and vertical directions. Four coefficients B, C, D and E

specify the characteristics of the tire. *D* is the peak factor, *B* is stiffness factor, *C* is the shape factor and *E* is the curvature factor. Figure 4.9 illustrates the influence of each factor on the appearance of Magic Formula graph.

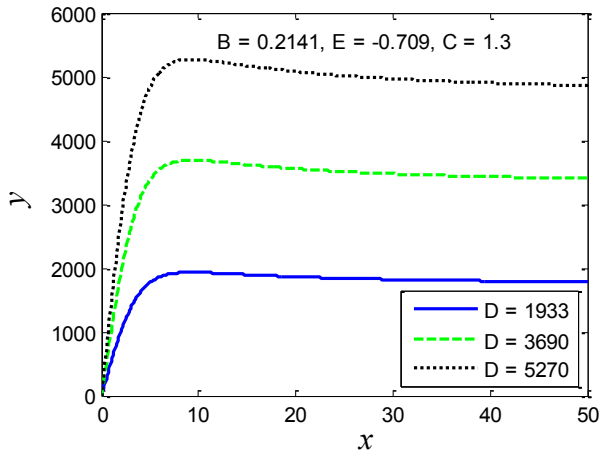

(a)

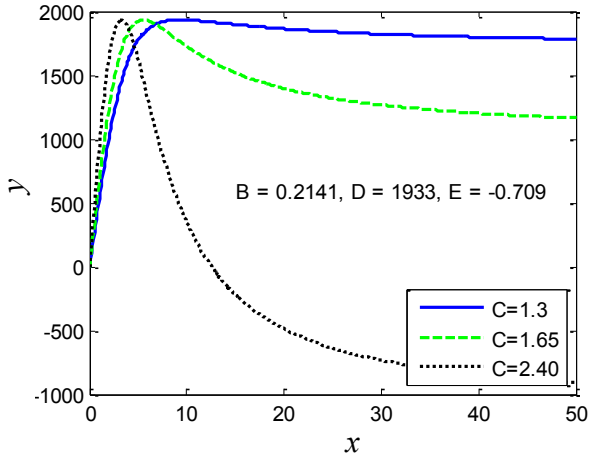

(b)

Figure 4.9: The impact of changing coefficients D and C on the outputs of Magic Formula.

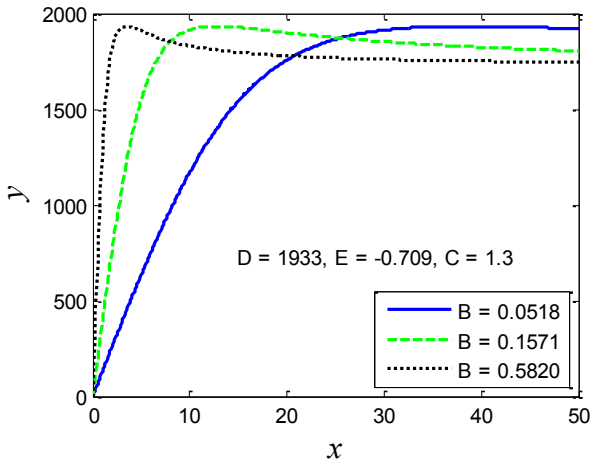

(a)

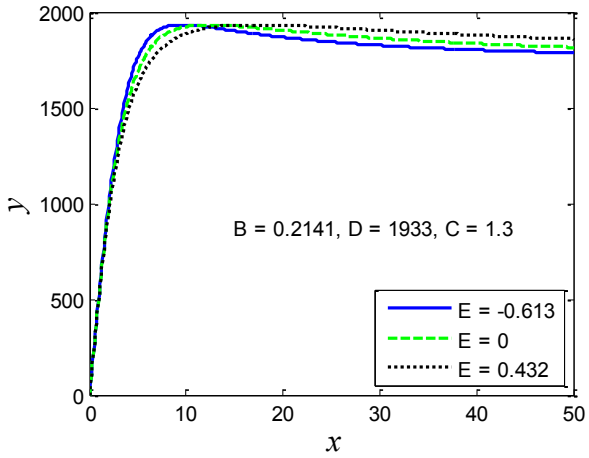

(b)

Figure 4.10: The impact of changing coefficients B and E on the outputs of Magic Formula.

Changing *D* factor in Figure 4.9(a) results the changing magnitude of the graph. The *C* factor defines the shape of the curve that looks like a lateral force ($C = 1.30$), a braking force ($C = 1.65$) or a self-aligning moment ($C = 2.40$) as shown in Figure 4.9(b). If the peak value *D* and the shape factor *C* are defined and remain constant, only the *B* value controls the stiffness as in Figure 4.10(a). The curvature factor *E* that adjusts the

extra stretch or compression of the curve, does not affect the peak value and the stiffness as in Figure 4.10(b).

4.4 THE OVERALL MODEL AND SIMULATION

The lateral and longitudinal controller provides the steering angle and the necessary wheel torque to the vehicle. In this section, a nonlinear vehicle model including the longitudinal, lateral, yaw and roll motion is used to represent the real vehicle. The overall model of the longitudinal and lateral control is illustrated in Figure 4.11.

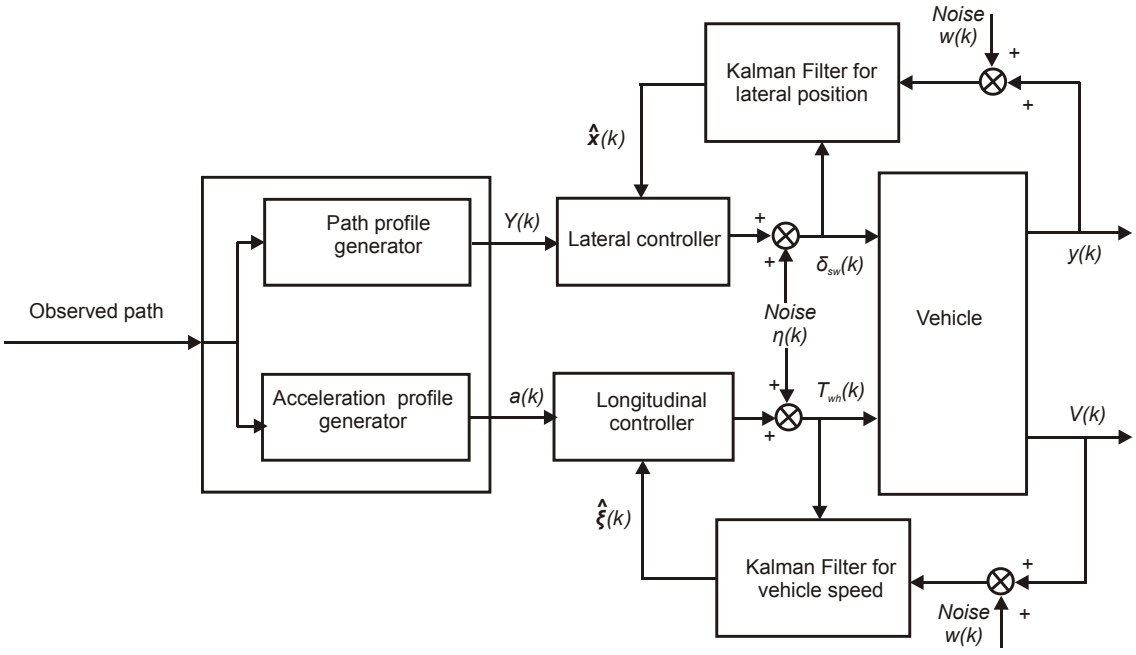

Figure 4.11: The overall model of vehicle control

From the investigation of the equations in the nonlinear vehicle model, the speed of the vehicle is affected not only by the wheel torque but also by the steering angle. Both the steering angle and the wheel torque affect to the lateral position of the vehicle. Errors are encountered between the output of the linear models and the same type of physical

quantity of the nonlinear model. For instances, the lateral position calculated in the lateral controller is different from the lateral position measured in the nonlinear model when both the steering angle and the wheel torque are applied.

The Kalman filter is used to estimate the states for the linear model and to eliminate additive noise due to the inputs and the measurements. The vehicle dynamics is subjected to disturbances. One type of disturbances is the errors of equipment such as sensors, cameras and speedometers. To count for that, noise is added to the observer. The other disturbances are the external forces such as wind and fluctuating road surface. This type of disturbances directly affects to the vehicle states and it is modeled as noise added to the inputs.

The lateral vehicle model can be represented as [103]:

$$\boldsymbol{x}_{k+1} = \boldsymbol{A_d}\boldsymbol{x_k} + \boldsymbol{B_d}\delta_{sw,k} + \boldsymbol{\Lambda} w_k \tag{4.56}$$

where w_k is a white Gaussian noise with the zero-mean and the intensity of W_y. The lateral position observer is established as:

$$y_k = \boldsymbol{H}_y \boldsymbol{x_k} + \eta_k \tag{4.57}$$

where $\boldsymbol{H_y}$ denotes the observer matrix, $\boldsymbol{H_y}$=[0 0 1 0] and η_k is a white Gaussian noise with the zero-mean and the intensity of N_y. The estimated state at the instant before performing the measurement is:

$$\hat{\boldsymbol{x}}_k(-) = \boldsymbol{A_d}\hat{\boldsymbol{x}}_{k-1}(+) + \boldsymbol{B_d}\delta_{sw,k-1} \tag{4.58}$$

The covariance before and after the measurement are:

$$\boldsymbol{P_k}(-) = \boldsymbol{A_d}\boldsymbol{P_{k-1}}(+)\boldsymbol{A_d^T} + \boldsymbol{\Lambda}_y W_y \boldsymbol{\Lambda}_y{}^T \tag{4.59}$$

$$\boldsymbol{P_k}(+) = \left[\boldsymbol{P_k^{-1}}(-) + \boldsymbol{H}_y^T N_y^{-1} \boldsymbol{H}_y\right]^{-1} \tag{4.60}$$

The estimation of the state as the feedback to the lateral controller is [104]:

$$\hat{\boldsymbol{x}}_k(+) = \hat{\boldsymbol{x}}_k(-) + \boldsymbol{K}_{f,k}\left[y_k - \boldsymbol{H}_y\hat{\boldsymbol{x}}_k(-)\right] \tag{4.61}$$

where $K_{f,k}$ is the Kalman gain as:

$$\boldsymbol{K}_{f,k} = \boldsymbol{P}_k(-)\boldsymbol{H}_y^T\left[\boldsymbol{H}_y\boldsymbol{P}_k(-)\boldsymbol{H}_y^T + N_y\right]^{-1} \tag{4.62}$$

For the longitudinal estimation, the vehicle with disturbances is modeled as:

$$\boldsymbol{\xi}_{k+1} = \boldsymbol{F}_d\boldsymbol{\xi}_k + \boldsymbol{G}_d\boldsymbol{T}_{wh,k} + \boldsymbol{\Lambda}_s w_k \tag{4.63}$$

and the velocity is measured as:

$$V_k = \boldsymbol{H}_s\boldsymbol{\xi}_k + \eta_k \tag{4.64}$$

where $\boldsymbol{H}_s$=[1 0 0], w_k and η_k are white Gaussian noises with the zero-means and the intensities of W_s and N_s respectively. The means and covariances using the Kalman filter are:

$$\hat{\boldsymbol{\xi}}_k(-) = \boldsymbol{F}_d\hat{\boldsymbol{\xi}}_{k-1}(+) + \boldsymbol{G}_d\boldsymbol{T}_{wh,k-1} \tag{4.65}$$

$$\boldsymbol{P}_k(-) = \boldsymbol{F}_d\boldsymbol{P}_{k-1}(+)\boldsymbol{F}_d^T + \boldsymbol{\Lambda}_s W_s \boldsymbol{\Lambda}_s^T \tag{4.66}$$

$$\boldsymbol{P}_k(+) = \left[\boldsymbol{P}_k^{-1}(-) + \boldsymbol{H}_s^T N_s^{-1}\boldsymbol{H}_s\right]^{-1} \tag{4.67}$$

$$\boldsymbol{K}_{f,k} = \boldsymbol{P}_k(-)\boldsymbol{H}_s^T\left[\boldsymbol{H}_s\boldsymbol{P}_k(-)\boldsymbol{H}_s^T + N_s\right]^{-1} \tag{4.68}$$

$$\hat{\boldsymbol{\xi}}_k(+) = \hat{\boldsymbol{\xi}}_k(-) + \boldsymbol{K}_{f,k}\left[V_k - \boldsymbol{H}_s\hat{\boldsymbol{\xi}}_k(-)\right] \tag{4.69}$$

The simulation is performed to evaluate the controllers and the estimators. First, no disturbance is added to the inputs and the measurements. From the observed path, many velocity profiles may be generated. The chosen profile is in the consideration of the vehicle and road conditions. In the simulation, three velocity profiles are tested. The velocity profile 1 corresponds to the high level of acceleration and deceleration while the

velocity profile 3 is for the low level of acceleration and deceleration. The total torque applied to the wheels is illustrated in Figure 4.12(a). The higher torque is required to follow the velocity profile 1. In Figure 4.12(b), three histories of the vehicle speed are recorded. The vehicle gradually accelerates and decelerates when it enters and exits the curve.

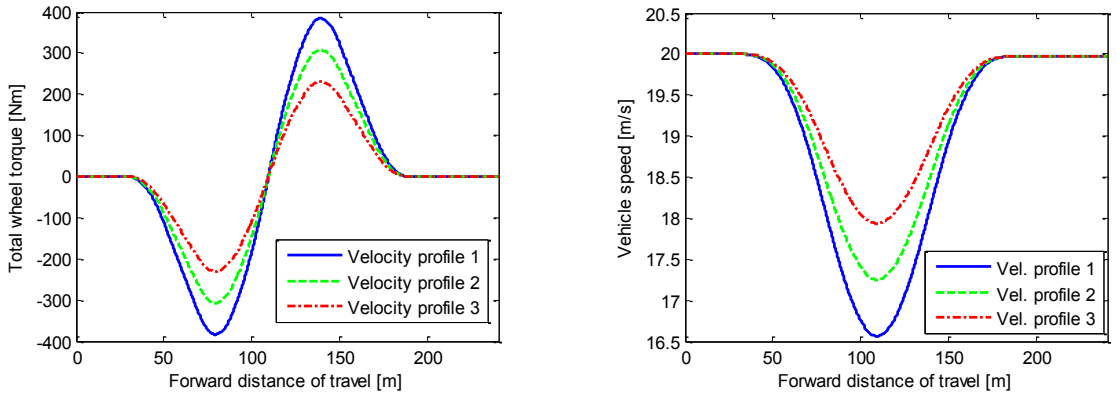

(a) *(b)*

Figure 4.12: Longitudinal performance

The path position provides the future information to the preview controller for the path following task. The vehicle performs a left turn and its position is detected as in Figure 4.13(a). Although there is only one observed path input, the steering varies due to the different wheel torques. In Figure 4.13(b), the steering corresponding to the velocity profile 1 is higher than the one for the velocity profile 3. A close look of the lateral displacement at the corner as in Figure 4.13(c) shows that the vehicle follows the observed path with the small lateral deviation. The difference of three trajectories is not significant.

A Kalman filter is capable of reducing the effect of noise on the vehicle state estimation. In reality, the filter is required due to the existence of disturbances affecting

the position and speed measurement. On the other hand, the vehicle is a complex dynamic system and the filter is considered as an estimator that provides the approximation for vehicle states based on the measured parameter. The states are necessary for the linear controller that needs feedback to calculate the next steering and torque inputs.

In the following simulation, the white Gaussian noises are added to the input from the measurements. The true position and the estimated position of the vehicle are illustrated in Figure 4.14(a). Although the measurement fluctuates due to the additive noise (±0.3m) as in Figure 4.14(b), the estimation is very close to the true state. The steering angle input as in Figure 4.14(c) is highly affected by disturbances. The large fluctuation of the steering angle comes from the corrupted noise and the noise that is partly filled by the Kalman filter.

The measurement of the vehicle speed is assumed to also be corrupted by noise (±0.4m/s) as illustrated in Figure 4.15(b). The Kalman filter performs estimation from the noise speed measurement. It provides the estimated vehicle speed and wheel angular velocities to the linear controller. The difference between the true vehicle speed and the estimated speed is not significant as in Figure 4.15(a). The wheel torque is computed from the estimated states with the presence of noise as in Figure 4.15(c).

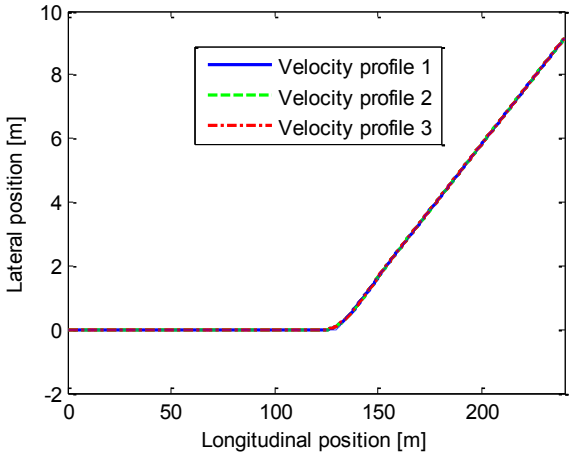

(a)

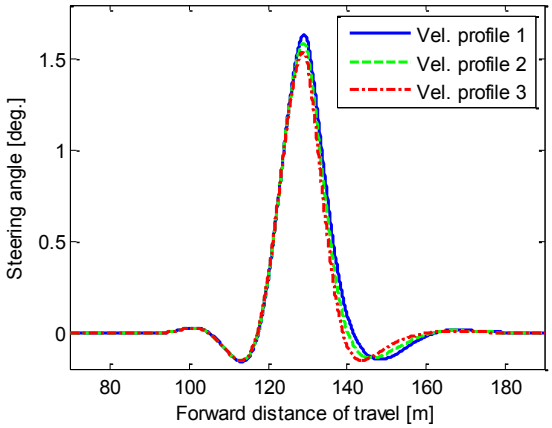

(b)

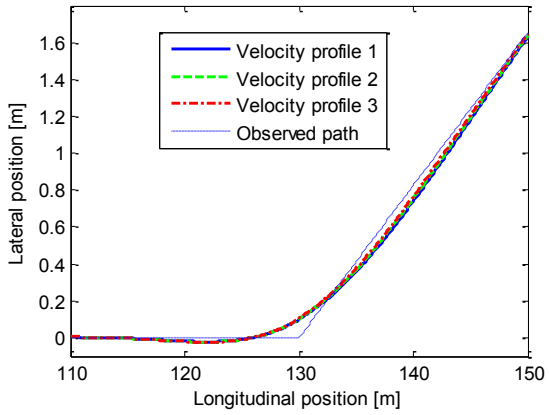

(c)

Figure 4.13: Lateral performance

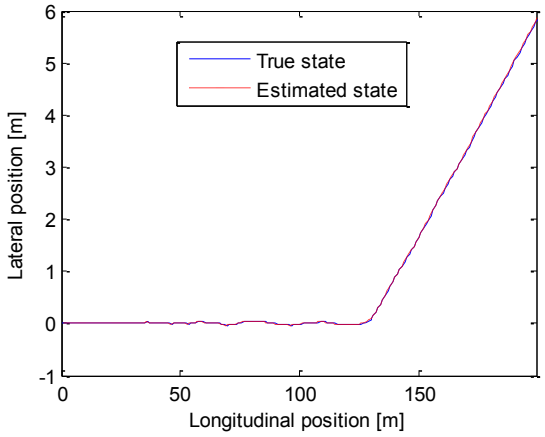

(a)

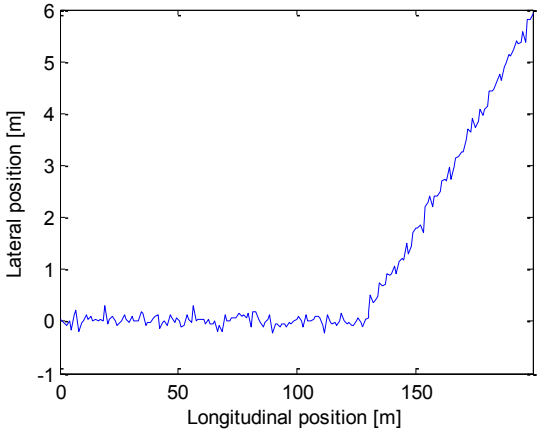

(b)

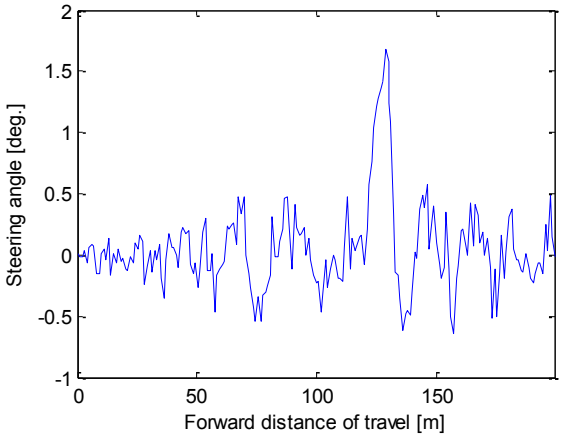

(c)

Figure 4.14: Lateral performance with disturbances

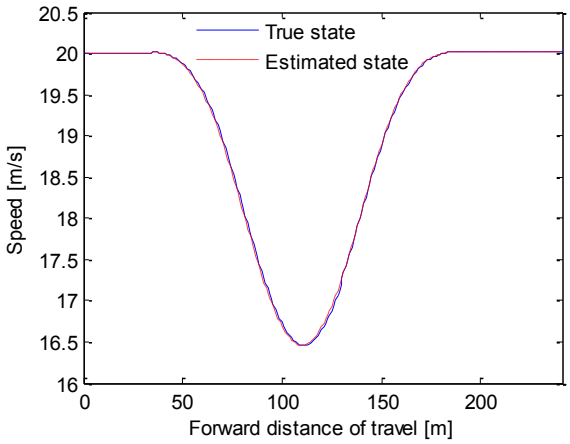

(a)

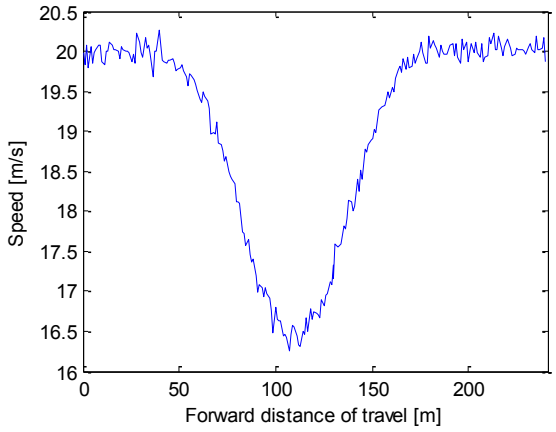

(b)

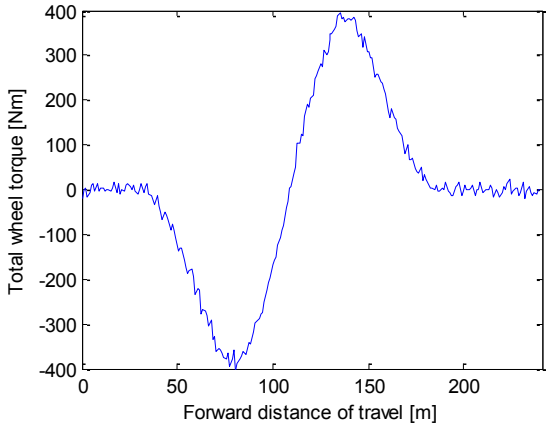

(c)

Figure 4.15: Longitudinal performance with disturbances

4.5 CONCLUSION

The investigation proposes a new method for the longitudinal and lateral planning that may be implemented on autonomous vehicles. The linear models of steering control and speed control are derived. The preview control is applied to enhance the performance of the vehicle when the future path is available. The Kalman filter is used to estimate the vehicle states based on the nonlinear model with disturbances. The simulation shows that the controllers perform a good path following and speed regulating.

The most important part of the controller and the filters are the computation of control gains and filter gains. These tasks deal with an enormous amount of calculation and matrixes of large dimension. These gains can be pre-calculated and stored in the hardware of controller. The computational time is shortened which allows the vehicle to operate real time while the road information is frequently updated. The proposed controller introduces a feasible application for autonomous vehicles.

Chapter 5

NEURAL NETWORK
USED TO CONTROL AUTONOMOUS VEHICLES

5.1 INTRODUCTION

Artificial Neural Networks (ANNs) have displayed the potential applications for control of nonlinear systems with high degrees of noise and variability [108]. In particular, Neural Networks (NNs) may be represented as human drivers to manipulate vehicles since the NNs are capable of emulating the drivers' behavior. The flexibility of adjusting the network weights provides the possibility of a wide range of autonomous vehicles' tasks including navigation and speeding.

The techniques which enable the NNs to learn the driver's performance were developed by Pomerleau et al (1992) [109]. By watching a human driver, the NN system was trained to autonomously control a vehicle in a variety of circumstances. The NN is a single hidden layer receiving camera input from a road scene [110]. The network uses the back-propagation to activate the NN output to adjust the current steering. The proposed technique is based on the image processing that allows the vehicle to follow the pre-defined path without the knowledge of the vehicle and disturbances. The network weights are pre-determined that does not support the online retraining.

Kehtarnavaz et al (1998) [111] proposed a NN module for autonomous vehicle which may change its steering and speed depending on the lead vehicle. Range and head angle were collected from the experiment with a human driver. The NN was capable of

leaning the nonlinear characterization of vehicle and reproducing the human driving. The control mechanism is transportable regardless of vehicle dynamics.

In this chapter, a new approach is introduced to use NN in autonomous vehicles. This method is a result of LQR used to design the controller for autonomous vehicle in the steady state. The NN structure is designed in the reference of the driver model. Two single neurons perform as the path filter where the previewed path is weighted. The vehicle model with nonlinear dynamics represents a real vehicle. The NN weights adapt to various road shapes. Finally, the trained NNs are tested through the F1 Montreal circuit in order to evaluate the vehicle performance in navigation and speed control.

5.2 NETWORK ARCHITECTURE

The investigation on the steering angle obtained in equation (4.14) reveals that the control gains $\boldsymbol{K}_{yk}$ consists of two components, the state gains and the path gains. If the stability of the system is satisfied, the gains will converge to the constants that may be pre-calculated and stored in the hardware. The state gains include lateral velocity, yaw rate, lateral position and head angle gains. The path gains represent the ability of observing the path to improve path following. The steering angle then is written as:

$$\delta_{sw}(k) = \mathbf{K}_v \mathbf{x}(k) + \mathbf{V}\mathbf{y}_v(k) \tag{5.1}$$

where the state gains $\mathbf{K}_v=[k_v\ k_r\ k_y\ k_\psi]$ and the path gains $\mathbf{V}=[v_1\ v_2\ \ldots\ v_n]$. The steering angle is computed from the contribution of the state feedback and the path preview.

For the lane-change test as in Figure 3.2, the contribution of each part is illustrated in Figure 5.1(a). The steering angle from the observed path provides a positive

feedback while the angle generated from vehicle states provides a negative feedback. Combining the two components yields the steering angle as in Figure 5.1(b) that drives the vehicle with the least lateral deviation. When the vehicle follows a straight path, the balance of the positive and negative parts results the zero steering angle.

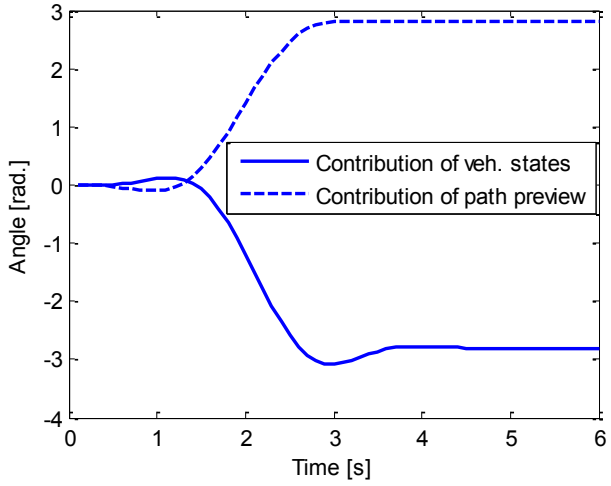

(a)

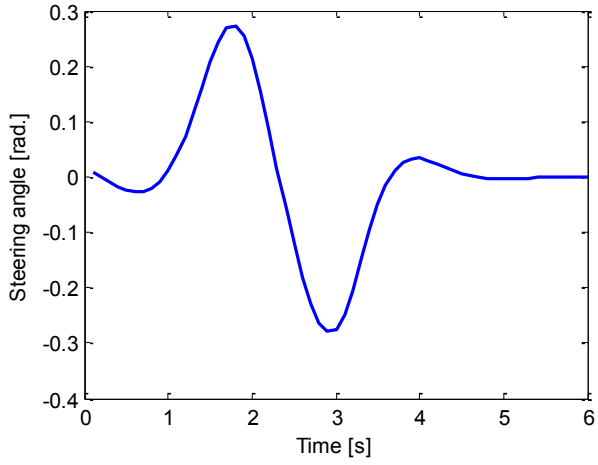

(b)

Figure 5.1: The contribution of vehicle states and path preview in generating the steering angle

The contribution of the path may be illustrated as a network with n inputs and one output. In Figure 5.2, n lateral positions of the path provide as the inputs to the NN. The network gain corresponding to each lateral position is the path gain. The activation function $\sigma(\cdot)$ is taken as linear so that:

$$y_{out} = v_1 y_{v1} + v_2 y_{v2} + \ldots + v_n y_{vn} = \sum_{i=1}^{n} v_i y_{vi} \tag{5.2}$$

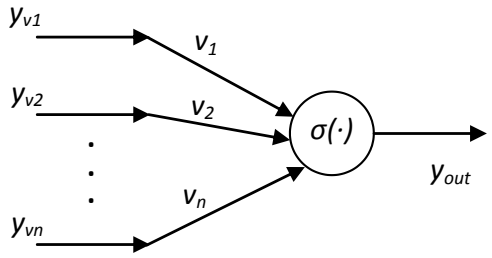

Figure 5.2: The NN presenting the path preview

Processing the previewed path through a series of delays provides a sequence of lateral positions ahead of the vehicle. The value $y_v(k+n)$ is the latest information observed from the path while the value $y_v(k)$ indicates the current desired position. Figure 5.3 illustrates the structure for lateral and longitudinal control. This schematic diagram yields the steering angle as in equation (5.1) for vehicle navigation. The previewed path is weighted by going through a single neuron.

The lateral velocity, yaw rate, lateral position and head angle are measured and then provided as the negative feedback. The technique to identify the state gains $\boldsymbol{K}_v$ is discussed in section 2.5. The gains are considered as the ratio of the future vehicle

position to the initial condition for a specific preview time. The state gains are unique and they are obtained through the initial tests.

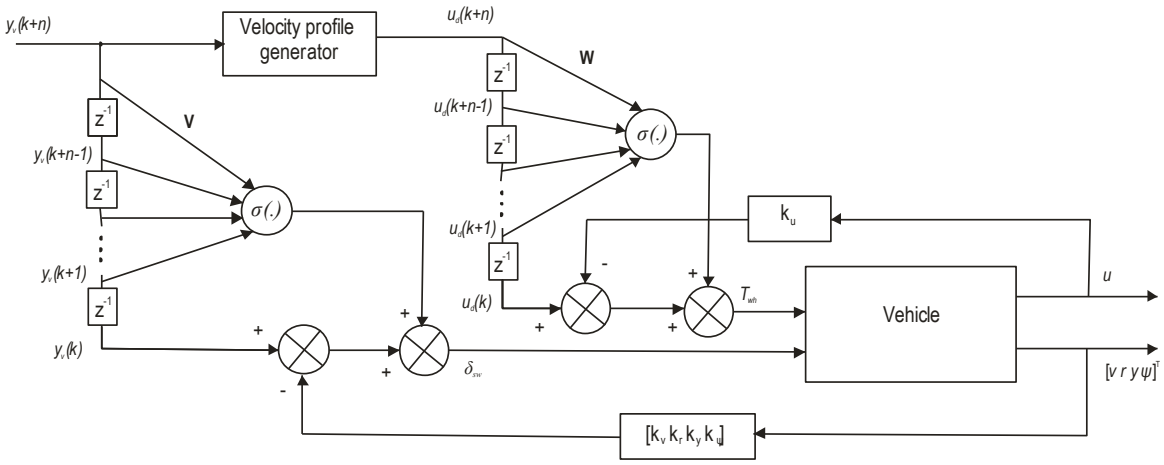

Figure 5.3: The structure of autonomous vehicle controller

It is expected that the similar scheme may be used to compute the required torque. The velocity profile generator provides the desired speed based on the previewed path. A single neuron collects the delayed speed to calculate the additional torque. The desired speed $u_d(k+n)$ after n delays is the current desired speed $u_d(k)$ that the vehicle must achieve at the next instant. The negative feedback is proportional to the measured vehicle speed. Therefore, the proportional control diagram is used if the NN is ignored.

The technique to create the curvature and velocity profile is described in section 4.2. Since the data collected from the path is discrete, three parts of the continuous curvature are constructed. The velocity profile generator computes the curvature and then builds the velocity profile by referring to the experiment results. The desired speed

depends on not only the curvature but also the road conditions and the characteristics of the vehicle.

The nonlinear vehicle model is derived in section 4.3. The 8 DOF model includes the longitudinal and lateral dynamics. The vehicle speed is interfered by changing the wheel torque T_{wh}. The position is achieved by applying a steering angle. The nonlinear dynamics of the tires is also included so that the vehicle may work when there is the high demand of the road. The vehicle model may be represented as a real vehicle for training and testing the NNs.

5.3 TRAINING ARTIFICIAL NEURAL NETWORK

In this section, the NN is trained by using the gradient descent tuning [112]. Let $v_i(k)$ be the weight at the iteration k, the NN output then is:

$$y_{out}(k) = \sum_{i=1}^{n} v_i(k) y_{vi} \tag{5.3}$$

where y_{vi} is the lateral position that stays constant during the iterating step. The relationship in equation (5.3) only mentions a pair of ($\boldsymbol{y}_v$, y_{out}). The vector $\boldsymbol{y}_v$ consists of lateral positions y_{vi} while y_{out} is a scalar output. In the practical situation, $\boldsymbol{y}_v$ are multiple input vectors. At the current instant, $\boldsymbol{y}_v(k)$ takes the set of [y_{v1} y_{v2} ... y_{vn}]. For the next instant, $\boldsymbol{y}_v(k+1)$ takes the different set. The output values y_{out} corresponding to $\boldsymbol{y}_v$ are $y_{out}(k)$, $y_{out}(k+1)$, … $y_{out}(k+n)$. The batch NN weight update is used to perform the iteration. Defining the inputs as a matrix yields:

$$\boldsymbol{y}=[\boldsymbol{y}_v(k)\ \boldsymbol{y}_v(k+1)\ \ldots\ \boldsymbol{y}_v(k+n)] \tag{5.4}$$

The output vector is defined as:

$$\boldsymbol{y}_{out}=[\boldsymbol{y}_{out}(k)\ \boldsymbol{y}_{out}(k+1)\ \ldots\ \boldsymbol{y}_{out}(k+n)] \tag{5.5}$$

At the initial stage, the NN with the predefined weights produces large errors. The training process is performed to achieve the accepted errors. The recursive update equation of weights is given as:

$$v_i(k+1)=v_i(k)-\alpha\frac{\partial E(k)}{\partial v_i(k)} \tag{5.6}$$

The algorithm insures that the cost function decreases after each update. The learning rate α is a value in the range of (0, 1). If the chosen α is too small, the number of iterations is large. If α is close to 1, the value of gain $v_i(k)$ may diverge that increases the value of the cost function.

Defining the cost function as the least-square error yields:

$$E(k)=\frac{1}{2}\sum_{i=1}^{n}e_i^2(k)=\frac{1}{2}\sum_{i=1}^{n}\left[y_{des,i}(k)-y_{out,i}(k)\right]^2 \tag{5.7}$$

The first derivative of the cost function with respect to the weights is given as:

$$\frac{\partial E(k)}{\partial v_i(k)}=-e_i(k)y_{vi}(k) \tag{5.8}$$

Therefore the weight update algorithm for the least-square error becomes as:

$$v_i(k+1)=v_i(k)+\alpha e_i(k)y_{vi}(k) \tag{5.9}$$

The training process begins while the previewed path is not provided. The vehicle follows the path only based on the current measured lateral position. The closed-loop system consists of a proportional controller which minimizes the deviation. The vehicle trajectory is illustrated as in Figure 5.4. The vehicle is lagged behind the desired path. The lateral errors between the vehicle trajectory and the desired path are recorded.

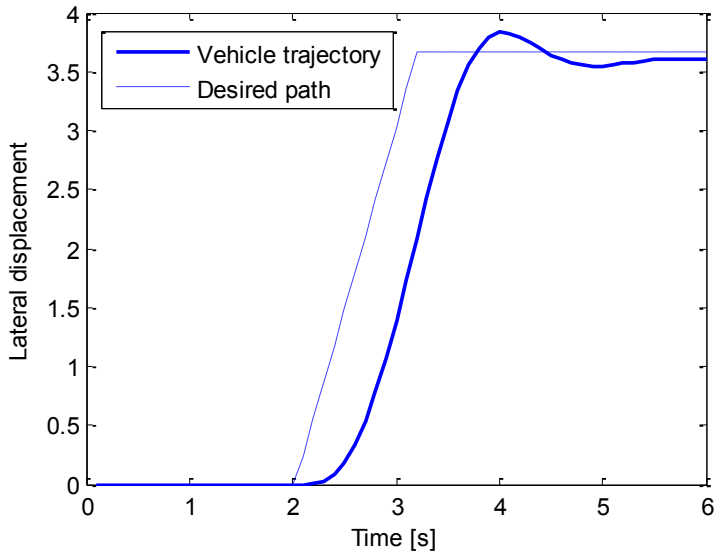

Figure 5.4: Vehicle trajectory with a proportional controller

In next step, the steering angles are computed from the lateral errors. They are the additional steering that is expected to draw the vehicle closer to the path. Then the additional steering is added to the proportion controller. The process is repeated until achieving the small lateral errors. The additional steering angles are considered as the desired outputs of the NN.

Theoretically, the NN gains (**V** and **W**) may be initially chosen as arbitrary sets of random numbers between -1 and 1. The training process tunes these gains so that the least-square errors are minimized. An example of NN weights after training is illustrated in Figure 5.5. The single neuron with 60 inputs and one output is used. The NN outputs are very close to the desired values that are the additional steering angles added to the system without preview information as in Figure 5.5(b). The gains are achieved as in Figure 5.5(a) after 500 iterations. The trained gains may be different if the different initial values of gains are selected.

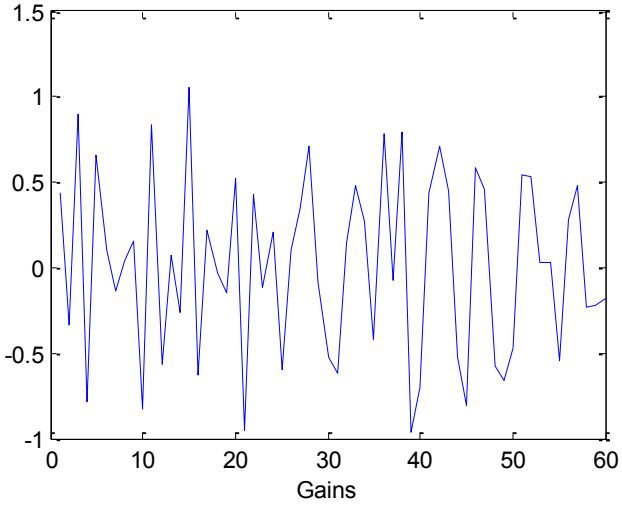

(a)

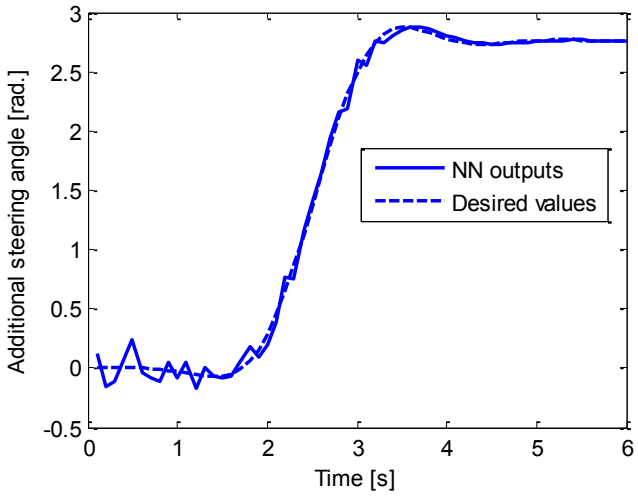

(b)

Figure 5.5: NN training with arbitrary pre-defined gains

The studies of the driver model in Chapter 3 provide another approach to initiate the gain values. Figure 5.6 illustrates the steady state control gains for the previewed path. In general, the gain for the path which is close to the vehicle is higher than that at a large distance from the vehicle. If the path is too far, it has a negligible effect on the driver's decision. The ordered gains improve the performance of the vehicle when

following a path with frequent changes. The NN gains for the nonlinear vehicle may be taken in a similar manner. At the beginning, the control gains as in Figure 5.6 are applied to the NN weights **V**. Then the weights are updated by using the gradient descent tuning as discussed in the beginning of the section.

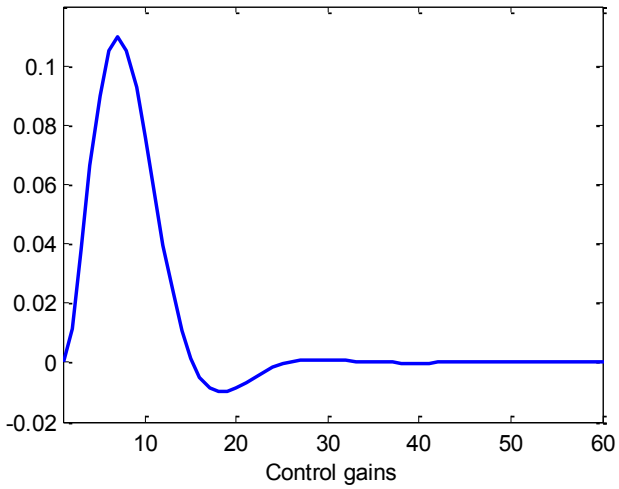

Figure 5.6: Control gains of LQR driver model

The trained weights are illustrated as in Figure 5.7. The NN weights are slightly changed after iteration and reach the steady values when the iteration steps are large. The updating algorithm maintains the shape of gains. The gains for the path which is far from the vehicle is close to zero. The peak gain is 0.101 which is lower than the initial value by 10%.

The gradient descent tuning is also applied to train the NN for the speed control. In this stage, only speed regulation is considered. The vehicle is required to follow a desired velocity profile. The initial values of **W** are chosen so that the gains for the desired speeds close to the vehicle are larger than that far from the vehicle. The reason is

that the speed controller likely relies on the near future desired speeds. Therefore, the similar gain shape as gains **V** is used. In Figure 5.8, the trained weights after 100 iterations slightly differ from the initial weights. The weights inherit the driver model performance in filtering the desired speed.

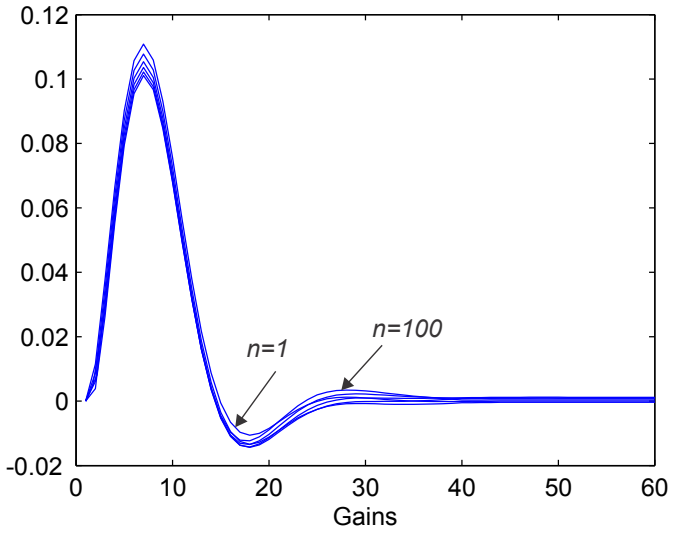

Figure 5.7: NN weights for nonlinear vehicle

The NNs are then trained by applying both steering angles and wheel torques. The vehicle performs a lane-change and decreases the speed. The errors between the desired path and the real position are measured. The tuning algorithm uses these errors to adjust the weights of **V**. The vehicle velocity is also compared to the velocity profile. The weights of **W** are updated to minimize the velocity errors. Various road shapes are used to train the NNs such as double lane-change, turning and slalom. After going through each shape, the NN adjusts its weights. When the vehicle performs all tests, the NNs are trained so that they can work with many types of path inputs.

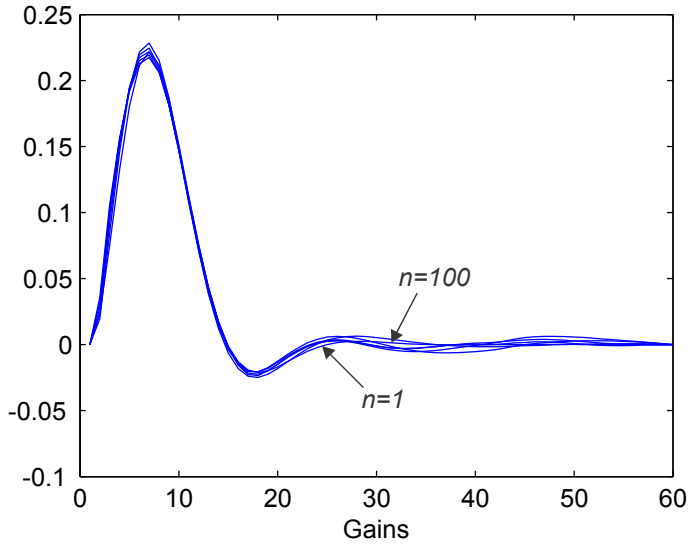

Figure 5.8: NN weights for velocity control

The robustness of the closed-loop system is evaluated by using the frequency response analysis. The robustness of the system represents its ability to maintain the desired performance. The method defines the curvature threshold at which the vehicle may perform. The path inputs are taken as sine functions with varying frequency. A road path is illustrated in Figure 5.9. The vehicle is required to follow the path that is continuously turning left and right. The peak lateral displacements for both sides are 3.66m that is the width of the lane. The vehicle completes a cycle when finishing one left turn and one right turn. The frequency of the road path is calculated as the number of cycles in one second. The velocity profile is computed from the lateral path. The change of the frequency yields various path curvature and velocity profiles.

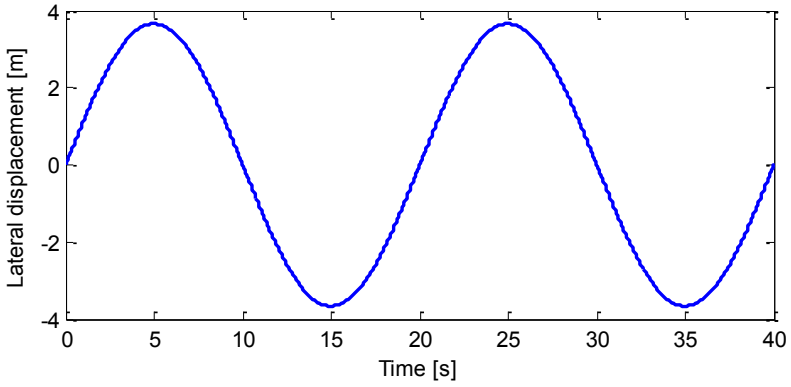

Figure 5.9: The road path used in the frequency response analysis

The Bode plot of the frequency response is presented in Figure 5.10 for lateral position. The path frequency increases from 0.01Hz to 1Hz. The magnitude of lateral position M_{lat} is the logarithmic gain calculated as:

$$M_{lat} = 20\log_{10}\left(\frac{y_{path}}{y_{out}}\right) \tag{5.10}$$

where y_{path} is the peak value of lateral path, y_{path}=3.66. y_{out} is the peak lateral output of the vehicle. The unit of M_{lat} is decibel (dB). For the low frequency (f < 0.1Hz), the magnitude close to zero means that the vehicle output meets the path input. In other words, the vehicle follows the path with small errors. For the higher frequency (f > 1Hz), the magnitude takes negative values that means the vehicle cannot accurately follow the path and produces large errors. The bandwidth of the system is 0.4Hz at which the magnitude is equal to -3dB. The vehicle maintains a good path-following when the path frequency is lower than 0.4Hz.

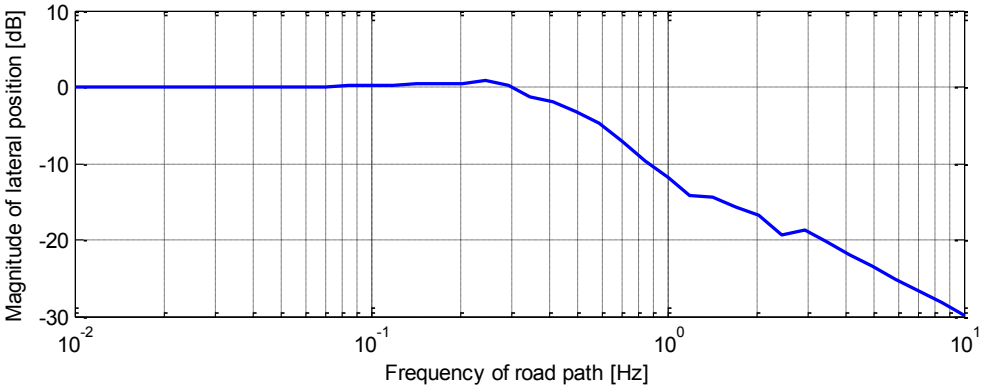

Figure 5.10: Frequency response of the lateral position

The frequency response of vehicle speed is illustrated in Figure 5.11. The magnitude of speed M_{sp} is the logarithmic gain calculated as:

$$M_{sp} = 20\log_{10}\left(\frac{v_{path}}{v_{out}}\right) \tag{5.11}$$

where v_{path} is the peak value of velocity profile. v_{out} is the peak speed output of the vehicle. The magnitude takes negative values in the entire frequency range. The vehicle speed decreases when the frequency increases from 0.01Hz to 0.4Hz. The errors reach stable values when the frequency is larger than 0.4Hz. Although the vehicle speed is always smaller than the desired speed, the difference between the response and the input is about -1.2dB. The small errors allow the vehicle to perform good speed control. In addition, the speed controller may perform at the high frequency which contrasts with the position controller.

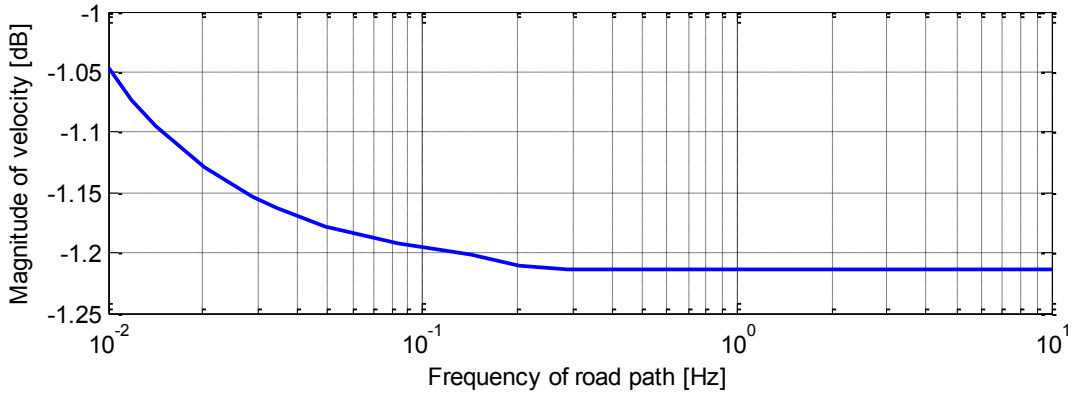

Figure 5.11: Frequency response of the vehicle speed

In this section, the training process for the NNs is discussed. The NN weights are initiated by learning the driver model behavior. Using offline training, the NN inherits the properties of the tested paths so that it may work with different path inputs latter. The frequency response analysis is performed to define the working range of the autonomous vehicle. The vehicle is capable of running with the regular paths where the path frequency is less than 0.4Hz. In next section, the position and speed performance of the vehicle is evaluated by using a complete road circuit.

5.4 SIMULATION RESULTS

The vehicle model with the trained NNs is tested by using the F1 Montreal Circuit as in Figure 5.12. The starting point is at the coordinate of (0, 0) and the moving direction is counterclockwise. The vehicle completes a cycle consisting of various path curvatures. The vehicle is required to follow the path and also to regulate its speed. Several important points are marked on the circuit such as the corner AB, CE and GH. The section AB is

similar to a lane change. The sections CE and GH have the largest curvature. The sections BC and FG are approximated as the straight path where the vehicle may perform the maximum speed.

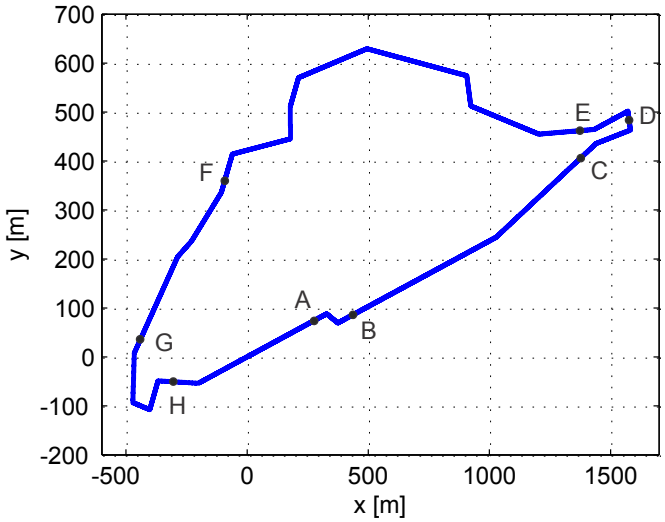

Figure 5.12: F1 Montreal Grand Prix circuit

The desired speed is calculated from the path curvature. As discussed in Chapter 4, the driver may choose an appropriate velocity profile that is lower than the limit. In this simulation, three levels of speed are considered to evaluate the influence of tracking forces on the lateral performance. The lateral position and speed of the vehicle are recorded for three velocity profiles in order to evaluate its capabilities of path-following and speed-regulating.

The gains of NNs for longitudinal and lateral control after training with various paths are illustrated in Figure 5.13. Although the values of **V** and **W** are different, their attitudes are similar. Almost half of the 60 values are negligible. The peak value is not the first gain but it falls in about the gain number eight. In general, the part of gains for weighting the path near the vehicle is large. The arrangement improves the ability of

tracking the desired path. The adjustment does not depend too much on the path next to the vehicle and the controller does not allow the path away from the vehicle affect the current performance.

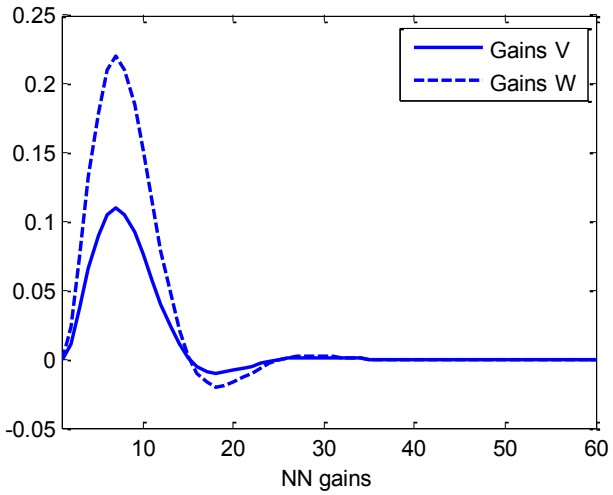

Figure 5.13: NN gains after training

Figure 5.14 illustrates the vehicle speed along the circuit at a reference velocity profile. The regular velocity profile is chosen where the maximum speed is 20m/s for the straight path. The vehicle speed reaches the highest value of 20m/s in the sections BC and FG where the curvature is considered small (κ<0.005m^{-1}). The vehicle reduces its speed at the corners. For instance, the lowest speed (12m/s) is in the sections CE and GH where the curvature is about 0.02m^{-1}. The vehicle chooses an appropriate speed corresponding to a curvature. The similar responses are found if the low velocity profile and high velocity profile are used.

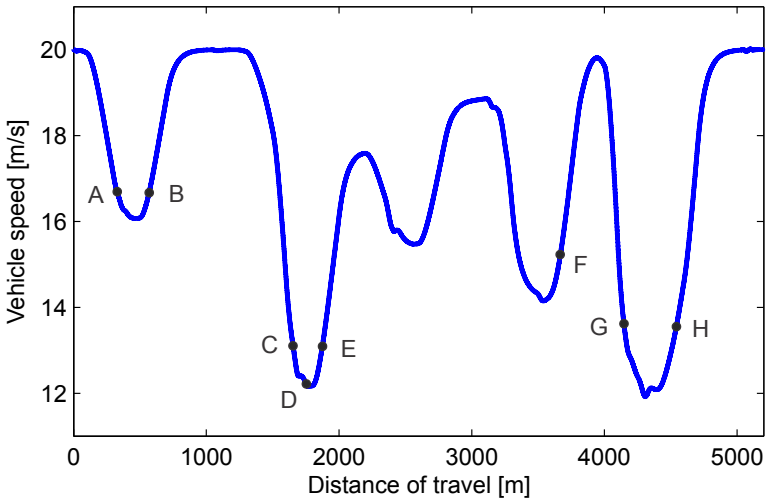

Figure 5.14: Vehicle speed

The vehicle position at the section AB is recorded as in Figure 5.15. The vehicle performs the test with three levels of velocity profile. The velocity profile 1 corresponds to the lowest velocity while the velocity profile 3 indicates the highest velocity. The maximum speeds are 22m/s, 20m/s and 18m/s for the high velocity profile, regular velocity profile and low velocity profile respectively. At the corner, the vehicle running with the high speed produces the larger deviation. With the velocity profile 1, the vehicle position is mostly coincided to the desired path. The profile 3 generates larger errors which the maximum recorded value is 2m. The differences of speeds have negligible effects on the lateral performance when the vehicle going along a straight line as the entrance and the exit of the corner.

The road as the section DE of the circuit is very high demanding as shown in Figure 5.16. The vehicle performs a difficult path following task while maintaining a suitable speed. Although the controller reduces the required speed (e.g. 12m/s), the errors are higher than that at the corner AB. The high speed results in the larger deviation. For

the high velocity profile, the error at the corner is 4m higher than that for the low velocity profile. The vehicle may not perform within the safe margin if the velocity profile is chosen too high.

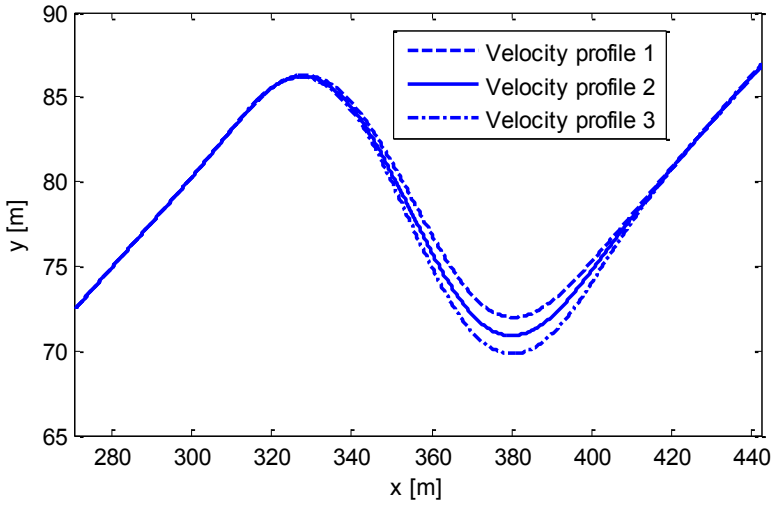

Figure 5.15: Vehicle position for the section AB

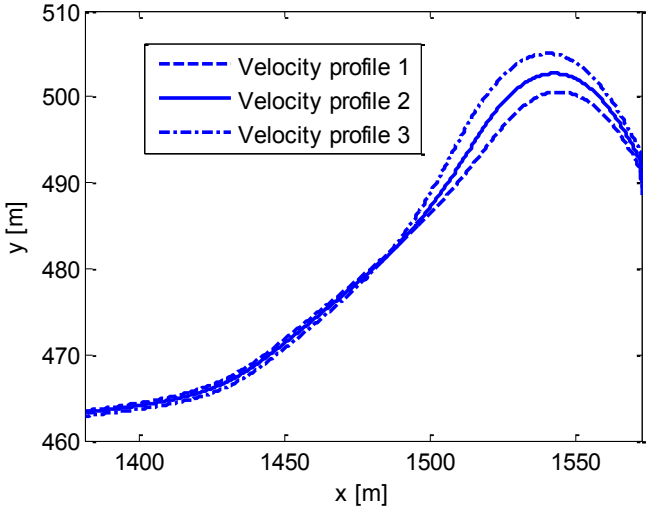

Figure 5.16: Vehicle position for the section DE

5.5 CONCOLUSION

This chapter discusses a new approach to design the longitudinal and lateral controller for the autonomous vehicle. The method is based on the knowledge of driver behavior in maintaining along a path and adjusting vehicle speed. The NN is used to weight the previewed path before providing an additional input to the vehicle. The NN weights are trained by the gradient descent tuning with various road shapes.

The NN architecture improves the longitudinal and lateral performance by using the ordered weights. After going through the NNs, the future path provides a preparation that helps the vehicle moves smoothly. The simulation for a complete F1 circuit shows that the NN controllers properly work with the changing curvature path. The vehicle may adjust its speed depending on the previewed path.

Chapter 6

CONCLUSION AND FUTURE WORK

6.1 CONCLUSION

The thesis presents the research on the driver-vehicle model for safe driving and the design of vehicle controller based on the knowledge of driver behavior. As stated in the literature review, the previous research in driver model only focuses on the optimal driving. The impaired driver model is proposed to present the varying skills that may have adverse effects on the overall vehicle performance. The novel approach to autonomous vehicles is also introduced and discussed. The controllers adopt the driver's prediction by incorporating the preview path. The below list are the main contributions that the work has emphasized on.

1. The driving skills may be quantified by plotting the root locus of the driver-vehicle model as in section 2.4. The driving performance is investigated in the similar manner as the stability analysis. Increasing reaction time and decreasing preview time means decreasing the system stability. The impaired driver is seen as the system closer to the unstable state. The threshold, where the driver cannot drive the vehicle, is seen as a root located in the right plane. This situation occurs when the preview time is too short and the reaction time is too long.
2. The linear driver model may couple to a nonlinear vehicle model. Without the knowledge of nonlinear vehicle, the driver model follows the path within the

accepted errors. The vehicle is treated as a black box where its feedback gains are identified by initial tests. The steering, lateral velocity, yaw rate, lateral position and head angle gains are driver model parameters in prediction. They are the ratios of lateral position to the initial values for a specific preview time.

3. The neuromuscular characteristic of the human operator is introduced to model the driver using the LQR as in section 3.2. The driving is considered as the optimal performance with delay. The driver continuously maintains the small errors while governed by the transport delay due to the perception and action. The achieved control law is similar to the system without delay however the output fluctuates more due to the delayed feedback.
4. The proposed driver model is related to the experiments for various levels of BAC. After consuming alcohol, the driver generates higher SDLP as the impaired driver model does when reducing preview time, increasing reaction time and introducing larger errors in the control gains. A percentage of deterioration in the impaired driver model corresponds to a level of BAC for the human driver.
5. The integration of the longitudinal and lateral planning for autonomous vehicle is proposed. The core of the controller is the approximation of the nonlinear vehicle. The LQR control calculates the steering angles and tracking torque based on the linear model. The lateral position and the velocity profile of the preview path provide the future information to improve the performance of the driver-vehicle.
6. The NNs are used to weight the preview path before feeding it to the steering and speed controllers. The NN weights are initiated in the fashion as the driver

observes the path. After training, the vehicle may track the path and regulate its speed for various curvatures of the road.

The research also proposes some modifications that improve the previous works.

1. Including the steering angle to the cost function improves the path following of the MacAdam model [27].
2. Introducing the update mechanism that draws the model closer to the driver behavior in path observation.
3. Adapting vehicle parameters such as tire pressure to impaired drivers improves the safe driving

Over the duration of the research project, the author has investigated the other aspects forming the background of the thesis. Some of them are listed below:

1. The comprehensive literature review covers the vehicle models, driver models, impaired drivers and autonomous vehicles. The advantages and disadvantages of the previous research are identified and the potential results are used in the thesis.
2. A bicycle and 8 DOF nonlinear vehicle models are carefully investigated. Although they have been frequently used in control and simulation, their suitability for modeling an impaired driver and simulating an autonomous vehicle is validated.
3. The broad range of control tools such as the classical control dealing with root locus, the LQR, the preview control, the Kalman filter and the NNs is studied and implemented. Comparison among these methods helps to choose the right tool that suits to a specific circumstance.
4. The computation throughout the thesis uses the MATLAB® software. MATLAB® is a powerful tool as the bridge links engineering to mathematics. Some features of

the software are used in the thesis such as control tool, Simulink, Kalman filter and NNs.

6.2 FUTURE WORK

Two major directions may be followed to extend the current work: setting up experiments for impaired drivers and testing the autonomous vehicle controller.

About experimental validation, there are some challenges since the driver adapts to the simulation environment. The performance is significantly improved if a driver performs a task again. Furthermore, an impaired driver is aware of the surveillance. The results may not reflect the reality. The experimental set-up must eliminate these factors. Such tests in academic environment need carefully be planned. The further investigation may be performed to identify the threshold, at which the driver-vehicle system becomes unsafe for specific conditions of road, traffic and weather.

About testing autonomous vehicles, the key issue is to develop a visual detector. The vehicle equipped with sensors and cameras may obtain the desired path. The difficulties are the uncertainties of the road such as obstacles, pedestrians, traffic signals and other vehicles. The pattern recognition is developed to classify the type of images. On the other hand, the system must distinguish motion from static. The computer vision also enables to plan a road path by incorporating digital maps and observed path. The control system is capable of determining the absolute position of the vehicle and its relative position to other traffic means.

The relative position of the vehicle is also considered since the vision system is in the moving vehicle in not only the longitudinal direction but also the lateral direction.

The measurement of relative distance for another moving object is quite difficult since the equipment is in the moving vehicle. Even the calculation of the distance for a stationary object ahead the vehicle remains a challenge due to the 2D images. A laser sensor may be incorporated to 2D data for distance measurement. The set-up of two cameras to reconstruct the 3D images from 2D ones is an alternative solution.

When the future path is available, the controller of the autonomous vehicle computes the steering angle and torque. The experiments on the autonomous vehicle need to be carried out to evaluate the performance in terms of the position, the speed and the safety criteria. The experimental results may be significantly different from the simulation results because the computer performs real time computation. The autonomous vehicle must overcome the issue of computational time in order to effectively operate.

REFERENCES

1. Traffic Injury Research Foundation of Canada. *Alcohol-crash problem in Canada: 2008*. Transport Canada, 2010.

2. National Highway Traffic Safety Administration (NHTSA). *The driver drowsy system field operational test: data collection method.* US Department of Transportation Technical Report, 2008

3. Rajamani R, Tan H, Law B et al. Demonstration of integrated longitudinal and lateral control for the operation of automated vehicle in platoons. *IEEE Transaction on control system technology* Jul. 2000; 8 (4): 695-708.

4. Ackermann J, Odenthal D, and Bunte T. Advantages of active steering for vehicle dynamics control, *Proc. 32nd Int. Symp. Autom. Technol. Autom.* 1999, pp. 263-270.

5. Han D and Yi K. A driver-adaptive range policy for adaptive cruise control. *Journal of automobile engineering* 2006; 220: 321-334.

6. Bose A, and Ioannou P. *Analysis of traffic flow with mixed manual and intelligent cruise control vehicles: theory and experiments*. California PATH research report, UCB-ITS-PRR-2001-13, 2001.

7. Wong JY. *Theory of ground vehicle* 3rd Edition. New York: John Wiley and Sons, 2001.

8. Jazar RN. *Vehicle dynamics: Theory and application*. Springer, 2008.

9. Abe M. *Vehicle handling dynamics: Theory and application.* Oxford: Elsevier, 2009.

10. Shim T and Ghike C. Understanding the limitations of different vehicle models for dynamics study. *Vehicle system dynamics* Mar. 2007*;* 45(3): 191-216.

11. Sayers W and Han D. A generic vehicle model for simulation handling and braking. *Vehicle system dynamics* 2006; 25: 599-613.

12. Pacejka HB. Tyre modeling for use in vehicle dynamics studies, *SAE Paper* No. 870421, 1987

13. UMTRI, Rollover of heavy commercial vehicles. *UMTRI research review* Dec. 2000; 31(4):1-21.

14. Allen R and McRuer D. The man/machine control interface pursuit control. *Automatica* 1979; 15: 683-686.

15. Hess RA. Modeling the effects of display quality upon human pilot dynamics and perceived vehicle handling qualities. *IEEE transactions on systems, man, and cybernetics* 1995; 25(2): 338-344.

16. Weir DH and McRuer DT. Dynamics of driver vehicle steering control. *Automatica* 1970; 6: 87-98.

17. McRuer D and Jex HR. A review of quasi-linear pilot models. *IEEE transactions on human factors in electronics* 1967; HFE-8(3): 231-249.

18. McRuer D. Human dynamics in man-machine systems. *Automatica* 1980; 16: 237-253.

19. McRuer D and Krendel ES. *Mathematical models of human pilot behavior.* Report No. 146, Systems technology, INC, CA, US, 1974.

20. McRuer D, Weir DH, Jex HR et al. Measurement of driver-vehicle multi-loop response properties with a single disturbance input. *IEEE transactions on system, man, and cybernetics* 1975; SMC-5(5): 490-497.

21. Hess RA and Moditahedzadel A. A control theoretic model of driver steering behavior. *IEEE international conference on system, man and cybernetics* 1990, pp. 504-509.

22. Sherian TB. Three models of preview control. *IEEE Transaction on human factors in electronics* 1966; HFE. 7(2): 91-102.

23. Cho YH and Kim J. Stability analysis of the human controlled vehicle moving along a curved path. *Vehicle system dynamics* 1996; 25: 51-69.

24. Hess RA and Modjtahedzadeh A. A preview control model of driver steering behavior. *Proceedings of the IEEE International Conference on Systems, Man and Cybernetics* 1989, pp. 504-509.

25. Plochl M and Edelmann J. Driver models in automobile dynamics application. *Vehicle Syst. Dyn.* 2007; 45(7-8): 699-741.

26. MacAdam C. An optimal preview control for linear systems. *Journal of dynamic systems, measurement, and control* 1980; 102: 188-190.

27. MacAdam C. Application of an optimal preview control for simulation of closed-loop automobile driving. *IEEE Transactions on systems, man, and cybernetics* 1981*;* 11(6): 393-399.

28. MacAdam C. Understanding and modeling human driver. *Vehicle system dynamics* 2003; 40: 101-134.

29. MacAdam C. *Development of driver/vehicle steering interaction models for dynamic analysis.* Technical report for the US army tank automotive command, Report No. UMTRI-88-53, University of Michigan 1998.

30. Gou K and Guan H. Modeling of driver/vehicle directional control system. *Vehicle system dynamics* 1993; 22: 141-184.

31. Yang X. *A closed-loop driver/vehicle directional dynamics predictor*. PhD Thesis, Concordia University, Canada, 1999.

32. Sharp RS. Optimal linear time-invariant preview steering control for motorcycles. *Vehicle system dynamics* 44(S1): 329-340.

33. Thomyppillai M, Evangelou S and Sharp RS. Car driving at the limit by adaptive optimal preview control. *Vehicle system dynamics* 2009; 47(12): 1535-1550.

34. Sharp R and Valtetsiotis V. Optimal preview car steering control, *Vehicle system dynamics supplement* 2001; 35: 101-117.

35. Sharp RS. Driver steering control and a new perspective on car handling qualities, *Proc. IMechE Vol. 219 Part C: J. Mechanical engineering science 2005*; 219(10): 1041-1051.

36. Pick AJ and Cole DJ. A mathematical model of driver steering control including neuromuscular dynamics. *Journal of dynamic systems, measurement, and control* 2008; 130: 1-9.

37. Pick AJ and Cole DJ. Driver steering and muscle activity during a lane-change maneuver. *Vehicle system dynamics* 2007; 45(9): 781-805.

38. Pick AJ and Cole DJ. Dynamic properties of a driver's arm holding a steering wheel. *Journal of automobile engineering* 2007; 221: 1475-1486.

39. Pick AJ and Cole DJ. Neuro dynamics in the driver-vehicle system. *Vehicle system dynamics 2006*; 44(S1): 624-631.

40. Pick AJ. *Neuromuscular dynamics and the vehicle steering task*. PhD thesis, University of Cambridge, 2004.

41. Ungoren AY and Peng H. An adaptive lateral preview driver model. *Vehicle system dynamics* 2005; 43(4): 245-259.

42. Peng H. Evaluation of driver assistance systems–a human centered approach. *AVEC proceedings*, 2002.

43. Hessburg T, Peng H, Tomizuka M et al. An experimental study on lateral control of a vehicle. *American control conference*, 1991.

44. Peng H and Tomizuka M. *Lateral control of front-wheel-steering rubber-tire vehicles*. PATH report UCB-ITS-PRR-90-5, University of California at Berkeley, US, 1990.

45. Peng H and Tomizuka M. Vehicle lateral control for highway automation. *American control conference*, 1990.

46. MacAdam C and Johnson G. Application of elementary neural networks and preview sensors for representing driver steering control behavior. *Vehicle system dynamics* 1996; 25: 3-30.

47. Gou K, Cheng Y and Ding H. Analytical method for modeling driver in vehicle directional control. *Vehicle system dynamics* 2004; 41(S1): 401-410.

48. Lin Y, Tang P, Zhang WJ et al. Artificial neuron network modelling of driver handling behaviour in a driver-vehicle-environment system. *International journal of vehicle design* 2005; 37(1): 24-45.

49. Moskowitz H and Robinson D. *Effects of low dose alcohol on driving related skills: A review of evidence*. NHTSA Report, U.S Department of Transportation, Jul. 1988.

50. Moskowitz H and Fiorentino D. *A review of the literature on the effects of low dose of alcohol on driving-related skills.* NHTSA Report, U.S Department of Transportation, Apr. 2000.

51. Fillmore M, Carcadden J and Vogel-Sprott M. Alcohol, cognitive impairment an expectancies, *Journal of studies on alcohol* 1998; 59: 174-179.

52. Liu Y and Fu S. Changes in driver behaviour and cognitive performance with different breath alcohol concentration levels. *Traffic injury prevention* 2007*;* 8: 153-161.

53. Linoila M, Erwin C, Ramm D et al. Effects of age and alcohol on psychomotor performance of men. *Journal of studies on alcohol* 1980; 41(5): 488-495.

54. Andre JT, Tyrrell RA, Leibowitz HW et al. Measuring and predicting the effects of alcohol consumption on contrast sensitivity for stationary and moving gratings. *Perception and psychophysics*; 56(3): 261-267.

55. Hill J and Toffolon G, The effect of alcohol on sensory and sensorimotor visual functions. *Journal of studies on alcohol* 1990: 51(2): 108-113.

56. Rohrbaugh J, Stapleton J, Parasuraman R et al, Alcohol intoxication reduces visual sustained attention. *Psychopharmacology* 1998; 96: 442-446.

57. Frazzoli E, Dahleh M and Feron E. Real-time motion planning for agile autonomous vehicles. *Journal of guidance, control, and dynamics* 2002; 25(1): 116-129.

58. Shiller Z, and Gwo Y. Dynamic motion planning of autonomous vehicles. *IEEE transaction on robotics and automation* 1991; 7(2): 241-249.

59. Shladover S, Desoer C, Hedrick J et al. Automatic vehicle control developments in the PATH Program, *IEEE transactions on vehicular technology* February 1991; 40(1): 114-130.

60. Hedrick J, MacMahon D, Narendran V et al. Longitudinal vehicle controller design for IVHS system. *Proceeding of the 1992 American control conference*, Chicago, 1992, pp. 3107-3112.

61. Hedrick J, Tomizuka M and Varaiya P. Control issues in automated highway systems. *IEEE Control Syst. Mag* 1994; 14(6):21-32.

62. Peng H, Hessburg T, Tomizuka M et al, A theoretical and experimental study on vehicle lateral control. *Proceeding of the 1992 American control conference, Chicago*, 1992, pp. 1738-1742.

63. Pham H, Hedrick K and Tomizuka M. Combined lateral and longitudinal control of vehicles. *Proceeding of the American control conference*, Baltimore, Maryland, 1994, pp: 1205-1206.

64. Vahidi A and Eskandarian A. Research advances in intelligent collision avoidance and adaptive cruise control. *IEEE Transactions on Intelligent Transportation Systems* September 2003; 4(3): 143-153.

65. Fritz H. Neural speed control for autonomous road vehicle. *Control Engineering Practice* 1996; 4(4): 507-512.

66. Holzmann H, Halfmann C, Germann S et al, Longitudinal and lateral control and supervision of autonomous intelligent vehicles. *Control Engineering Practice* 1997; 5(11): 1599-1605.

67. Guo K, Ding H, Zhang J et al. Development of a longitudinal and lateral driver model for autonomous vehicle control. *Int. J. Vehicle Design 2004*; 36(1): 50-65.

68. Sharp RS, Casanova D and Symonds P. A mathematical model for driver steering control, with design, turning and performance results. *Vehicle system dynamics* 2000; 33: 289-326.

69. Baluja S. Evolution of an artificial neural network based autonomous land vehicle controller. *IEEE transactions on systems, man, and cybernetics, part B: Cybernetics* 1996; 26(3): 450-463.

70. Rosenblum M and Davis L. An improved radial basis function network for visual autonomous road following. *IEEE transactions on Neural Networks* 1996; 7(5): 1111-1120.

71. Dougherty M, A review of Neural Networks applied to transport. *Transportation research Part C: Engineering technologies* 1995; 34(3): 247-260.

72. Kumarawadu S and Lee T. Neuroadaptive combined lateral and longitudinal control of highway vehicles using RBF networks. *IEE transactions on intelligent transportation systems* 2006; 7(4): 500-5012.

73. Cole DJ, Pick AJ and Odhams MC. Predictive and linear quadratic methods for *potential* application to modeling driver steering control. *Vehicle System Dynamics*, 2006; 44(3): 259-284.

74. Naidu DS. *Optimal Control Systems.* CRC Press 2003.

75. Yang X, Rakheja S and Stiharu I. Structure of the driver model for articulated vehicle. *International Journal of Heavy Vehicle Systems*, 2002, 9(1), 27-51.

76. Yang X, Rakheja S and Stiharu I. Study of control characteristics of an articulated vehicle driver. *Heavy Vehicle Systems*, 1997*,* 4(2-4), 1-25.

77. McLean JR and Hoffmann ER. The effects of restricted preview on driver steering control and performance. *Human Factor* 1973; 15(4): 421-430.

78. Green M. "How long does it take to stop?" Methodological analysis of driver perception-brake times. *Transportation Human Factors* 2000; 2(3): 195-216.

79. Odenthal D, Bunte T and Ackermann J. Nonlinear steering and braking control for vehicle rollover avoidance. *European control conference*, Germany 1999.

80. Zheng S, Tang H, Han Z and Zhang Y. Controller design for vehicle stability enhancement. *Control Engineering Practice* 2006; 14(12): 1413-1421.

81. Tekin G and Unlosoy YS. Design and simulation of an integrated active yaw control for road vehicle system. *Int. J. Vehicle Design* 2010; 52 (1-4): 5-19.

82. Lewis F L. *Optimal Control*. New York: John Wiley & Sons, 1986.

83. Basin M and Gonzalez JR. A closed-form optimal control for linear systems with equal state and input delays. *Automatica* 2005; 41(5): 915-920.

84. Chyung DH. Discrete systems with delays in control. *IEEE transactions on automatic control* 1969; 14(2): 196-197.

85. Fujinaka T and Araki M. Discrete-time optimal control of systems with unilateral time-delays. *Automatica* 1987; 23(6): 763-765.

86. Drouin M, Abou-Kandil H and Bertrand P. Feedback control for linear discrete-time systems with time delays. *Automatica* 1985; 21(3): 323-327.

87. Mariani L and Nicoletti B. Optimal discrete systems with pure delays. *IEEE transactions on automatic control* 1973; 18(3): 311-313.

88. Hinmarch I, Kerr JS and Sherwood N. The effects of alcohol and other drugs on psychomotor performance and cognitive function. *Alcohol and Alcoholism* 1991; 26(1): 71-79.

89. Brookhuis KA, De Waard D and Fairclough S. Criteria for driver impairment. *Ergonomics* 2003; 46(5): 433-445.

90. Ogden E and Moskowitz H. Effects of alcohol and other drugs on driver performance. *Traffic Inj. Prev.* 2004; 5: 185-198.

91. Wilkinson I, Kim R and Purnell M. Alcohol and human eye movement. *Brain* 1974; 97: 785-792.

92. O'Hanlon JF, Haak TW, and Blaauw GJ. Diazepam impairs lateral position control in highway driving. *Science* 1982, 217: 79-81.

93. Mets MAJ, Kuipers E, Domis L et al. Effects of alcohol on highway driving in the STISIM driving simulator. *Hum. Psychopharmacol Clin. Exp.* 2011; 26: 434-439.

94. Rajamani R, Zhu C. Semi-autonomous adaptive cruise control systems. *Proceedings of the American control conference* 1999, San Diego, California US, pp. 1491-1495.

95. Falcone P, Borrelli F, Asgari J et al. Predictive active steering control for autonomous vehicle systems. *IEEE Transaction on Control System Technology* May 2007; 15(3): 566-580.

96. Falcone P, Borrelli F, Asgari J et al. A model predictive control approach for combined braking and steering in autonomous vehicles. *Mediterranean conference on control and automatio*n 2007, pp. 1-6.

97. Han D and Yi K. A Driver-adaptive range policy for adaptive cruise control. J*ournal of Automobile Engineering* 2006; 220: 321-334.

98. Wang C, Hu Z, and Uchimura K. Precise curvature estimation by cooperating with digital road map. *IEEE Intellegent Vehicle Symposium* 2008, pp. 859-864.

99. Lee T, Kang J and Yi K. Integration of longitudinal and lateral human driver models for evaluation of the vehicle active safety systems. *SAE Paper* No. 2010-01-0084, 2010.

100. Lee T, Kang J, Yi K et al. An investigation on the integrated human driver model for closed-loop simulation of intelligent safety systems. *Journal of mechanical and technology* 2010; 24(3): 761-767.

101. Dorf RC and Bishop RH. *Modern control systems* 11th edition. New York: Pearson Prentice Hall, 2008.

102. Sinha A. *Linear systems: Optimal and robust control*. New York: CRC press, 2007.

103. Maybeck P. *Stochastic models estimation and control* Volume 1. New York: Academic Press, 1979.

104. Stengel R. *Optimal control and estimation.* New York: Dover Publication Inc. 1994.

105. He J, Crolla DA, Levesley MC et al. Integrated active steering and variable torque distribution control for improving vehicle handling and stability. *SAE technical paper* No. 2004-01-1071, 2004.

106. Cabrera JA, Ortiz A, Carabias E et al. An alternative method to determine the Magic tyre model parameters using genetic algorithms. *Vehicle system dynamics* 2004; 41(2): 109-127.

107. Lee H and Tomizuka M. Coordinated longitudinal and lateral control of vehicles for IVHS. *Journal of dynamic systems, measurement, and control* 2001; 123: 535-543.

108. Pomerleau DA. *ALVINN: An autonomous land vehicle in a Neural Network*. Carnegie Mellon University, Pittsburgh, PA, USA, January 1992.

109. Pomerleau DA. *Neural network perception for mobile robot guidance*. Carnegie Mellon University, Pittsburgh, PA, USA, February 1992.

110. Pomerleau DA. Progress in Neural Network-based vision for autonomous robot driving. *Proceedings of the Intelligent Vehicles Symposium 1992*, pp. 391-396.

111. Kehtarnavaz N, Griswold N, Miller K et al. A transportable Neural-Network approach to autonomous vehicle following. *IEEE Transaction on Vehicle Technology* May 1998; 47(2): 694-702.

112. Sarangapani J. *Neural Network control of nonlinear discrete-time systems.* Boca Raton: Taylor and Francis, 2006.